Non-covalent and Covalent Interactions of Anti-aromatic Isophlorinoids

A Thesis

Submitted in Partial Fulfillment of the Requirements

for the Degree of

Doctor of Philosophy

By

Baddigam Kiran Reddy

ID: 20103064

Indian Institute of Science Education and Research (IISER), Pune

2016

Dedicated to my Family…

भारतीयविज्ञानशिक्षाएवंअनुसंधानसंस्थान, पुणे
INDIAN INSTITUTE OF SCIENCE EDUCATION AND RESEARCH (IISER), PUNE
Mendeleeve Block, Dr. Homi Bhabha Road, Pune – 411 008, Maharashtra, India

Dr. V. G. Anand
Associate Professor

Certificate

Certified that the work described in this thesis entitled "***Non-covalent and Covalent Interactions of Anti-aromatic Isophlorinoids***" submitted by *Mr. Baddigam Kiran Reddy* was carried out by the candidate, under my supervision. The work presented here or any part of it has not been included in any other thesis submitted previously for the award of any degree or diploma from any other university or institution.

Date: 18th April, 2016

V. G. Anand

Research Supervisor

Ph: +91-20-25908091 | Fax: +91-20-25899790 *Email: vg.anand@iiserpune.ac.in*

Declaration

I declare that this written submission represents my ideas in my own words and wherever other's ideas have been included; I have adequately cited and referenced the original sources. I also declare that I have adhered to all principles of academic honesty and integrity and have not misrepresented or fabricated or falsified any idea/data/fact/source in this submission. I understand that violation of the above will result in disciplinary actions by the Institute and can also evoke penal action from the sources, which have thus not been properly cited or from whom appropriate permission has not been taken when needed.

Date: 18th April, 2016

Baddigam Kiran Reddy

ID: 20103064

ACKNOWLEDGEMENTS

I express my deep sense of gratitude and heartfelt thanks to Dr. V. G. Anand, my research supervisor, whose guidance made me realize the dream of pursuing doctoral studies. It is his keen interest, constant support and encouragement which enabled me to successfully complete this research work.

I would also like to thank Prof. K. N. Ganesh, Director, IISER Pune for providing excellent research facilities and an outstanding research ambiance.

I am also grateful to the Research Advisory Committee members Dr. Rajesh G. Gonnade (NCL, Pune) and Dr. R. Boomishankar (IISER, Pune), for their suggestions and advices.

I would like to express my sincere thanks to Prof. Amitava Das (NCL, Pune) for Isothermal Titration Calorimetry facility and Dr. Jayaraman Sankar (IISER Bhopal) for EPR facility.

I would like to express my sincere thanks to Dr. T. S. Mahesh, Dr. Ramakrishna Bhat, Dr. H. N. Gopi, Dr. Jeetender Chugh, Dr. Srinivasa Hotha, Dr. M. Jayakannan, Dr. S. G. Srivatsan, Dr. R. Boomishankar, Dr. M. Musthafa, Dr. Sunil Nair and Dr. Surjeet Singh for their encouragement and timely help. In fact, I owe heartiest thank to every faculty in IISER-Pune.

I am extremely thankful to Dr. Umeshareddy Kacherki (deputy librarian) for library support.

I take this opportunity to thank Dr. T. Y. Gopalalrishna for his invaluable help during crystal solving and discussions. I thank Sappati Subrahmanyam and Sharath Thadeti for their valuable suggestions in theoretical studies.

I am really lucky to have wonderful lab mates. It's my pleasure to thank all the lovable Dr. VGA Lab members. Dr. T. Y. Gopalakrishna, Dr. Santosh Gadekar, Dr. Rashmi Prabhu, Dr. Neelam Shivran, Rakesh Gaur Santosh Panchal, Ashok Kumar, Madan Ambore, Uday, Jyotsna, Prachi, Prakhar, Raj Kumar and as they always maintained a very lively environment in lab.

I thank Dr. V. S. Rao and Santosh Nevse for their precious support and timely help. I extend my heartfelt thank IISER Pune administrative staff members especially

Tushar, Mayuresh, Nayana, Mahesh, Nitin, Yatish and Megha for their generous support.

I would like to thank Suresh Prajapat, Syed, Somnath and Pappu from UG lab IISER Pune. I thank Neeta Deo, Suresh and Sachin for IT support.

I acknowledge the help from Archana (SCXRD), Pooja Lunawat (NMR), Swati M. Dixit (MALDI), Swathi (HRMS) and Nayana (HRMS) for the instrumental support.

No words can ever convey my sense of gratitude felt for my parents (Mr. Rami Reddy, Mrs. Jyothi and Mr. Gopala Reddy, Mrs. Madhavi), my sister Mrs. Madhuri and my wife Mrs. Swarna, without their support, encouragement and sacrifice, this journey wouldn't have been possible.

I am extremely thankful to my undergraduate supervisor Mr. B. Venkateswara Rao and his family for their personal care on my studies and motivated me to do PhD.

I gratefully acknowledge to University Grants Commission (UGC) for Research Fellowship.

I thank all my friends and colleagues in IISER Pune for making my stay comfortable and memorable.

CONTENTS

CHAPTER II

Supramolecular Fullerene-Isophlorin Architectures

CHAPTER III

Synthesis and Characterization of *meso,meso* Linked Anti-aromatic Isophlorin

List of abbreviations used in the text

B3LYP	Becke, 3-parameter, Lee – Yang - Parr hybrid functional
BF_3	Boron trifluoride
COSY	Correlated Spectroscopy
d	doublet
DCM	dichloromethane
DDQ	2,3-dichloro-5,6-dicyano-1,4-benzoquinone
DFT	density functional theory
DNA	deoxyribose nucleic acid
DSC	differential scanning calorimetry
DPP	diphenyl porphyrin
ESI-TOF	electrospray ionisation with time of flight detection
EPR	electron paramagnetic resonance
eq.	Equivalents
Et_2O	diethylether
G	gram
h	hour
HOMO	highest occupied molecular orbital
Hz	hertz
ITC	isothermal titration calorimetry
J	joules
J	coupling constant
LUMO	lowest unoccupied molecular orbital
MALDI	matrix assisted laser desorption ionization
MHz	megahertz
mmol	milli mole(s)
ml	milli liter
mp	melting point
MS	mass spectrometry
N	normal
NOESY	Nuclear Overhausser Effect Spectroscopy
NMR	nuclear magnetic resonance
Ppm	parts per million
Rt	room temperature
TD-DFT	time dependent density functional theory
THF	tetrahydrofuran
TPP	5,10,15,20-tetraphenylporphyrin
UV	ultraviolet
XRD	X-ray diffraction

Synopsis

The thesis entitled ***"Non-covalent and Covalent Interactions of Anti-aromatic Isophlorinoids"*** is a study based on the anti-aromatic isophlorins. In an attempt to explore the reactivity of isophlorins, the thesis describes synthesis and characterization of non-covalent complexes obtained from π-π interaction between C_{60} fullerene and the π surface of the anti-aromatic macrocycle. In this endeavour, it was observed that the nature of the substituents on the macrocycle not only affects the strength of binding, but also induces dimerization of the macrocycle. Unlike aromatic porphyrins, the anti-aromatic isophlorins have electron deficient core and rich electron density at the periphery of the macrocycle. Prior to this work, there were no reports on non-covalent and covalent reactivity of this unique property of π system. This is mainly attributed to the limited number of stable and planar anti-aromatic isophlorins known to date. This thesis describes the synthesis and non-covalent interactions between the anti-aromatic π surface of stable and planar *meso* free isophlorins and the fullerene C_{60}. The limited reactivity of the *meso* free carbons led to design the first covalent anti-aromatic dimer through a possible diradical intermediate. This unstable diradical isophlorin dimer could be stabilized with a diradical character upon expanding the macrocyclic skeleton to an expanded isophlorin through a systematic synthetic methodology. The products obtained from various reactions have been characterized unambiguously through experimental and computational studies. Quantum mechanical calculations were also employed for the better understanding aromatic and anti-aromatic characteristics of these molecules. The results of this research have been described in four chapters.

The first chapter describes the importance of non-covalent interactions in the construction of self-assembled/co-assembled architectures. The π-π interactions play a major role with planar and nonplanar π-conjugated systems in heterogeneous as-well-as homogeneous assembly. Particularly, it highlights the literature reports on synthesis and characterization of porphyrin-C_{60} covalent and non-covalent complexes which also includes the effect of *meso* substitution on non-covalent interaction. The prelude

to this thesis defines the first ever attempts to explore the possibility of 4nπ systems as synthons for supramolecular chemistry. It originated from the idea to explore the planar π surface of anti-aromatic molecules for non-covalent interactions. It can be expected that such planar isophlorins can exhibit non-covalent interactions with fullerene, in a fashion similar to that observed for porphyrins. Further, the first ever attempts to synthesize a covalent dimer of an isophlorin and expanded isophlorin described in this thesis.

Chapter 2 describes the molecular complexes of fullerene with *meso*-substituted anti-aromatic isophlorin were obtained and successfully characterized by single crystal X-ray diffraction studies. The close contacts between fullerenes and isophlorin arise from a favorable van der Waals attraction of the curved π surface of a fullerene towards the anti-aromatic π surface of isophlorin. These values are much shorter than C_{60} and porphyrin assembly. The non-covalent interaction between isophlorin and fullerene was confirmed in solution state by ITC and variable temperature NMR studies. These results strongly favoured the formation of 1:1 complex in solution state in support of the non-covalent interaction between the 20π anti-aromatic tetraoxa isophlorin surface and the curved π surface of C_{60}. The estimated binding constants confirmed moderate interaction between the isophlorins and C_{60} in the solution state. These studies suggest that, anti-aromatic characteristics of a π surface can be as good as aromatic surfaces for binding fullerenes. Isophlorin can bind C_{60}-fullerene through conventional π-π contacts, highlighting the utility of isophlorin as a synthon for supramolecular chemistry.

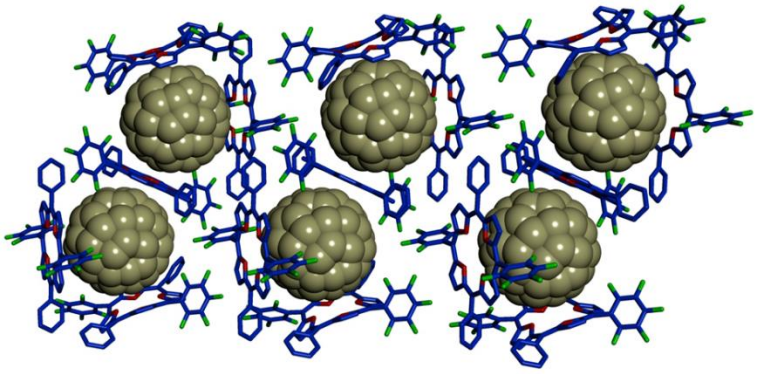

Synopsis

Chapter 3 describes the role of *meso* substituents in isophlorins in binding the C_{60} fullerene. Less number of substituents enhanced the binding strength as observed from mass spectrometry, NMR and ITC titrations. At the same time, the reactivity of *meso* free isophlorins has also been explored for the first time. It appears that *meso* unsubstituted isophlorins are very reactive and perhaps leads to reactive radical species. In this process, the first synthesis of a covalent dimer of an anti-aromatic molecule was discovered serendipitously. All attempts to dimerize *meso* free isophlorins into *meso-meso* link dimer, in a fashion similar to the dimerization of *meso* free porphyrin, went futile. It is apparent that conventional oxidative coupling reactions may not be successful with 4nπ systems and novel methodologies need to be explored for their functionalization. In this process, an alternative procedure was developed to synthesize the *meso*, *meso* linked tetraoxa isophlorin dimer.

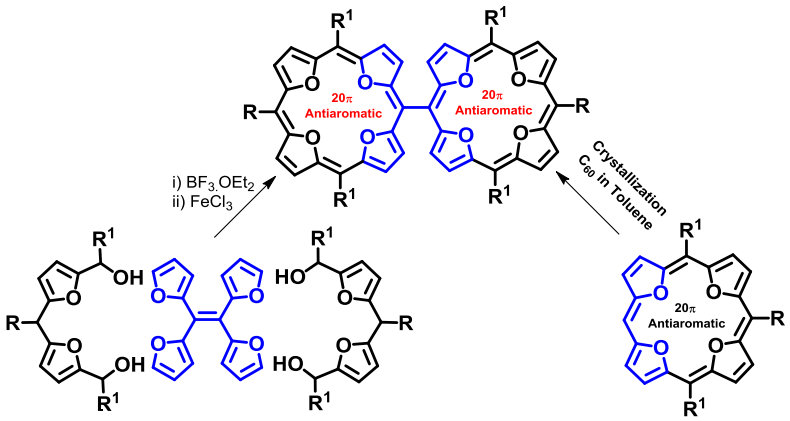

Chapter 4 describes the bicyclic expanded isophlorin obtained from a one-pot synthesis which was characterized to have a stable singlet diradical character. The molecular structure was confirmed by single crystal X-ray diffraction analysis. The ESR and SQUID measurements confirmed that macrocycle existed in a singlet diradical form (open shell configuration) instead of closed shell. The energy gap between singlet (S_0) and triplet (T_1) states was determined to be 0.3113 k.cal./mol. Such small ΔE_{S-T} value allows the facile thermal excitation to the higher energy triplet diradical state. The two symmetrical 22π aromatic cores are only possible when the two diradicals are accommodated in the naphthalene ring. The NICS and AICD

calculations also support that two symmetrical 22π aromatic cores with open shell biradical system could be the most possible structure.

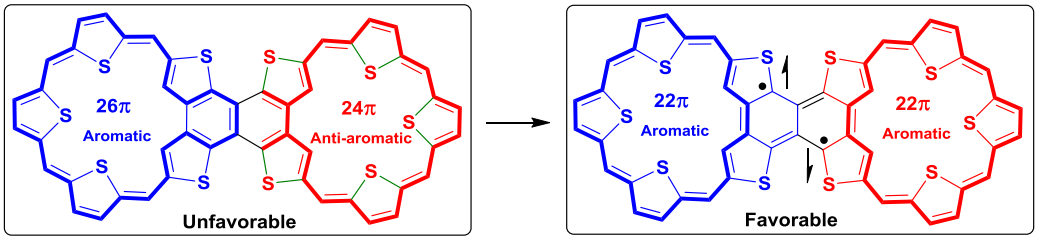

These observations suggest that, the molecule may not exist with the combination of both aromatic and anti-aromatic closed shell property; instead it could exist in a stable aromatic-aromatic delocalized open shell property. To date, there are no examples of direct fusion between aromatic and anti-aromatic sub-units. This molecule represents one such unexplored situation that tries to understand the electronics of fusing anti-aromatic behaviour with aromaticity. It can be foreseen that such covalent interactions predominantly support aromatization leading the formation of a stable biradical.

Publications

- **Baddigam Kiran Reddy**, Santosh C. Gadekar, and V. G. Anand, *Chem. Commun.*, **2016**, *52*, 3007-3009. The synthesis and characterization of the *meso-meso* linked anti-aromatic tetraoxa isophlorin dimer.
- **Baddigam Kiran Reddy**, Santosh C. Gadekar, and V. G. Anand, *Chem. Commun.*, **2015**, *51*, 8276-8279. Non-covalent composites of anti-aromatic isophlorin–fullerene.

Chapter 1

Role of Non-covalent Interactions in the Design of Supramolecular Architectures

I.1. Supramolecular Chemistry

Supramolecular chemistry involves the synthesis of complex chemical systems employing non-covalent interactions between molecules, rather than synthesis of molecules with covalent bonds.[1] A supramolecular system is a well-organized complex entity that can be created from association of two or more chemical species held together by non-covalent interactions. Invariably, supramolecular chemistry involves the chemistry of multiple non-covalent bonds.

I.2. Non-covalent interactions

Non-covalent interaction differs from a covalent interaction in that it does not involve the sharing of electrons, but instead involves more dispersed variations of electronic interactions between molecules, or within a molecule which can be either attractive or repulsive in nature. These interactions are of fundamental importance in chemistry, materials and biology. Molecular recognition through intermolecular bonds is a remarkable concept that originated from non-covalent interactions. Nature has clearly selected several non-covalent interactions, over the too strong covalent bonds, which is ubiquitous in protein folding, drug design, self-assembled materials, separation technologies, *etc*.

I.3. Classification of Non-covalent Interactions

The non-covalent interactions can be classified[2] as:

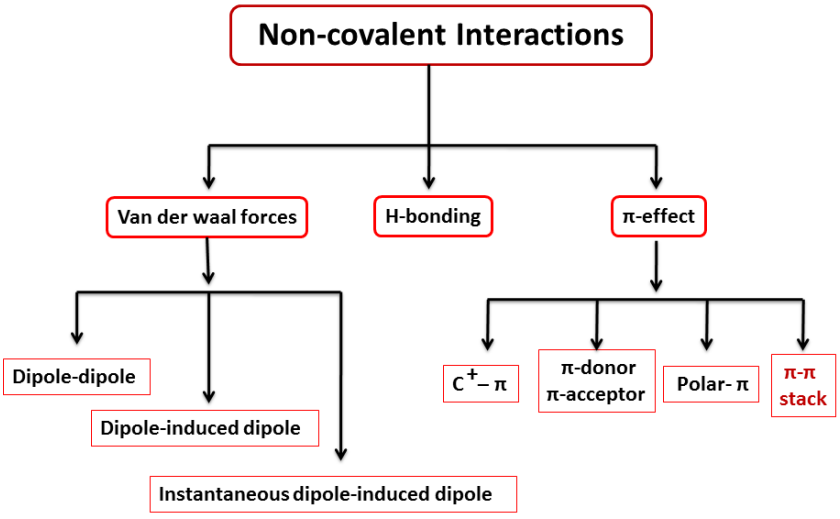

I.3.1. Intermolecular Forces

Intermolecular forces are predominantly considered to be attractive forces that occur between molecules. They are weaker than either ionic or covalent forces. However, the varying strengths of different types of intermolecular forces are responsible for formation of molecular complexes, self-assembled structures and physical properties of molecular compounds such as melting and boiling points. Amongst all the non-covalent interactions, Van der Waals force is the weakest intermolecular force consisting of dipole-dipole forces and dispersion forces.

I.3.1.a. Dipole-dipole interactions

Dipole-dipole forces are the attractive forces that occur among polar molecules (Figure 1.1). For example, a molecule of acetone has a partially positive carbonyl carbon atom and a partially negative oxygen atom. A collection of many acetone molecules will align themselves so that the oppositely charged regions of neighbouring molecules are near each other.

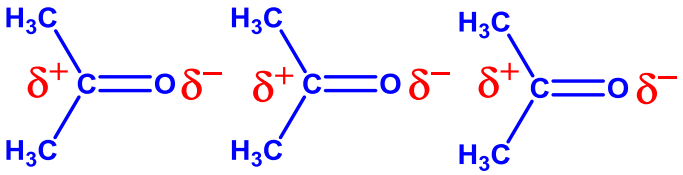

Figure 1.1. Acetone molecules aligned according to attractions of their partially positive regions and partially negative regions (dipole-dipole interactions).

I.3.1.b. Dipole-induced dipole forces

The electrostatic attraction resulting when a permanent dipole (polar molecule) gets close to temporary dipole (non-polar molecule) is called dipole-induced dipole interaction. For example, a solution of oxygen in water, the water molecule causes (induces) a temporary dipole in the oxygen molecule due to the closer proximity of oxygen to the polar water molecule. This induced dipole is temporary and forms only when the two molecules are extremely close to one another. This attraction is called a dipole-induced dipole attraction, because the dipole (the polar molecule) induces or causes the non-polar particle to behave as a dipole.

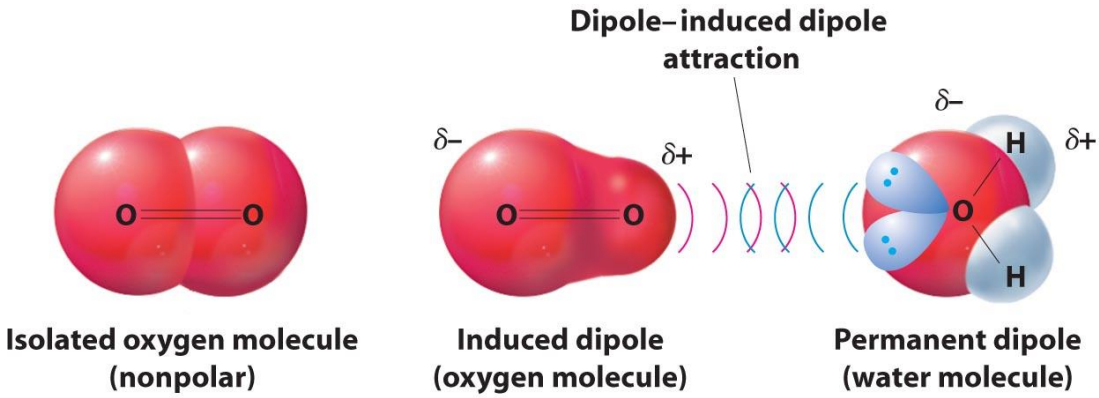

Figure 1.2. Permanent dipole of water molecule creates induced dipole in the neighbouring non-polar oxygen molecule. (Copyright© 2007 Pearson Education Inc., publishing as Pearson Addsion Wesley.)

I.3.1.c. Instantaneous dipole-induced dipole forces (London dispersion forces)

The electrostatic attraction between temporary dipoles is called dispersion forces. These are also considered a type of van der Waals force and are the weakest of all intermolecular forces. They are often called as London forces. London dispersion forces are intermolecular forces that occur between all atoms and molecules due to the random motion of electrons. An important landmark in the history of understanding these attracting forces is represented by the liquefaction of helium in experiments by Kamerlingh-Onnes.[48] Existence of liquid helium provides the most conclusive argument about the existence of attractive intermolecular forces acting between small spherical rare gas atoms such as helium (Figure 1.3), not bearing any charge or permanent electric multipole moment.

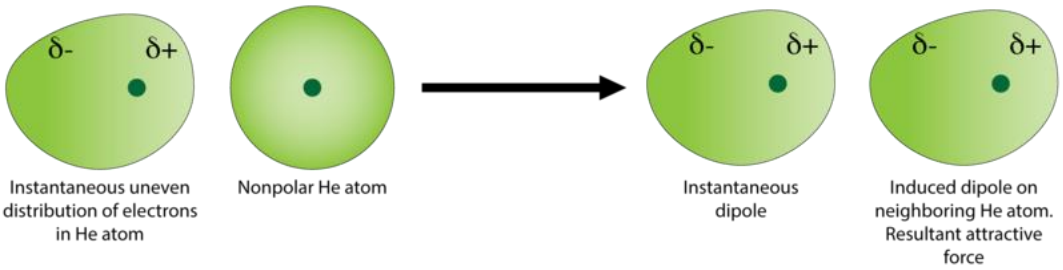

Figure 1.3. Fluctuation in the electron density of a helium atom results in instantaneous dipole which creates an induced dipoles in neighbouring helium molecules[3] (Image reproduced from Wikipedia).

The electron cloud of a helium atom contains two electrons, and, when averaged over time, these electrons will distribute themselves evenly around the nucleus. However, at any given moment, the electron distribution may be uneven, resulting in

an instantaneous dipole. This weak and temporary dipole can subsequently influence neighbouring helium atoms through electrostatic attraction and repulsion. The instantaneous and induced dipoles are weakly attracted to one another. The strength of dispersion forces increases as the total number of electrons in the atoms or non-polar molecules increases. These temporary dipoles change constantly, but the net result of their existence is to produce attractive forces between non-polar molecules.

I.3.1.d. Hydrogen bond

Hydrogen bond is an electrostatic attractive interaction between a hydrogen atom from a molecule or a molecular fragment XH in which X is more electronegative than H, and an atom or a group of atoms in the same or a different molecule, in which there is evidence of bond formation.[4] These hydrogen-bond attractions can occur between molecules (intermolecular) or within different parts of a single molecule (intramolecular).

Inter-molecular hydrogen bonding

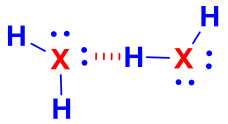

X = O

Intra-molecular hydrogen bonding

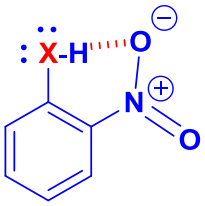

I.3.1.e. Cation-π interaction

Cation–π interaction[5] is a non-covalent interaction between the face of an electron-rich π system (*ex:* benzene, ethylene, acetylene) and cation (e.g. Li^+, Na^+).

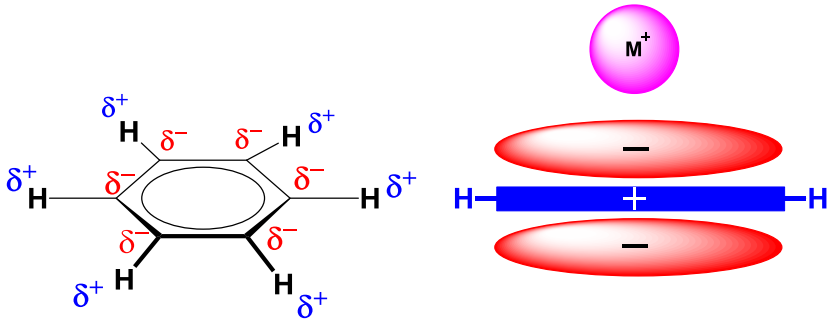

Figure 1.4. Schematic representation of cation-π interaction.[5]

Table 1. Experimental Measurements of Gas-Phase Ion Molecule Binding Energies[6]

Ion M^+	Molecule	Binding Energy kcal/mol
Li^+	C_6H_6	38.3
Na^+	C_6H_6	20.0
K^+	C_6H_6	19.2

I.3.1.f. Polar-π interaction

Apart from interactions between individual atoms of independent molecules, interactions between charged species and a neutral molecule is also observed. Either an anion or cation can interact with electron rich species with delocalized π-electrons density. Polar-π interaction involves interaction of a polar molecule and quadrupole moment of π system. The permanent dipoles of polar molecule interact with π surface of the aromatic ring.[7]

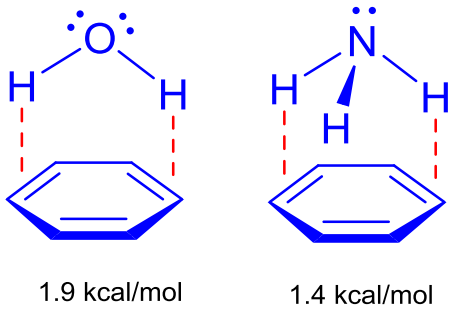

I.3.1.g. Donor-Acceptor π interactions

A donor-acceptor interaction occurs between two molecules with respect to a low energy empty orbital (acceptor) and high energy filled orbital (donor). The basic requirement for good donor is its low ionization potential and the acceptor should have high electron affinity.

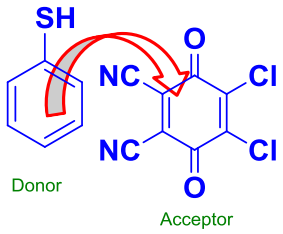

Figure 1.5. Charge transfer complex between electron rich thiol (donor) and electron deficient DDQ (acceptor) molecules.[8]

I.3.1.h. π–π stacking

Non-covalent interactions between neutral molecules are very common amongst aromatic units. A non-covalent attractive force between delocalized π-systems in which the interplanar distance varies between 3.3 and 3.8 Å is usually referred to as π-stacking.[9]

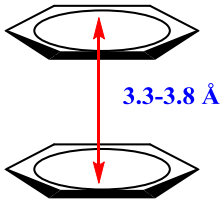

When the aromatic rings face each other, the overlap of π-electron orbitals results in an energetic gain. Alignment of positive electrostatic potential on one ring with negative electrostatic potential on another ring forms an offset stack in pure benzene[10] π–π interactions occur between aromatic rings, and these sometimes provide important contributions to molecular recognition. For example, the double-strand structure of DNA is partially stabilized through π–π interactions between neighbouring base-pairs.[11] The π–π interactions also play a key role in designing self-assembled architectures,[12] binding properties of polyaromatic macrocycles,[13] complexation in many host-guest systems,[14] porphyrin aggregations[15] and functional nanomaterials.[16]

For example, consider benzene dimer, there will be three possibilities to interact with each other.

- Face-to-face or sandwich π-stacking
- Point to face or T-shaped π- interaction
- Offset or Slipped sandwich π-stacking

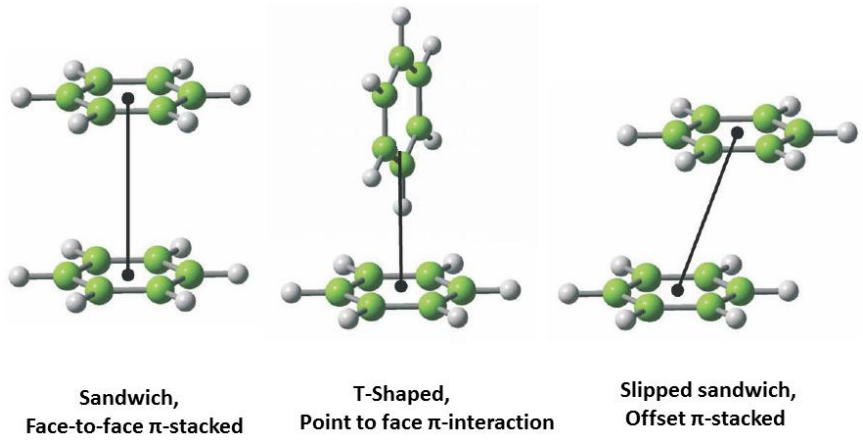

Figure 1.6. Possible orientation of π–π interactions in benzene dimer.[17]

The benzene dimer shows either slipped sandwich π-stacking or T-shaped C-H π-interaction.[17] It will not exhibit face-to-face or sandwich π-stacking because of the repulsions between π electrons. Benzene and hexafluorobenzene displayed face-to-face or sandwich type of π-stacking due to complimentary quadrupole moments. The combination of two liquids, benzene and hexafluorobenzene produces an intimate 1:1 solid complex in which the basic short range order is a face-to-face stack.[18] The driving force for this specific mixing comes from the quadrupole moment and van der Waals surface of benzene and hexafluorobenzene.

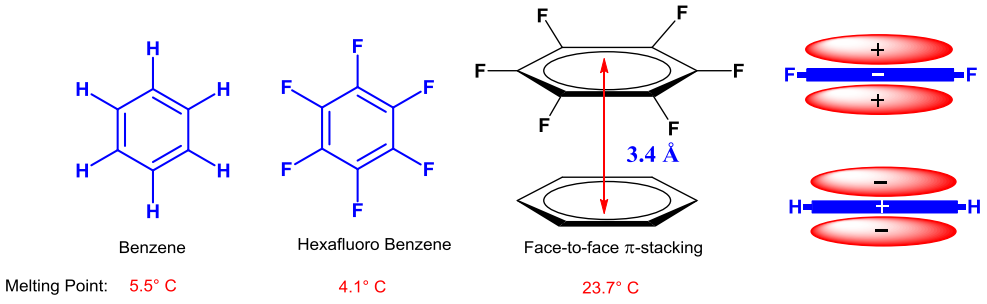

Figure 1.7. π–π interactions between benzene and hexafluorobenzene.[18]

These π–π interactions are not only limited for planar π-systems, but they can exist even in non-planar π systems also. Based on literature, π–π interactions can be classified into three types.

(i) Flat *vs.* Flat π-π interaction

(ii) Concave-convex π-π interaction

(iii) Flat *vs* Curved π-π interaction

(i) Flat *vs*. Flat π-π interaction

Strong attractive interactions between π-systems have been known for over half a century. Majority of the π–π interactions studied till date are predominantly based on planar delocalized π-systems. Such interactions are not limited only to π-rich systems. π-deficient systems can also interact with electron rich akin to electrostatic interactions. A 1:1 complex of *sym*-triphenylbenzene and *sym*-tris(perfluoro phenethynyl)benzene displays face-to-face π–π stacking.[19] The pure compound **1** melted at 142-146 °C (visual inspection), 144 °C (differential scanning calorimetry DSC) while **1-F$_{15}$** was found to melt at 199-201 °C (visual inspection), 201 °C (differential scanning calorimetry (DSC)). Equimolar amounts of **1** and **1-F$_{15}$** recrystallized from *n*-hexane/dicloromethane yielded cocrystals of **1**: **1-F$_{15}$**. The melting point of these cocrystals were higher than either of the two pure compounds (235-239 °C, visual inspection; 239 °C, DSC). The sharp and the higher melting point of the mixture indicated that a solid compound had formed and it was inferred that unusual phenyl/perfluorophenyl interaction was involved, in there cocrystals.

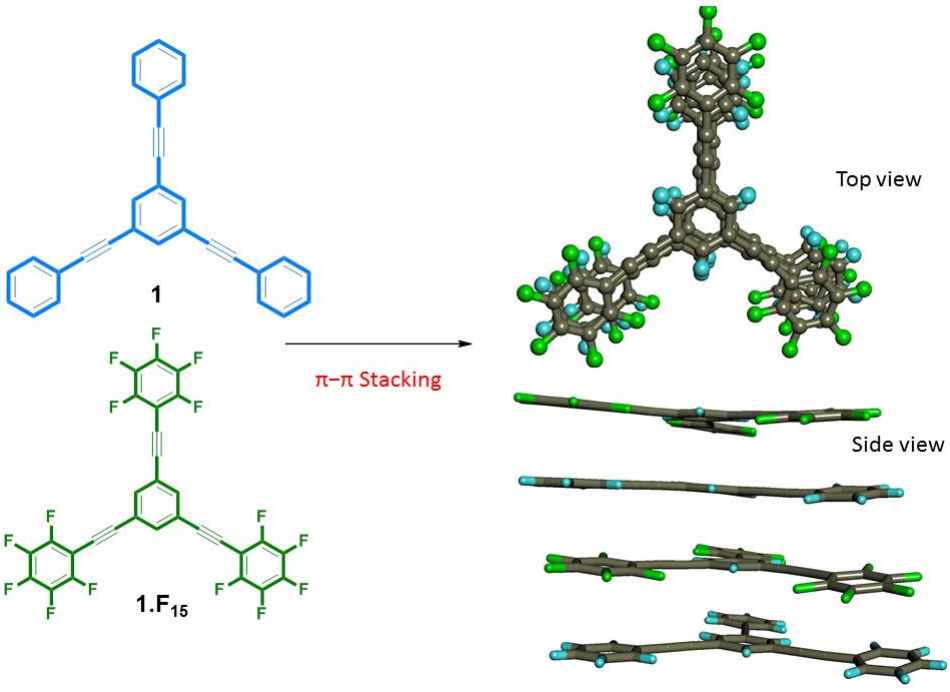

Figure 1.8. π–π interactions between**1** and **1.F$_{15}$**.[19]

Large delocalized aromatic π systems like porphyrins also exhibit π–π interaction. The aromatic 18π system of zinc diphenyl porphyrin displayed slipped sandwich type of π–π stacking in its crystal packing. The interplanar distance between the two planar π surfaces was found to be 3.65 Å.[20]

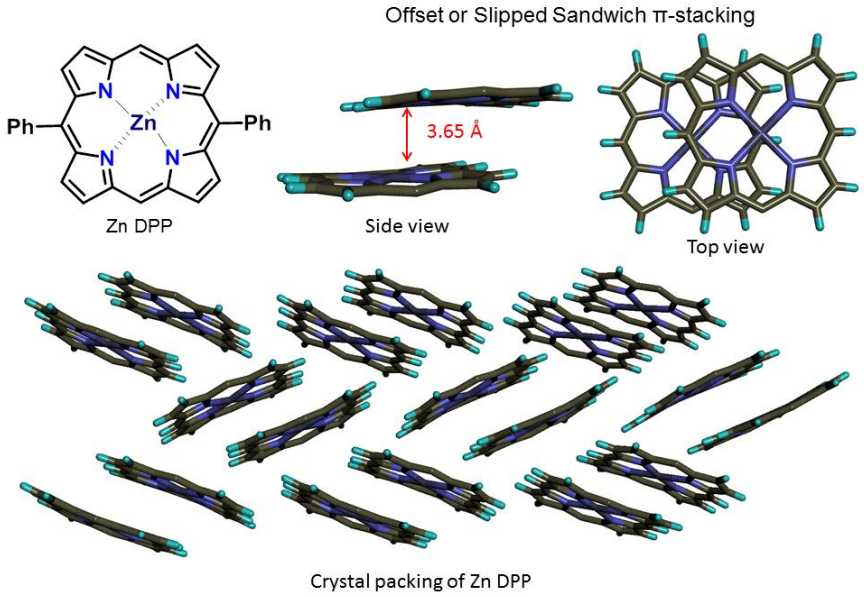

Figure 1.9. Crystal packing of Zn DPP showed strong π–π interaction.[20]

(ii) Concave-convex π-π interaction

The strength of the π–π interaction is essentially a function of the surface area of contact and the polarizability of electron shells. A larger surface area invariably enhances the non-covalent interaction between the molecules. The bowl-shaped polycyclic aromatic hydrocarbons with carbon networks related to fullerenes appear to be ideal candidates for molecular receptors with the ability to recognize curved-surface fullerene cages through concave-convex "ball-and-socket" π-π interactions.[21]

Pentacene functionalized fullerene derivatives also exhibit concave−convex π–π interactions. The intermolecular short contact distances of 3.1 and 3.2 Å have been observed from single crystal X-ray diffraction analysis.[23]

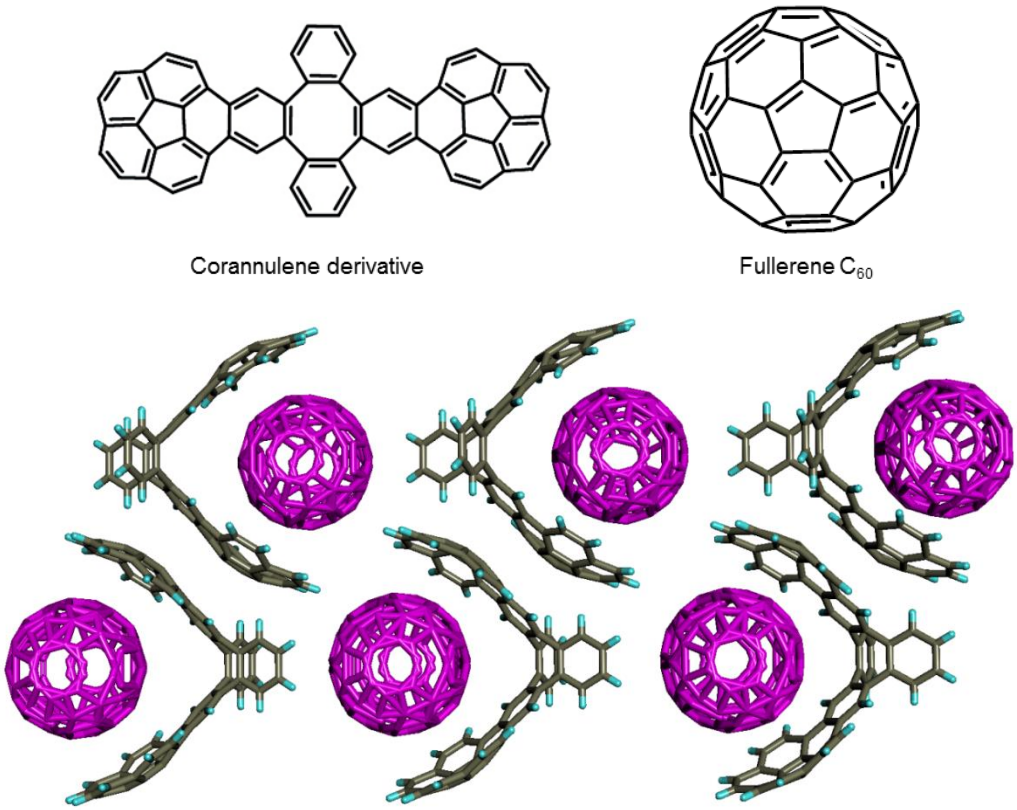

Figure 1.10. X-ray crystal structure determination of inclusion complex formed by attractive concave−convex π−π interactions between fullerene and corannulene derivative.[22]

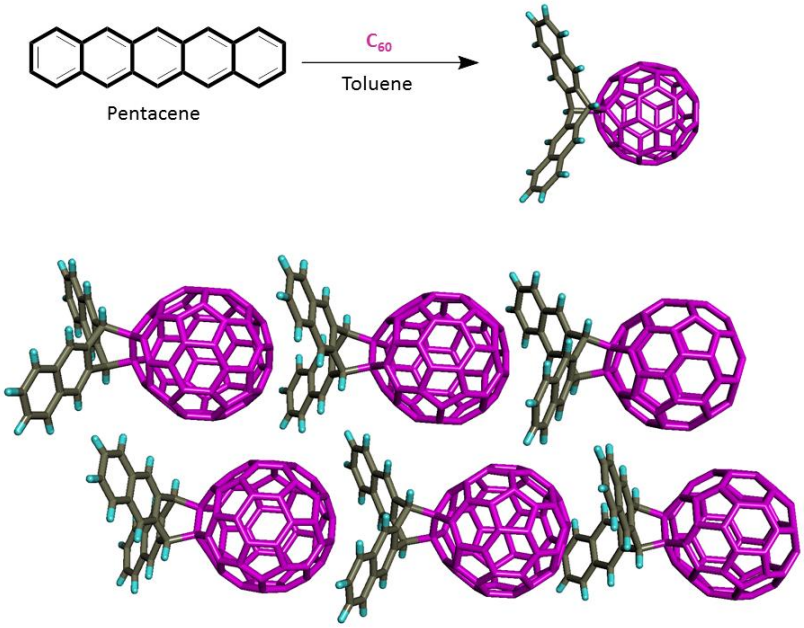

Figure 1.11. Molecular packing of pentacene functionalized fullerene derivative.[23]

(iii) Flat *vs* Curved π-π interaction

Porphyrin and fullerene π system belong to this class of interaction. The porphyrins large and flat planar aromatic π-surface is ideal to encourage π-π interaction with the curved π surface of the fullerene. The fullerene carbon atom to the centre of the neighbouring tetraphenylporphyrin plane was found to be separated by a distance of 2.75 Å, which was notably shorter than familiar π-π interactions.[24]

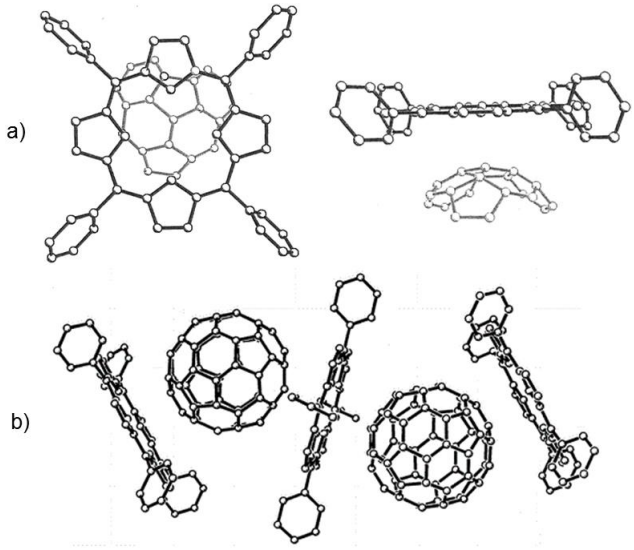

Figure I.12. (a) 6:6 ring junction oriented at the centre of the H_2TPP (b). Zig-zag arrangement of porphyrin H_2TPP/C_{60} chain.[24]

I.4. Chemistry of C_{60} Fullerene

Fullerene C_{60} is an allotrope of carbon with spheroid geometry.[25] It was discovered for the first time in 1985 by a group of scientists including Richard Smalley, Robert Curl and Harry Kroto. The structure of the C_{60} is a combination of 12 pentagonal and 20 hexagonal rings, forming a spheroid shape. Figure 1.13 shows the structure of the molecule, which reveals how the pentagonal rings sit at the vertices of an icosahedron such that no two pentagonal rings are next to each other. The localization of the double bonds at the edges of the hexagons can be investigated. These bonds are named [6,6] bonds. Their length of 1.36 Å is significantly shorter than the 1.47 Å of the [5,6] bonds between pentagons and hexagons which is shown in Figure 1.13.

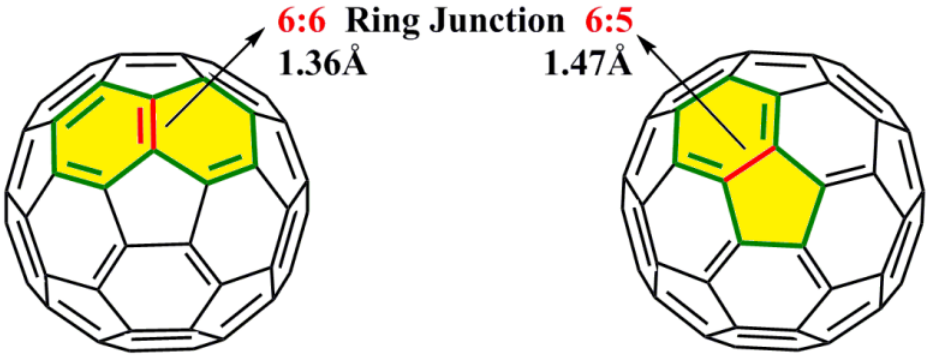

Figure 1.13. Schematic representation of fullerene C_{60} with the lengths of the two different bonds in the molecule.

Due to these alternant double bonds and the high electron affinity, C_{60} is not considered as an aromatic but it behaves as an electron deficient polyolefin. The Buckminster fullerene C_{60} exhibits I_h symmetry like a regular soccer ball. Each carbon atom in C_{60} is identical as concluded from the ^{13}C NMR spectrum which displayed only a single peak at δ 143.2 ppm.[47] C_{60} exhibits reversible reduction up to six electrons. This high electron affinity results from the presence of triply-degenerate low-lying LUMO's (lowest unoccupied molecular orbital). Oxidation of the molecule has also been observed; but, oxidation found to be irreversible. The high electron-affinity nature of C_{60} makes it the best acceptor component currently available. Fullerenes also show important non-covalent van der Waal's interaction due to the delocalised π electron density across its outer curved π surface. This leads to self-aggregation and attractive interactions with large planar π surface of porphyrins. Cocrystallates of fullerenes with a wide range of compounds have been reported, including with porphyrins,[26] and planar electron-rich molecules such as thiafulvalenes.[27] A weak charge transfer interactions between π-electron deficient fullerenes and π-electron rich molecules is a key observation in the complex formation. Large macrocyclic compounds such as calix[n]arenes[28] have also been shown to encapsulate fullerenes, and this encapsulation has been used in selective extraction of specific fullerenes from mixtures of fullerenes.[29] Fullerenes are now a well-established subject of research in many areas of chemistry. Fullerene chemistry plays a noticeable role in fields, such as supramolecular chemistry, nanotechnology and materials chemistry.[21]

I.5. Porphyrin-Fullerene π–π interaction

Conjugated π-molecules such as fullerenes and porphyrins with tunable electronic properties are appealing building blocks for the construction of functional materials with exceptional electrochemical and photophysical properties. The self-assembly of porphyrins and C_{60} is chiefly driven by π-π interactions and are widely explored topic of research. There are a large number of molecular structures of simple porphyrins with C_{60} organized by π-π interactions and dispersion forces. The close attractive interaction of a fullerene and a porphyrin was first recognized in the molecular packing of a crystal structure containing a covalent fullerene-porphyrin conjugate.[30] Later, many examples of the attractive interaction between the planar π surface of porphyrins and the curved π surface of fullerenes have been documented in the literature. One such example shows close interaction of tetraphenylporphyrin with C_{60} in the solid state with a porphyrin mean plane-fullerene distance of 2.72 Å.[24] This is supported by molecular modelling studies which suggest that this interaction is largely due to van der Waals forces. These interactions not only exist in the solid state, but observed even in solution state studies also. This was confirmed by the upfield shifts in ^{1}H NMR spectra of porphyrins and ^{13}C NMR spectra of fullerenes.[24] In addition to the observed π-π interactions, an attractive interaction between the electropositive centre of the porphyrin and the electron-rich 6:6 ring junction of the fullerene is observed in crystal structures, with the 6:6 ring junction being centred over the centre of the porphyrin.

I.6. Effects of *meso*-substituents on Porphyrin in C_{60} Binding and Molecular packing

The substituents on *meso*-position of a porphyrin are known to modulate the strength of the interaction between the porphyrin and the fullerene,[24,31] depending on whether the orientation of the substituents is favourable for interaction with the fullerene. However, porphyrin-fullerene interactions occur without requirement for additional recognition elements. Some representative examples are described further.

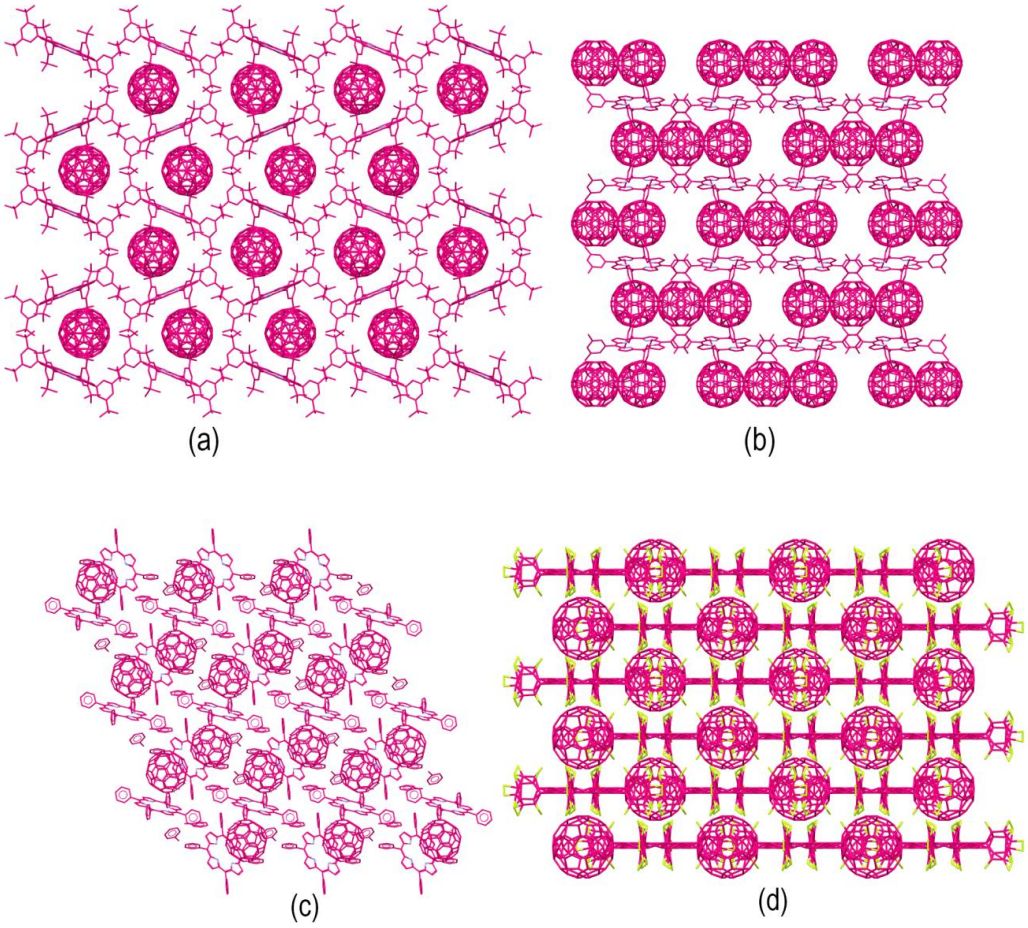

Figure 1.14. Molecular packing of $H_2T_{3,5\text{-dibutyl}}PP.C_{60}$ (a), $H_2T_{3,5\text{-dimethyl}}PP.C_{60}$ (b) $H_2TPP.C_{60}$ (c) and $H_2TPFPP{\cdot}C_{60}$ (d) complexes.[24,31]

H_2TPFPP-C_{60}, Porphyrin Sheets: The crystals were grown in *p*-xylene solvent by slow evaporation of 1:1 solutions of H_2TPFPP and C_{60} at room temperature. Figure 1.15 shows the familiar porphyrin/fullerene supramolecular assembly in an alternating columnar stack. The fullerene oriented on porphyrin with its closest C atom to the mean 24-atom plane at distances of 2.65 and 2.71 Å.[24] These short contact distances, suggested that the electron withdrawing effect of the pentafluorophenyl substituents on the porphyrin enhance the binding with C_{60}. On the other hand, the 6:6 ring juncture "double" bonds (electron rich site) of fullerene approach over centre of the porphyrin (electron deficient site). The 6:6 approach is more common than the 6:5 consistent with maximization of electron density in the π–π interaction.

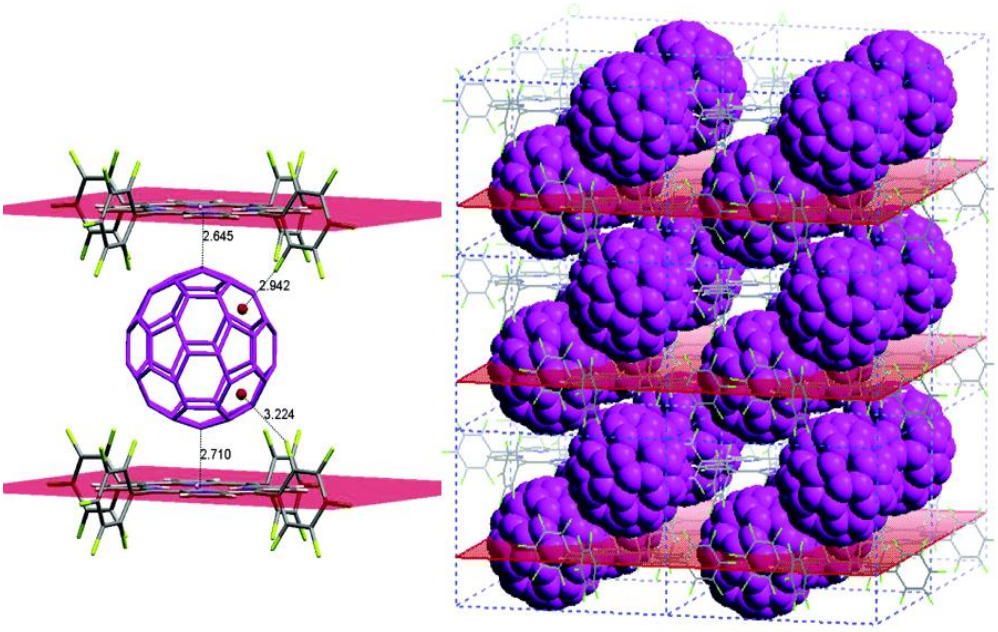

Figure 1.15. a) Close approach of C_{60} to centre of the porphyrin, and *ortho* F atoms to the centres of the fullerene six-membered rings in $H_2TPFPP \cdot C_{60}$,. b) Alternating layered porphyrin sheets (stick model) separated by C_{60} molecules (space filling) in $H_2TPFPP \cdot C_{60}$.[31]

To complete the description of the crystal packing of H_2TPFPP-C_{60} (Figure 1.14d), it can best described as two interpenetrating identical sets of tetragonally stacked porphyrin layers with fullerene pillars resulting in alternating layered sheet structure as shown in Figure 1.15. The separation of porphyrin layer to layer was found to be 12.26 Å.

$3H_2TPFPP$-$2C_{60}$, Porphyrin Prisms: When the solvent was changed from *p*-xylene to toluene, a 1:1 complex of C_{60} and H_2TPFPP couldn't be observed. Rather, the stoichiometry was three porphyrins and two fullerenes with trigonal prismatic arrangement molecular packing. There are close approaches of one mean (24 atoms) porphyrin plane with the 6:6 ring (2.78, 2.86 Å) and 6:5 ring junctions to rest of the two porphyrins (2.78, 2.89, 2.88, 2.99 Å). To make up the complete structure, the molecules projected (Figure 1.16) in a 2D honeycomb are repeated along the perpendicular 3-fold axes such that the inter-fullerene spacing is quite large (> 7.7 Å).

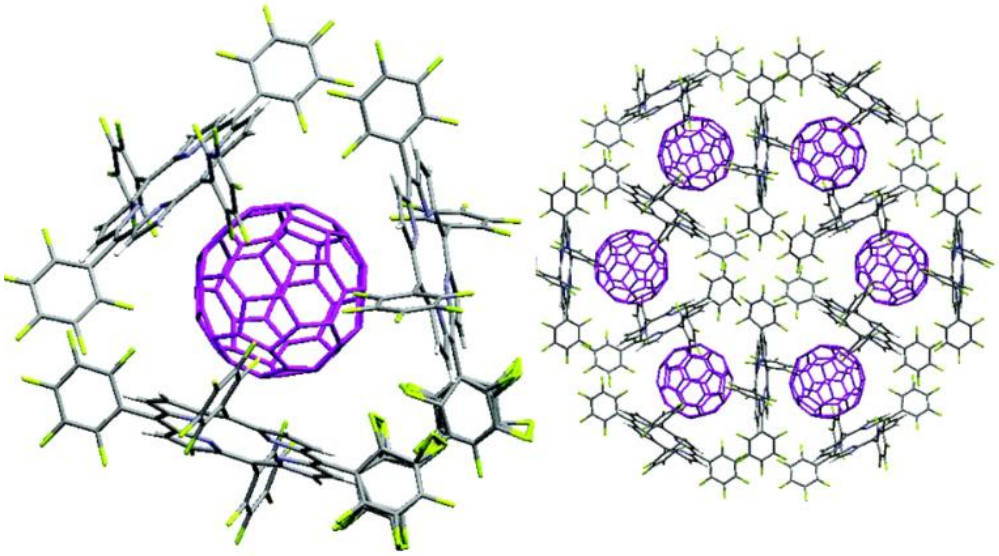

Figure 1.16. a) Prismatic arrangement of three $(H_2TPFPP)_3$:$2C_{60}$ complex. b) The 2D honeycomb arrangement of fullerenes and porphyrins.[31]

Table 2. The intermolecular short contacts in molecular complexes of $H_2TPP.C_{60}$, $H_2T_{3,5\text{-dibutyl}}PP.C_{60}$, $H_2T_{3,5\text{-dimethyl}}PP.C_{60}$ and $H_2TPFPP{\cdot}C_{60}$. [24,31]

Complex	Porphyrin plane-Fullerene distances (Å)	Porphyrin-Porphyrin angle (deg)	Fullerene-Fullerene Contact
$H_2T_{3,5\text{-dibutyl}}PP.C_{60}$	2.69, 2.83, 2.88, 2.97	45.3	0.0
$H_2T_{3,5\text{-dimethyl}}PP.C_{60}$	2.71, 2.72, 2.87, 2.92	31.6	3.59
$H_2TPP.C_{60}$	2.75, 2.72, 2.79, 2.99	45.2	3.37
$H_2TPFPP{\cdot}C_{60}$	2.65, 2.71, 2.74, 2.80	0.0	0.0

All the above literature results suggested that electron withdrawing and electron donating substituents at *meso* position of the porphyrin shows different binding interactions and molecular packing with fullerene C_{60}. The aromatic solvents also play a key role in the molecular packing.

I.7. Radical Reactions of Fullerene C_{60}

Apart from the utility of fullerenes and supramolecular synthons, the chemistry of these spheroids has been explored extensively. The discovery of fullerenes, species as electron deficient polyalkenes with weakly conjugated double bonds, has opened novel opportunities for the radical chemistry. A great number of weakly conjugated

double bonds in fullerenes make them reactive toward different radicals. The photoreduction of acetophenone, benzophenone, or acetone in the presence of various alcohols (*i.e.*, 2-propanol) have been investigated.[32] The *tert*-butoxyradical or the photoexcited carbonyl group of the various ketones, respectively, abstracts a hydrogen atom from the alcohols and subsequent formation of $H^{\bullet}C_{60}$ is the result of a sequential electron/proton transfer reaction.

$$R_1\,R_2\dot{C}(OH) + {}^1C_{60} / {}^3C_{60} \rightarrow [R_1\,R_2\,C^{+}(OH) + \dot{C}_{60}^{-}] \rightarrow R_1\,R_2CO + H\dot{C}_{60}$$

$$H\dot{C}_{60} + H\dot{C}_{60} \rightarrow (C_{60}H)_2$$

In the above mentioned reaction, $R_1R_2\dot{C}(OH)$ is derived from activated alcohol or photoreduced ketone in the first or second method, respectively. Moreover, similar to the alkyl fullerenyl radical analogues ($R\dot{C}_{60}$),[33] $H\dot{C}_{60}$ tends to dimerize to form$(C_{60}H)_2$.[34]

Fluorination on C_{60}

Fluorination of C_{60} with fluorine gas produces fluorofullerene with a different number of fluorines depending on the time of fluorination at 275 °C. The maximum number of fluorines is 48.[35]

$$C_{60} \xrightarrow[275\ ^{\circ}C]{F_2\ gas} C_{60}F_{48}$$

Chlorination on C_{60}

Chlorination of C_{60} by chlorine gas at 250° gives an orange product indicated by chlorine uptake to be $C_{60}Cl_{24}$.[36]

$$C_{60} \xrightarrow[250\ ^{\circ}C]{Cl_2\ gas} C_{60}Cl_{24}$$

I.8. Catalytic activity of fullerene C_{60}

A recent report claimed that fullerene is a non-metal catalyst for molecular activation of hydrogen, and that its catalytic activity is comparable to that of a noble metal catalyst.[37] The hydrogenation of aromatic nitro compounds to amino aromatics is achieved on this catalyst with high yield and selectivity under 1 atmospheric pressure of H_2 and light irradiation at room temperature. More interestingly, there exists a cooperative effect between C_{60} and C_{60}^{-}. At C_{60}:C_{60}^{-} 2:1 ratio, ~100% conversion and ~100% selectivity is achieved under conditions of 120-160 °C and 4-5 MPa of H_2 pressure without light irradiation.

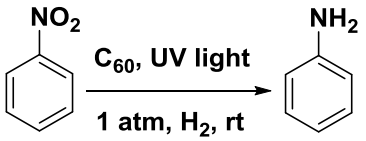

Scheme 1.1. Hydrogenation of nitrobenzene to aniline under light irradiation with fullerene catalyst at room temperature[38]

The catalytic performance is comparable with that of the noble metal catalyst. Fullerene is an excellent hydrogenation catalyst not only for nitrobenzene but also for aromatic nitro compounds such as 4-nitrobenzonitrile, 4-nitroacetophenone and 4-chloronitrobenzene. Based on these results, it can be conjectured that electronically excited C_{60} or C_{70}, H_2 and nitrobenzene form a synergistic exciplex, which activates the H_2 molecule and achieves transfer of hydrogen atoms to the nitro group to form aniline.

I.9. Applications of porphyrin-C_{60} Assembly

Based on the structural observation of fullerene-porphyrin complexes, its interaction had been proposed as the basis for selectivity in fullerene chromatography using zinc porphyrin-appended silica stationary phases.[39] Long retention times are associated with larger-sized fullerenes, consistent with greater π–π contact areas. Columns of porphyrin-appended silica are also superior for the separation of endohedral metallo-fullerenes such as Ln.C_{82}.[29] Very recently, cyclic porphyrin dimers have been shown to selectively extract higher fullerenes.[40] Porphyrin-

fullerene materials can form long-lived charge-separated states; they represent an excellent system for components of organic electronics and photoactive devices. Recent literature has shown that the combination of more than one specifically designed non-covalent interaction can increase the stability and prevent the degradation of order of the molecules in the material.[41]

I.10. Outline of this Thesis:

Isophlorin

Predominantly π-interactions are observed with aromatic molecules. Even though anti-aromatic molecules have similar π framework, they are seldom employed in supramolecular chemistry due to the perceived unstable nature of the 4nπ systems. Cyclobutadiene and cyclooctatetraene are the simplest of the anti-aromatic systems to explore the chemistry of 4nπ systems. A much larger framework of 20π electrons, referred to as Isophlorin (N, N'-dihydroporphyrin, **I.1**) was first hypothesized by Woodward[42] as a intermediate during the synthesis of chlorophyll. It was proposed that the cyclo condensation of four pyrrole units with aldehyde proceeded from the formation of porphyrinogen, **I.2**, to porphyrin, **I.3**, through the formation of isophlorin intermediate.

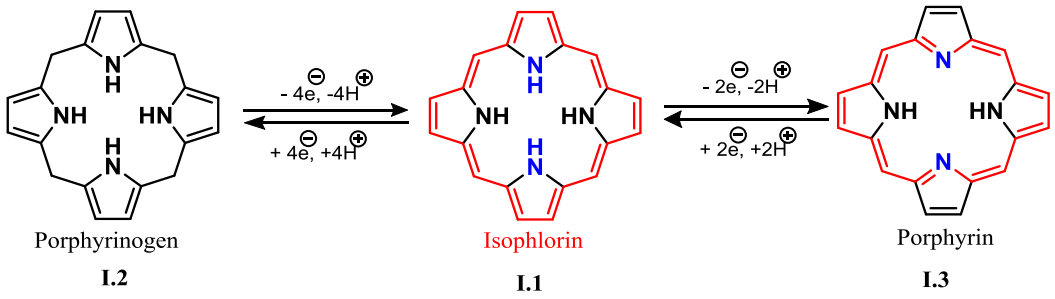

Scheme 1.2. Synthesis of porphyrin

Even though half a century ago Woodward hypothesized this anti-aromatic macrocycle, it still remains a synthetic challenge for chemists to stabilize the tetra-pyrrolic isophlorin, due to its high susceptibility for oxidation to 18π aromatic porphyrin, which makes its isolation rather difficult. This macrocycle signifies the anti-aromatic character of a porphyrin-like macrocycle. In addition, the pyrrole NH

also plays a key role in the proton-coupled two-electron oxidation of isophlorin to the aromatic porphyrin.

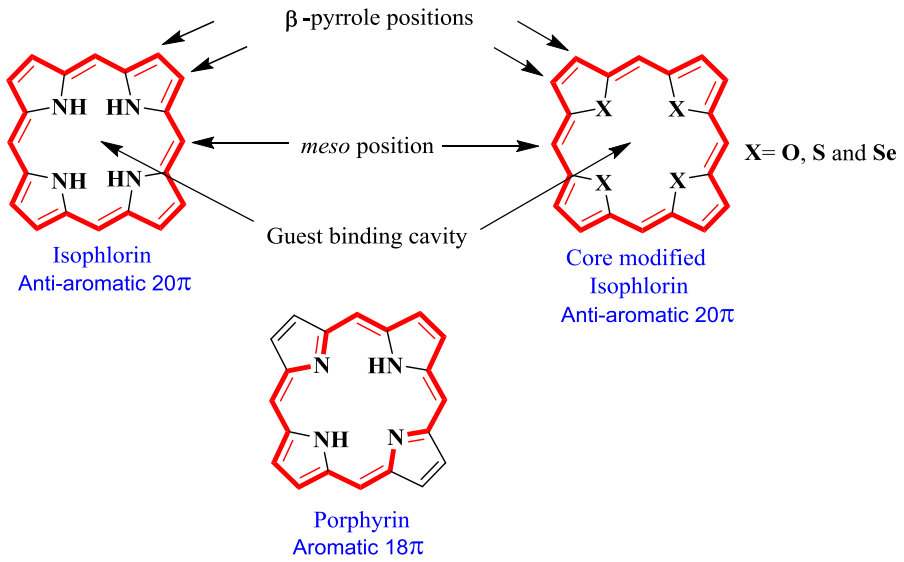

Figure 1.17. The basic difference between isophlorin and core modified isophlorin and porphyrin; Key substitution positions also shown; Red color indicates path of conjugation.

However, a major aspect of its unstable nature was attributed to its anti-aromatic character, which is understood to destabilize the macrocycle upon conjugation. Anti-aromaticity in general has not gained significant attention mainly due to the lack of stable 4nπ systems. Isophlorin or core modified Isophlorins are planar or near-planar macrocyclic compounds containing four five-membered hetero cyclic rings linked with methene groups and the conjugation flows through the carbon framework. The resulting electronic properties of the 20π macrocycles are different from the structurally similar porphyrin. There have been significant contributions in the design and synthesis of this anti-aromatic macrocycle. Vogel and co-workers pioneered rational synthetic strategies for 20π isophlorins.[43] Pyrrole was replaced by structurally similar heterocycles such as furan/thiophene/selenophene to prevent the proton-coupled electron transfer process which can oxidize the 20π to 18π macrocycle.

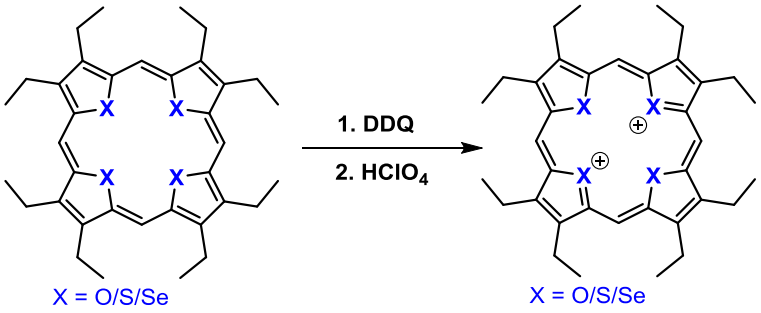

Initially, Vogel and co-workers were successful in the synthesis of tetra-(thia/oxa/selena) isophlorins with β-alkyl substituted heterocycles. These macrocycles underwent irreversible ring oxidation to the 18π porphyrin dication indicating the unstable nature of the 20π systems.[43]

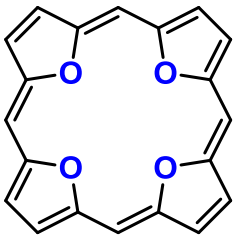

Later, the same group synthesized the tetraoxa isophlorin without any substituents on the furan rings and the *meso*-carbon atoms of the macrocycle.[43] It displayed remarkable up-field chemical shifts for the furan β-protons and the *meso*-protons in the ^{1}H NMR spectrum to confirm paratropic ring current effects as expected of 4nπ macrocycles. Finally tetraoxa isophlorin was isolated as air sensitive black crystals (could be stored at -78 °C).

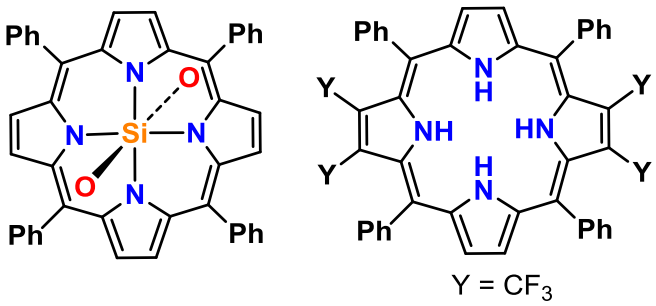

Vaid and co-workers[44] exploited the complexation of group (IV) elements such as silicon by stabilizing its +4 oxidation state through covalent bonds between silicon

and all the four nitrogens of the pyrrole. In an alternate synthetic route, Chen and co-workers[45] employed conditions strong enough to reduce a Cu(II) complex of porphyrin to 20π isophlorin. It represents one of the rare reactions to expose the possibility of reducing a tetrapyrrolic porphyrin to anti-aromatic isophlorin. All these reports conclude a common observation of unstable nature for the isophlorins under ambient conditions.

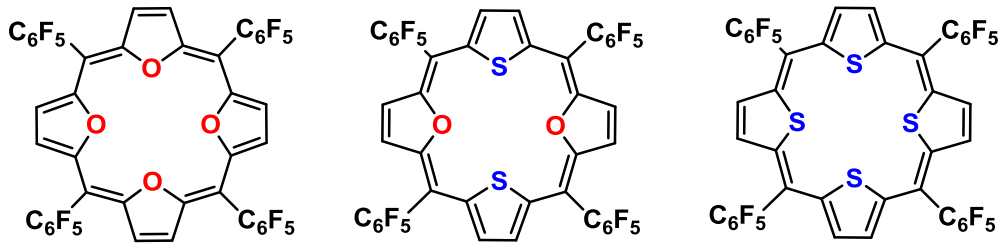

Scheme 1.3: Structural representation of stable isophlorins

Later on, Anand and co-workers[46] synthesized stable core-modified 20π isophlorins by introducing electron withdrawing pentafluorophenyl substituents on *meso* positions of the macrocycle. The robust chemical stability was further confirmed by their resistance to be oxidized to 18π porphyrin dication with strong oxidizing agents.

This thesis describes the first ever attempts to explore the possibility of 4nπ systems as synthons for supramolecular chemistry. It originated from the idea to explore the planar π surface of anti-aromatic molecules for non-covalent interactions. It can be expected that such planar isophlorins can exhibit non-covalent interactions with fullerene, in a fashion similar to that observed for porphyrins. Further, the first ever attempts to synthesize a covalent dimer of an isophlorin and expanded isophlorin will be described in this thesis.

1.11 References

[1] Lehn, J. M. Supramolecular Chemistry Concepts and Perspectives; VCH: New York, 1995.

[2] Vögtle, F. Suparmolecular Chemistry; John Wiley & Sons: New York, 1991.

[3] J. O. Hirschfelder, C. F. Curtiss and R. B. Bird, Molecular Theory of Gases and Liquids, Wiley, New York, 1954.

[4] E. Arunan, R. Desiraju Gautam, A. Klein Roger, J. Sadlej, S. Scheiner, I. Alkorta, C. Clary David, H. Crabtree Robert, J. Dannenberg Joseph, P. Hobza, G. Kjaergaard Henrik, C. Legon Anthony, B. Mennucci, J. Nesbitt David, in *Pure and Applied Chemistry, Vol. 83*, **2011**, p. 1619.

[5] D. A. Dougherty, *Science* **1996**, *271*, 163.

[6] J. C. Ma, D. A. Dougherty, *Chemical Reviews* **1997**, *97*, 1303.

[7] K. P. Gierszal, J. G. Davis, M. D. Hands, D. S. Wilcox, L. V. Slipchenko, D. Ben-Amotz, *The Journal of Physical Chemistry Letters* **2011**, *2*, 2930.

[8] P. Kalimuthu, A. Sivanesan, S. A. John, *The Journal of Physical Chemistry A* **2007**, *111*, 12086.

[9] C. Janiak, *Journal of the Chemical Society, Dalton Transactions* **2000**, 3885.

[10] C. A. Hunter, J. K. M. Sanders, *Journal of the American Chemical Society* **1990**, *112*, 5525.

[11] C. A. Hunter, X.-J. Lu, *Journal of Molecular Biology* **1997**, *265*, 603.

[12] P. D. W. Boyd, C. A. Reed, *Accounts of Chemical Research* **2005**, *38*, 235

[13] C. A. Hunter, P. Leighton, J. K. M. Sanders, *Journal of the Chemical Society, Perkin Transactions 1* **1989**, 547.

[14] B. Askew, P. Ballester, C. Buhr, K. S. Jeong, S. Jones, K. Parris, K. Williams, J. Rebek, *Journal of the American Chemical Society* **1989**, *111*, 1082; b) T. J. Shepodd, M. A. Petti, D. A. Dougherty, *Journal of the American Chemical Society* **1988**, *110*, 1983

[15] A. E. Alexander, *Journal of the Chemical Society (Resumed)* **1937**, 1813.

[16] V. Georgakilas, F. Pellarini, M. Prato, D. M. Guldi, M. Melle-Franco, F. Zerbetto, *Proceedings of the National Academy of Sciences* **2002**, *99*, 5075.

[17] M. O. Sinnokrot, E. F. Valeev, C. D. Sherrill, *Journal of the American Chemical Society* **2002**, *124*, 10887.

[18] C. R. Patrick, G. S. Prosser, *Nature* **1960**, *187*, 1021.

[19] F. Ponzini, R. Zagha, K. Hardcastle, J. S. Siegel, *Angewandte Chemie International Edition* **2000**, *39*, 2323.

[20] A. D. Bond, N. Feeder, J. E. Redman, S. J. Teat, J. K. M. Sanders, *Crystal Growth & Design* **2002**, *2*, 27.

[21] T. Kawase, H. Kurata, *Chemical Reviews* **2006**, *106*, 5250.

[22] A. Sygula, F. R. Fronczek, R. Sygula, P. W. Rabideau, M. M. Olmstead, *Journal of the American Chemical Society* **2007**, *129*, 3842.

[23] G. P. Miller, J. Briggs, J. Mack, P. A. Lord, M. M. Olmstead, A. L. Balch, *Organic Letters* **2003**, *5*, 4199.

[24] P. D. W. Boyd, M. C. Hodgson, C. E. F. Rickard, A. G. Oliver, L. Chaker, P. J. Brothers, R. D. Bolskar, F. S. Tham, C. A. Reed, *Journal of the American Chemical Society* **1999**, *121*, 10487.

[25] W. J. Anton, R. W. Stephen, I. S. David , Biological Applications of Fullerenes. New York City, NY: ElsevierScience, **1996**.

[26] L. Sánchez, N. Martín, D. M. Guldi, *Angewandte Chemie International Edition* **2005**, *44*, 5374.

[27] TTF Chemistry: Fundamentals and Applications of Tetrathiafulvalene, J. Yamada and T. Sugimoto (eds); Kodansha-Springer, (2004).

[28] (a) J. L. Atwood, G. A. Koutsantonis and C. L. Raston, *Nature*, 1994, **368**, 229- 231; (b) T. Suzuki, K. Nakashima and S. Shinkai, *Chem. Lett.*, 1994, 699-702

[29] Xiao, J.; Savina, M. R.; Martin, G. B.; Francis, A. H.; Meyerhoff, M. E. Efficient HPLC Purification of Endohedral Metallofullerenes on a Porphyrin-Silica Stationary Phase. J. Am. Chem. Soc. **1994**, 116, 9341-9342.

[30] Y. Sun, T. Drovetskaya, R. D. Bolskar, R. Bau, P. D. W. Boyd, C. A. Reed, *The Journal of Organic Chemistry* **1997**, *62*, 3642.

[31] A. Hosseini, M. C. Hodgson, F. S. Tham, C. A. Reed, P. D. W. Boyd, *Crystal Growth & Design* **2006**, *6*, 397.

[32] R. Klemt, E. Roduner, H. Fischer, *Chemical Physics Letters* **1994**, *229*, 524.

[33] J. R. Morton, K. F. Preston, P. J. Krusic, S. A. Hill, E. Wasserman, *Journal of the American Chemical Society* **1992**, *114*, 5454.

[34] a) J. R. Morton, K. F. Preston, P. J. Krusic, E. Wasserman, *Journal of the Chemical Society, Perkin Transactions 2* **1992**, 1425; b) T. Tanaka, K. Komatsu, *Journal of the Chemical Society, Perkin Transactions 1* **1999**, 1671.

[35] P. B. Shevlin, *Journal of the American Chemical Society* **2000**, *122*, 4846.

[36] G. A. Olah, I. Bucsi, C. Lambert, R. Aniszfeld, N. J. Trivedi, D. K. Sensharma, G. K. S. Prakash, *Journal of the American Chemical Society* **1991**, *113*, 9385.

[37] B. Li, Z. Xu, *Journal of the American Chemical Society* **2009**, *131*, 16380.

[38] B. Li, Z. Xu, *Journal of the American Chemical Society* **2009**, *131*, 16380.

[39] J. Xiao, M. R. Savina, G. B. Martin, A. H. Francis, M. E. Meyerhoff, *Journal of the American Chemical Society* **1994**, *116*, 9341.

[40] Y. Shoji, K. Tashiro, T. Aida, *Journal of the American Chemical Society* **2004**, *126*, 6570.

[41] a) H. Sato, K. Tashiro, H. Shinmori, A. Osuka, Y. Murata, K. Komatsu, T. Aida, *Journal of the American Chemical Society* **2005**, *127*, 13086; b) M. Yanagisawa, K. Tashiro, M. Yamasaki, T. Aida, *Journal of the American Chemical Society* **2007**, *129*, 11912.

[42] R. B. Woodward, *Angewandte Chemie* **1960**, *72*, 651.

[43] a) E. Vogel, in *Pure and Applied Chemistry, Vol. 65*, **1993**, p. 143; b) E. Vogel, P. Röhrig, M. Sicken, B. Knipp, A. Herrmann, M. Pohl, H. Schmickler, J. Lex, *Angewandte Chemie International Edition in English* **1989**, *28*, 1651.

[44] J. A. Cissell, T. P. Vaid, A. L. Rheingold, *Journal of the American Chemical Society* **2005**, *127*, 12212.

[45] C. Liu, D. -M. Shen, Q. -Y. Chen, *Journal of the American Chemical Society* **2007**, *129*, 5814.

[46] J. S. Reddy, V. G. Anand, *Journal of the American Chemical Society* **2008**, *130*, 3718.

[47]. Taylor, R.; Hare, J. P.; Abdul-Sada, A. K.; Kroto, H, W. *J. Chem. Soc. Chem. Comm*. **1990**, 1423

[48]. H. Kamerlingh Onnes, The liquefaction of helium., in: KNAW, Proceedings, 11, 1908-1909, Amsterdam, **1909**, pp. 168-185

Chapter 2

Supramolecular Fullerene-Isophlorin Architectures

II.1. Introduction to Porphyrin - Fullerene Systems

The curved π surface of fullerene has attracted significant attention in the synthesis of heterogeneous self-assembled architectures. It was discovered that fullerene and calixarene can form molecular complex through non-covalent interaction.[1] Their binding was found to be dependent on the size of the spheroids interacting with the macrocyclic hosts. Boyd and co-workers[2] were the first to obtain X-ray crystallographic evidence of a close interaction between porphyrin and C_{60} in a covalently linked porphyrin-fullerene dyad (**1**, Figure 2.1). Later, it was also observed that molecules with a flat surface such as porphyrin or its metal derivatives possessing a π plane could harbor the curved π surface of fullerene. The 2.75 Å approach of a fullerene carbon atom to the centre of the neighboring porphyrin plane was shorter than the separations of familiar π-π interactions.

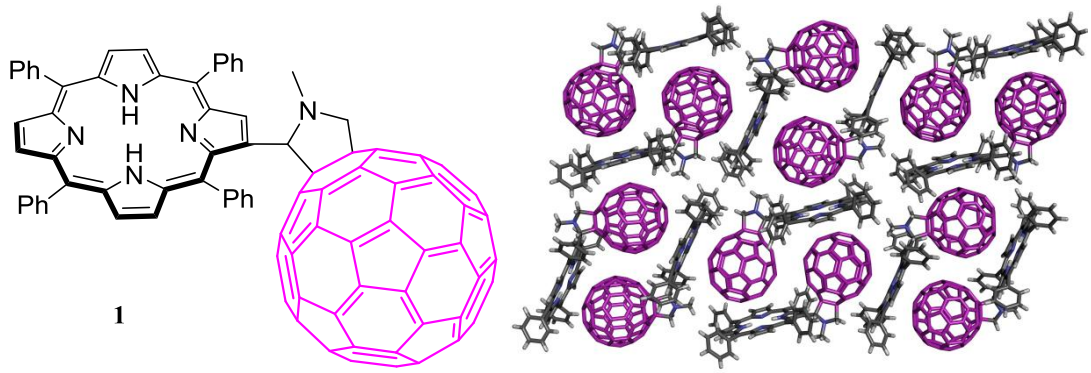

Figure 2.1. A covalently linked dyad **1** with a close porphyrin-fullerene assembly in the X-ray crystal structure.[2]

This intermolecular interaction between two dissimilar π systems is largely attributed to the van der Waals dispersion forces. Similarly, other planar systems also have the ability to form a non-covalent complex with the π surface of fullerene.[3] Even though π –π interaction is common between fullerene and flat molecules, the shape of these assemblies can be either non-linear or in the form of columnar stacks. A variety of hosts have been designed, synthesized and explored to bind the C_{60} spheroid.[4] In this context, the unique aromatic character of fullerene is a topic of intense discussion.[5] Small aromatic sub-units such as benzene, pyrrole, and thiophene[6] are a common feature of all such hosts that favour close contacts with C_{60}. However, π- surface is not unique only to aromatic systems, since anti-aromatic

and non-aromatic units also possess π bonds. In this context there are no significant reports on the ability of fullerene to interact with uncommon π-surfaces. Therefore, is aromaticity the only driving force to attract fullerene towards a planar π-surface? Unlike its interaction with aromatic molecules, it is rare to observe the binding of fullerene to anti-aromatic hosts. But, 4nπ systems are also understood to be pretty unstable in nature and not even a handfull of stable anti-aromatic molecules are available to explore its chemistry. Unlike cyclobutadiene and cyclooctatetraene, only core-modified isophlorins appear to be stable analogues of 4nπ systems. The parent Isophlorin,[7] **2**, is an unstable 20π anti-aromatic tetrapyrrolic macrocycle with a structural resemblance to porphyrin, **3** (Figure 2.2). Nonetheless, its furan/thiophene derivatives are stable under ambient conditions and sustain a planar π-surface very similar to that of a porphyrin.[8]

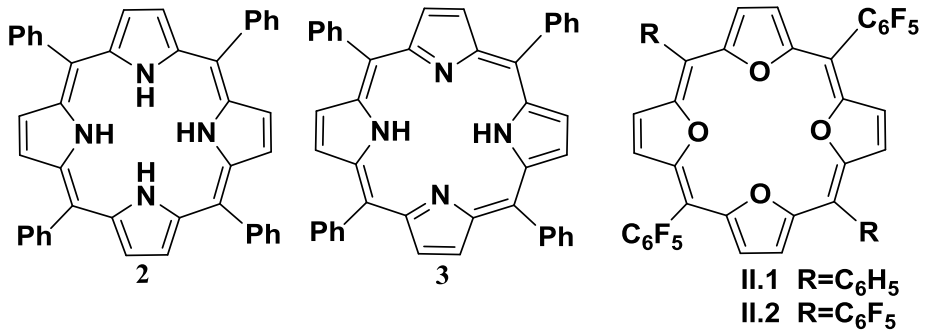

Figure 2.2. 20π anti-aromatic isophlorins (**2**), 18π aromatic porphyrin (**3**) and 20π anti-aromatic tetraoxa isophlorin (**II.2**).

They represent ideal examples to explore the interaction of fullerene with a 4nπ macrocyclic host. In addition, isophlorins do not exhibit π stacking which can favour better interaction with guest molecules. In this chapter the discrete nature of fullerene-isophlorin interaction along with the structural characterization of these non-covalent complexes will be described.

II.2. Synthesis of Anti-aromatic Isophlorin Hosts

meso-Substituents on the porphyrin ring provide cooperative effects in the binding of fullerene C_{60}. In this context, two different tetraoxa isophlorins, **II.1** and **II.2**, were employed by varying the substituents on the *meso*-carbon atoms. The

tetraoxa isophlorins **II.1** and **II.2** were synthesized by acid catalyzed reactions of suitable precursors, followed by oxidation (Scheme 2.1).

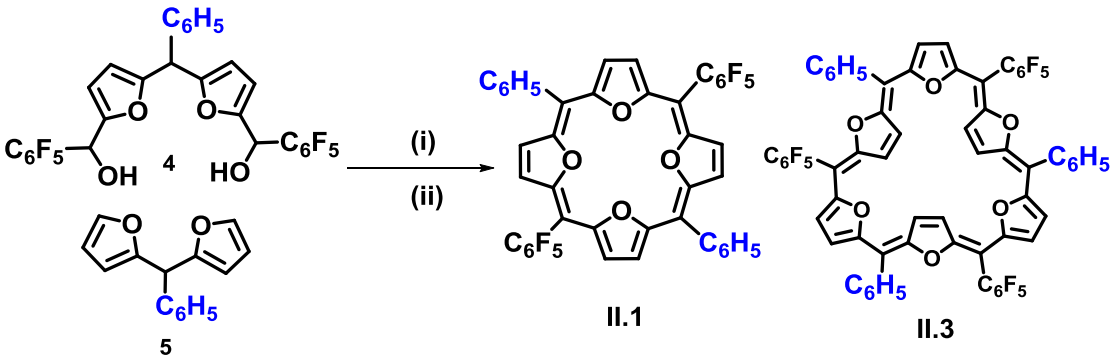

Scheme 2.1. Acid catalysed synthesis of 20π tetraoxa isophlorins **II.1**
Reaction conditions: (i) $BF_3.OEt_2$ (1 eq.), dry DCM (100 ml), rt, N_2, 2h (ii) $FeCl_3$ (5 eq.), 2h.

In a process similar to modified Rothemund type synthesis[9] (Scheme-2.1), *meso*-phenyl difuromethane dicarbinol, **4,** was condensed with the corresponding difuromethane **5**, under acidic conditions. An equimolar concentration of dicarbinol, **4,** and *meso*- phenyldifuromethane,[9c] **5**, was dissolved in 100 ml dry dichloromethane and degassed with Argon for ten minutes. Then, a catalytic amount of boron trifluoride diethyl etherate ($BF_3.OEt_2$) was added under dark. After stirring for two hours, five equivalents of $FeCl_3$ were added and stirring continued for an additional two hours. Apart from the expected product, a larger macrocycle was also detected in the MALDI-TOF mass spectrum of the reaction mixture. Then, few drops of triethyl amine were added and the resultant solution was passed through a short basic alumina column. This mixture was concentrated and further purified by size exclusion chromatography with Bio-Beads S-X1 (BIO-RAD) and toluene as a eluent. A yellowish green color band obtained was identified as **II.1** in 2.5% yield and pink color band identified as **II.3** in 5% yield. Their composition and structural details were confirmed by various spectroscopic techniques as described below.

II.3. Spectral Characterization of Isophlorins

The isophlorins **II.1** and **II.3** were analyzed through high resolution mass spectrometry, UV-Vis, NMR spectroscopy, and X-ray Crystallography.

II.3.1. Electronic Absorption Studies

The synthesized isophlorins **II.1** and **II.3** displayed green and pink color solutions respectively when dissolved in common organic solvents. The color of the solution is attributed to the extensive conjugation. **II.1** has a high energy absorption at 328 nm (ε = 83900) and 368 nm (ε =102300) followed by low energy absorptions in the region 400-500 nm. The higher analog **II.3** has absorption at 566 nm (ε =75049).

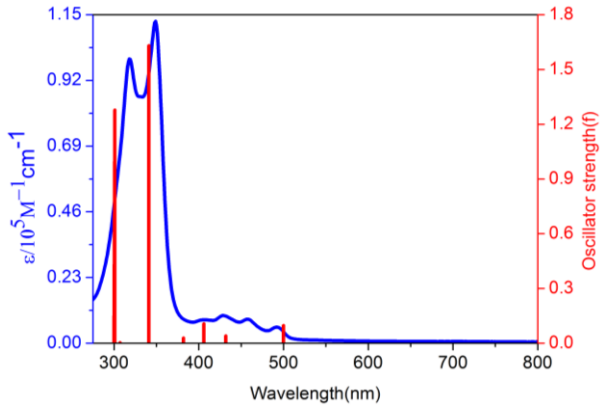

Figure 2.3. The steady state absorption spectra (blue line-experimental) of **II.1** recorded in CH_2Cl_2 along with the theoretical vertical excitation energies (red bar-theoretical) obtained from TD-DFT calculations carried out at the B3LYP/6-31G(d,p) level.

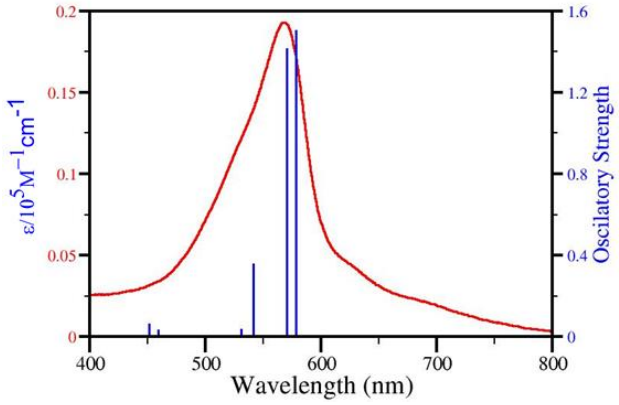

Figure 2.4. The steady state absorption spectra (red line-experimental) of **II.3** recorded in CH_2Cl_2 along with the theoretical vertical excitation energies (blue bar-theoretical) obtained from TD-DFT calculations carried out at the B3LYP/6-31G(d,p) level.

II.3.2. NMR Characterization

The ^{1}H NMR spectrum of **II.1** confirmed the paratropic ring current effects for a 4nπ anti-aromatic system arising from 20π electrons conjugated pathway and **II.3** confirmed the diatropic ring current effects for a (4n+2)π aromatic system because of

the 30π electrons along its conjugated pathway. Macrocycle **II.1** exhibited two doublets for the β hydrogens of furan at δ 2.53 and 2.17 ppm, and multiplets were observed for the *meso* substituted phenyl protons at δ 6.61 – 6.30 ppm, indicating strong paratropic ring current effects due to effective delocalization of the π electrons (Figure 2.5). Such high upfield shifts for β-hydrogens of the heterocyclic subunits are as expected for anti-aromatic systems. These values are in good agreement with the earlier reports.[10,8b]

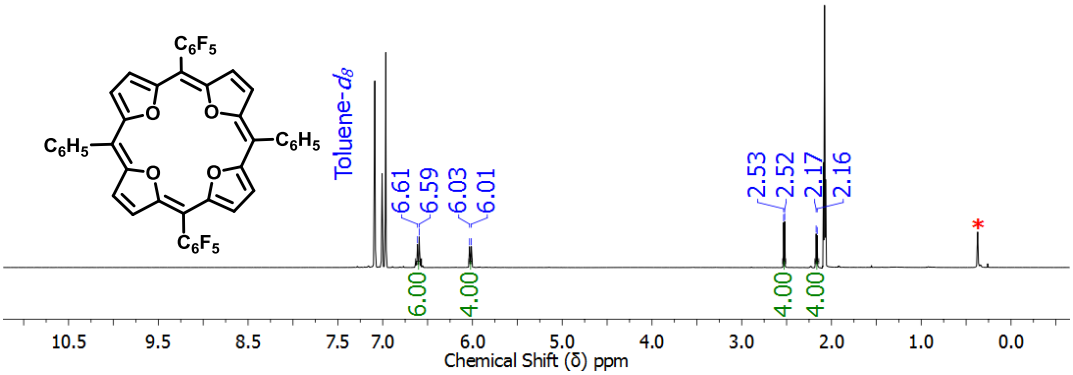

Figure 2.5. ^{1}H NMR of **II.1** in Toluene-d_8 at 298*K* (* H_20).

Compound **II.3** displayed four doublets in its room temperature ^{1}H NMR spectrum for β-hydrogens of furan. Of these, two doublets were observed in the upfield region at δ 2.31–2.20 ppm and the remaining two doublets resonated downfield at δ 8.27 and 7.89 ppm. The phenyl protons on the *meso*-carbon atoms were identified as multiplets in the region δ 8.10–7.54 ppm (Figure 2.6). This spectrum was suggestive of a C_3 symmetry in solution state with diatropic ring current effects and a near planar conformation for the macrocycle.

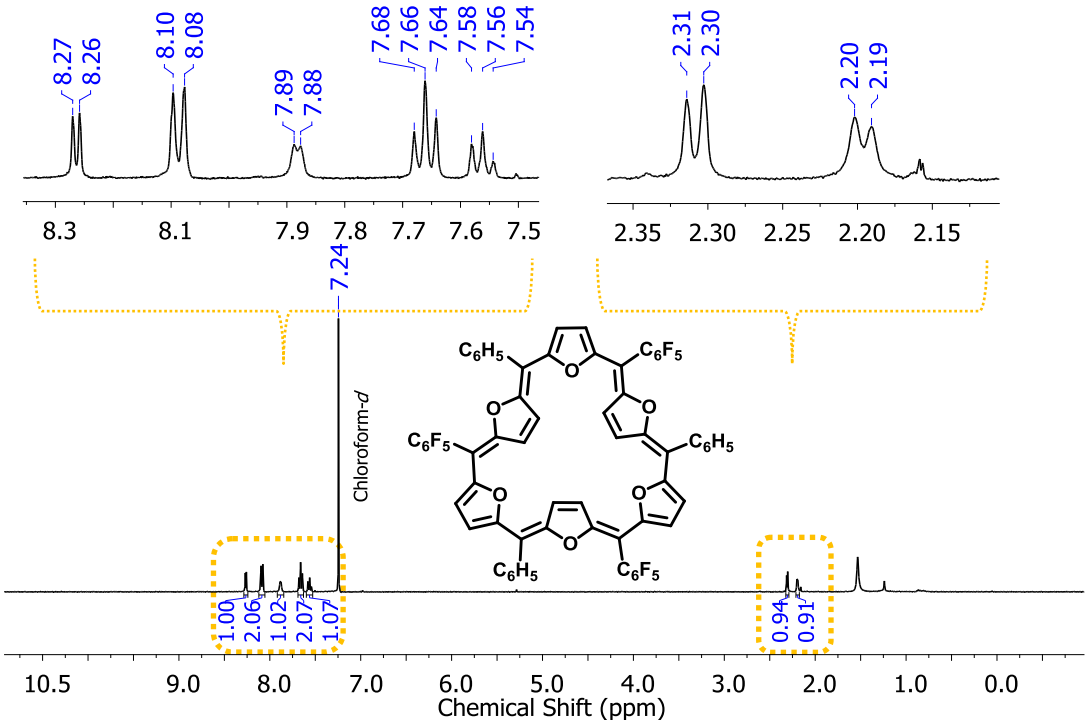

Figure 2.6. ^{1}H NMR of **II.3** in Chloroform-*d* at 298*K*.

II.3.3. Single Crystal X-ray Diffraction Studies

The structural features in solid state were confirmed from single crystal X-ray diffraction analysis. To confirm the molecular structures of **II.1** and **II.3**, good quality single crystals were grown in chloroform/*n*-hexane by using vapor diffusion method. The macrocycle crystallized in monoclinic system. The tetraoxa isophlorin **II.1** displayed a planar conformation with respect to the four-furans. All the four oxygen atoms from the four furans pointed towards the centre of the macrocycle and the phenyl rings were found to be orthogonal with respect to the mean macrocyclic plane. Macrocycle **II.3** displayed alternative furan ring inversion with a C_3 symmetry. The conformation of both macrocycles **II.1** and **II.3** in solid state (Figure 2.7), supported the solution state conformation inferred from their respective ^{1}H NMR spectrum.

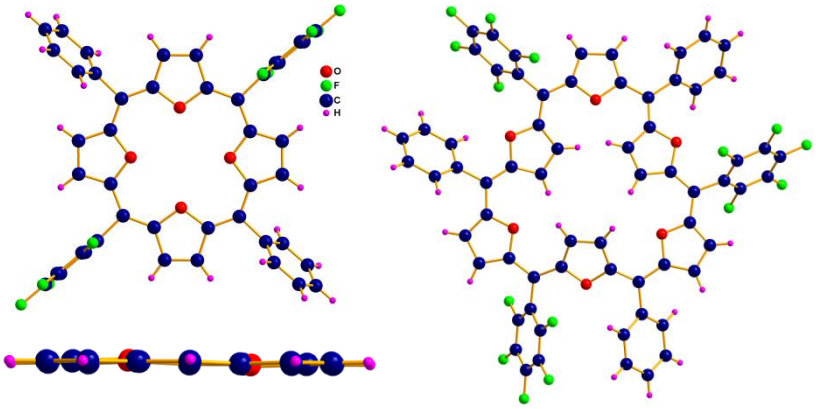

Figure 2.7. Molecular structures of **II.1** (left) and **II.3** (right). Phenyl groups are omitted in the side view.

II.4. Cocrystallization of Isophlorin (II.1 or II.2) with C_{60}

The solutions of these two anti-aromatic macrocycles were individually treated with a toluene solution of C_{60}. The color of the solution displayed a distinct change from green to brown upon the addition of fullerene, suggesting the formation of the π complex. Cocrystals of isophlorins (**II.1 and II.2**) and fullerene were grown from a combination of toluene-acetone/benzene solvents by slow evaporation method at room temperature, to yield black colored crystals.

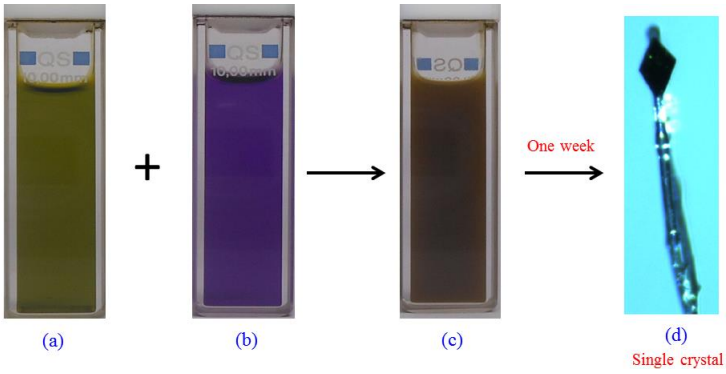

Figure 2.8. Color of the solutions displayed a distinct change from green to brown, upon the addition of fullerene.(a) **II.1** Isophlorin; (b) **C_{60}**in Toluene; (c) Slow evaporation of **II.1+C_{60}** solution and (d) Single crystal of **(II.1).C_{60}**

II.4.1. Methods used to confirm Isophlorin C_{60} interaction

The isolated cocrystals were subjected to following experimental techniques to confirm the interaction between anti-aromatic isophlorins (**II.1** and **II.2**) and C_{60}.

a) MALDI-TOF Mass Spectrometry
b) Isothermal Titration Calorimetry
c) Fluorescence Spectroscopic Titrations
d) Variable Temperature NMR experiments
e) Single Crystal X-ray analysis

II.4.1.a. MALDI-TOF Mass Spectrometry

As mass spectrometry is an excellent tool to confirm the composition of non-covalent complexes, the obtained cocrystals of **II.1(C_{60})** were dissolved in toluene and subjected to MALDI-TOF analysis. In its mass spectrum, two *m/z* values were observed, corresponding to individual mass of C_{60} and isophlorin mass rather than their combined mass. This suggested a weak interaction between the π surfaces of isophlorin and fullerene.

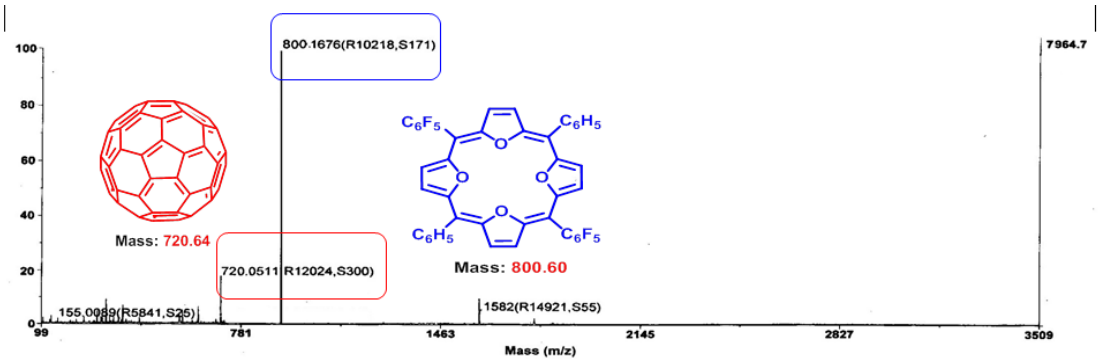

Figure 2.9. MALDI-TOF-TOF mass spectrum for **II.1(C_{60})** complex.

II.4.1.b. Isothermal Titration Calorimetry

Suspecting a weak interaction between the two molecules, the binding constant between isophlorin **II.1** and **C_{60}** was estimated using isothermal titration calorimetric (ITC) and fluorescence spectroscopic titrations.

Isothermal titration calorimetry (ITC)[11] was employed to quantify the complexation of the host (Isophlorin **II.1**) and guest (C_{60}) molecules in solution. The titration was carried out in toluene at 25 °C using an isothermal titration calorimeter (Microcal iTC-200) with stirring at 1000 rpm. About 200 µl of host (**II.1**) solution

was titrated with the guest (C_{60}) solution. A typical titration experiment consisted of 20 consecutive injections of 2 µl volume and 9s duration each, with a 90s interval between injections. Heat of dilution of the guest (C_{60}) were determined by injecting the guest solution into the solvent alone and the total observed heats of binding were corrected for the heat of dilution. A single set binding model fitted the binding isotherm, from where binding constant (K), binding stoichiometry (N), change of enthalpy (ΔH) and the change of entropy for the binding (ΔS) were obtained. The estimated association constant (K_a) was found to be 9.91 X 10^2 M^{-1} for **(II.1).C_{60}**.

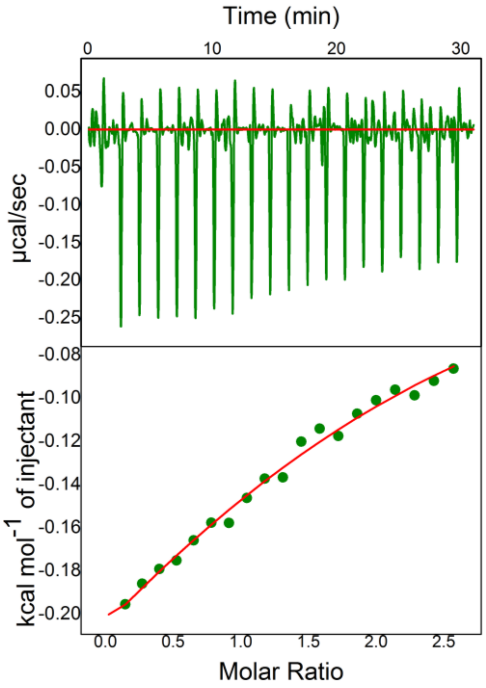

Figure 2.10. ITC profiles for the binding of guest (C_{60}) to host **II.1** at 25 ^{0}C in toluene. Top: raw data for the sequential 2 µl injection of C_{60} (0.4 mM) into **II.1** (5 mM). Bottom: plot of the heat evolved (kcal) per mole of C_{60} added, corrected for the heat of C_{60} dilution, against the molar ratio of C_{60} to **II.1**. The data (filled squares) were fitted to a single set binding model and the solid line represents the best fit.

The estimated thermodynamic parameters, ΔG (-5.24 k.cal.mol^{-1}), ΔH (-0.146 k.cal.mol^{-1}), and TΔS (-5.24 k.cal.mol^{-1}), for **(II.1).C_{60}** further confirmed a weak binding between isophlorin and C_{60}.

II.4.1.c. Fluorescence Spectroscopic Titrations

The isophlorins are poor emitters compared to porphyrin. However, it was observed that even the negligible fluorescence intensity reduced upon the addition of fullerene, which can be attributed to cluster formation between the two π conjugated molecules (Figure 2.11).

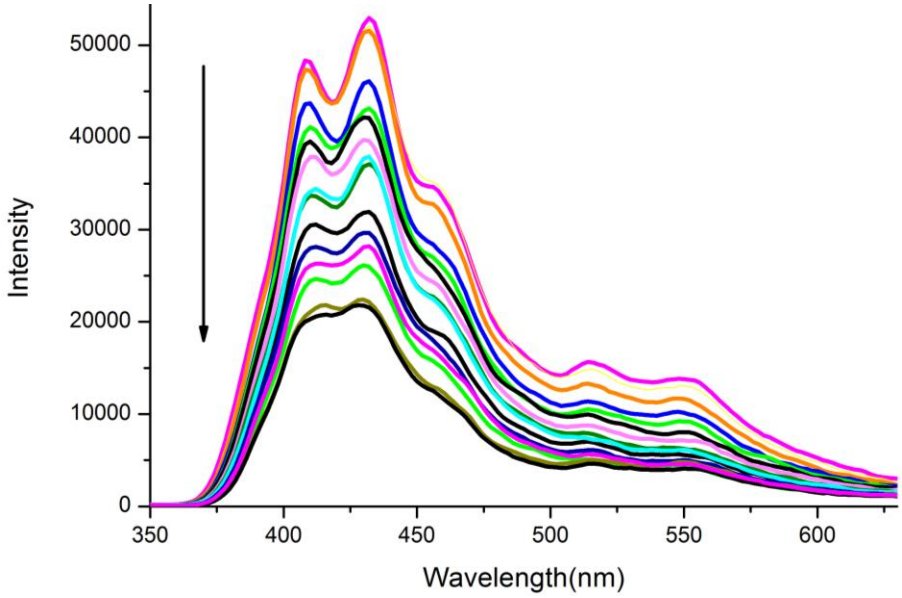

Figure 2.11. Fluorescence spectroscopic titration of Isophlorin **II.1** (1 μM, excited at 326 nm; slit = 2/3 nm) with 0−30 μM of **C_{60}**.

Benesi-Hildebrand plot for binding studies of [C_{60}] towards Isophlorin (II.1).

In order to determine the stoichiometry as well as binding constants of the inclusion complexes, the fluorescence intensity was analyzed using Benesi-Hildebrand (BH) plot[12] using the following equation (1).

$$\frac{1}{F\text{-}F_0} = \frac{1}{K(F_1\text{-}F_0)[host]} + \frac{1}{F_1\text{-}F_0} \qquad (1)$$

where F_0, F and F_1 are the fluorescence intensities of Isophlorin in absence, presence of host, and in the inclusion complex, respectively.

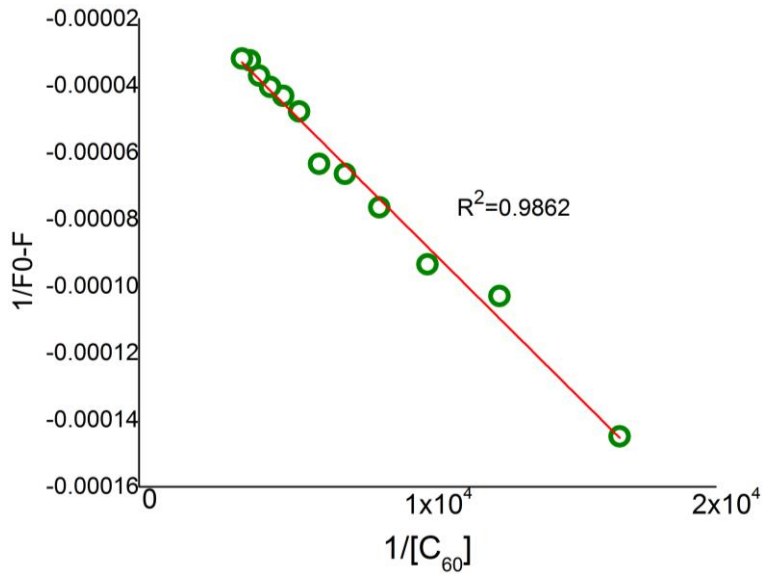

Figure 2.12. Benesi-Hildebrand plot of **II.1**(1 μM) for varying [C_{60}] (0 to 30 μM).

The fluorescence titration was conducted by with λ_{Ext} = 326. A good linear fit confirmed the 1: 1 binding stoichiometry in solution and the association constant (K_a) was estimated to be 3.712 x 10^3 M^{-1}. These values are in support of the results obtained from ITC measurements.

II.4.1.d. Variable Temperature NMR experiments

The interaction between fullerene and the isophlorin in solution was investigated by variable-temperature NMR experiments. Toluene-d_8 was chosen as solvent because of good solubility for both the molecules. The solution displayed remarkable shifts in both ^{13}C as well as ^{1}H NMR spectrum. A 1:1 solution of **II.1** and C_{60} displayed 0.03 ppm upfield shift for the β-hydrogens of furan and 0.03 ppm downfield shift for the *meso*-phenyl hydrogens (Figure 2.13).

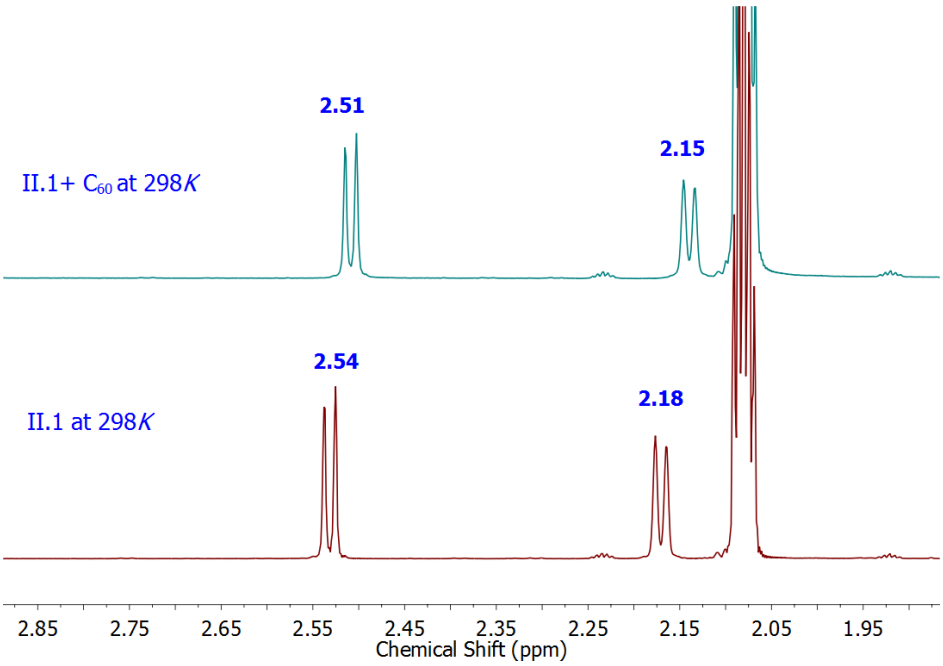

Figure 2.13. Partial ^{1}H NMR spectrum of **(II.1).C$_{60}$** complex in Toluene-d_8 at 298K.

Simultaneously, a 0.10 ppm shift was observed for the *ortho* fluorine atoms in ^{19}F NMR at room temperature (Figure 2.14). In the ^{13}C NMR, the C_{60} displayed a single resonance for **(II.1).C$_{60}$** at 298K with a marginal downfield shift of 0.26 ppm relative to free C_{60}. Upon cooling to 203K, this signal was further downfield shifted by 0.98 ppm. A large downfield shift of 1.33 ppm was observed upon cooling to 183K but accompanied with a significant broadening of the signal.[3a]

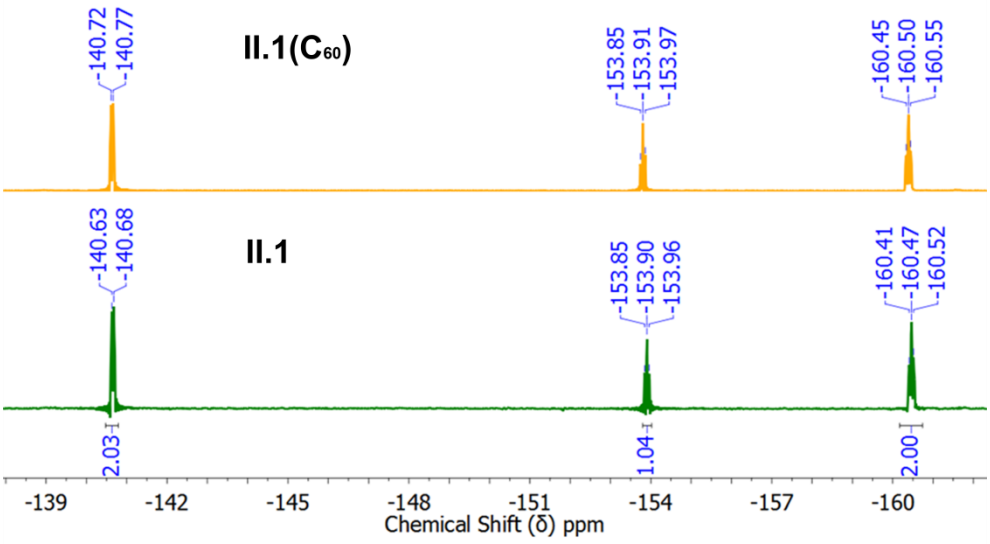

Figure 2.14. ^{19}F NMR spectrum of **(II.1).C$_{60}$** complex in Toluene-d_8 at 298*K*.

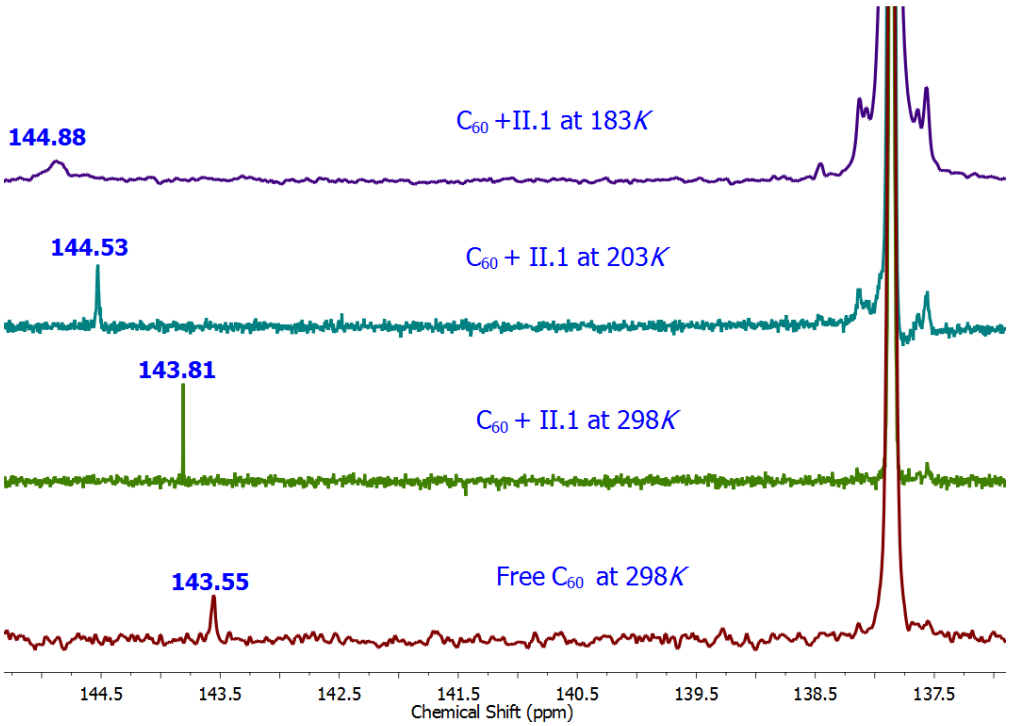

Figure 2.15. Variable temperature ^{13}C NMR spectrum of **(II.1) C_{60}** complex 1:1 ratio in Toluene-d_8.

The larger shift suggested significant interaction between C_{60} and isophlorin.

II.4.1.e. Single Crystal X-ray Diffraction analysis

Fullerene-Isophlorin Binding in Solid State

The attempts to cocrystallize different composition of C_{60}/isophlorin in various solvents selectively yielded 1:3 and 2:1 ratio of isophlorin **II.1**, while isophlorin **II.2** cocrystallized with C_{60} only in 1:1 ratio.

3:1 Molecular complex of II.1 with fullerene

The molecular complex of **$(II.1)_3.C_{60}$** revealed a fullerene trigonally engulfed by three isophlorins (a, b and c in Figure 2.16).[5b] The C_{60} is centred over the isophlorin with electron-deficient 5:6 ring juncture C-C bonds at a close distance to the plane of the isophlorin core (C to mean 24-atom plane distances C with a, b and c are 2.61 Å, 2.68 Å, and 2.76 Å respectively). No close fullerene/fullerene contacts were observed in the packing diagram for this crystal. The short contacts of *ortho*-F atoms of the isophlorin "a" and "c" to the nearest carbon atom of fullerene were found to be 3.09

and 3.10 Å respectively. Curiously, one of the isophlorin "c" was distorted from a regular planar structure in this non-covalent complex.

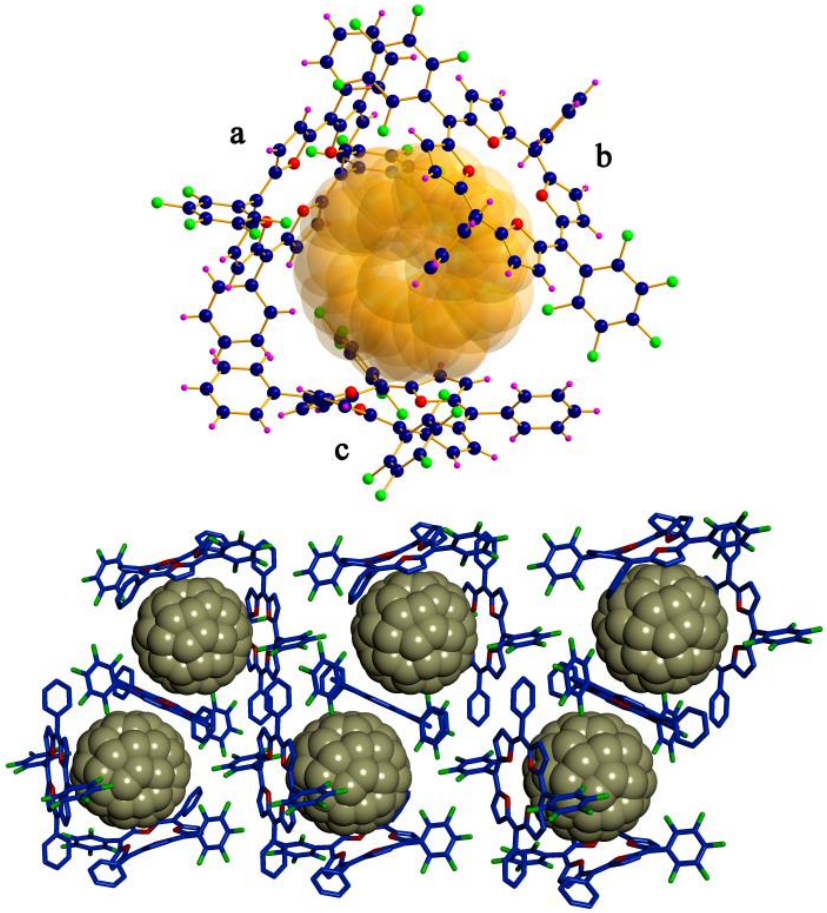

Figure 2.16. (Top) Molecular complex of $(\mathbf{II.1})_3.\mathbf{C_{60}}$ displayed prismatic arrangement of three isophlorin molecules around a C_{60}(transparent yellow color). (Below) Packing diagram of the prismatic arrangement. Color code: C_{60} in space filled gray color, O (red), C (blue), and F (green).

1:2 Molecular complex of II.1 with fullerene

Apart from the 1:3 complex described above, it was also observed that the macrocycle was sandwiched by two fullerene units,[13] $\mathbf{II.1.(C_{60})_2}$ (Figure 2.17). However, the distinction could be made only by the different morphology of the crystals with different ratios of isophlorin and fullerene. The close contacts observed between both the C_{60} and the macrocycle were 2.64 and 2.66 Å. These values are extremely short compared to conventional π-π stacking even in a homogeneous system.

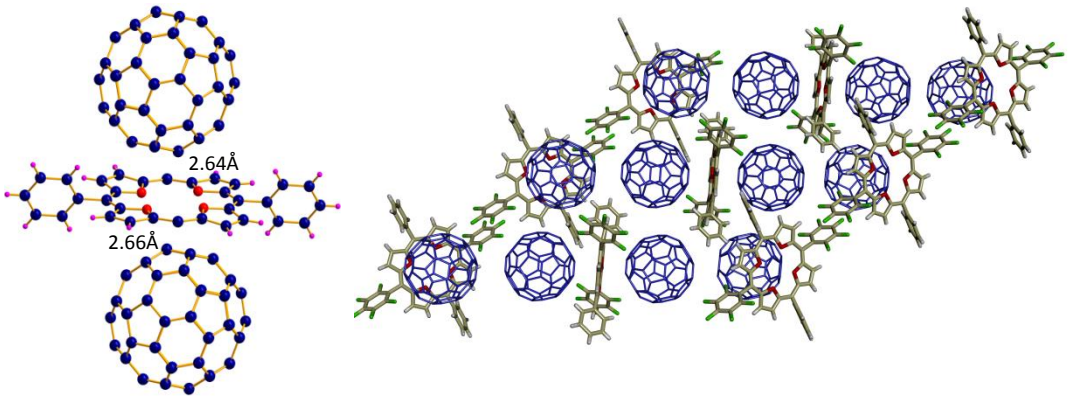

Figure 2.17. (a) 1:2 contact of a single isophlorin with fullerene in **II.1.(C_{60})$_2$** (left side). Pentafluorophenyl rings are omitted for clarity. (b) Molecular packing of **II.1.(C_{60})$_2$** (right side).

Molecular complex of II.2 and C_{60}

The crystal-packing diagram of **(II.2).C_{60}**, displayed a columnar stacking of 1:1 alternative C_{60}-isophlorin in benzene (Figure 2.18). A zig-zag assembly was not displayed and the isophlorin planes were found parallel, leading to a one-dimensional assembly. The C_{60} is centred over the isophlorin with electron-rich 6:6 ring-juncture C-C bonds in close approach to the plane of the isophlorin core (C to mean 24-atom plane distance) 2.62 Å. The closest atom-to-atom contacts were from the two 6:6 fullerene carbon atoms to the isophlorin oxygen atoms, which are in the range 2.94 to 3.76 Å. Short contacts between *ortho*-F atoms of the isophlorin and the nearest carbon atom of fullerene were found to be 3.16 and 3.18 Å, indicating that the *ortho* C-F bonds have relatively weak contribution to the association than in **(II.2).C_{60}**. In addition to the above mentioned interactions, weak C-F…H-C hydrogen bonding[14] was also observed between the isophlorin units. Interestingly, there were no close fullerene/fullerene contacts. Benzene molecules were found to occupy channels between columns, suggesting that aromatic solvents stabilized the non-covalent assembly (Figure 2.18 c).

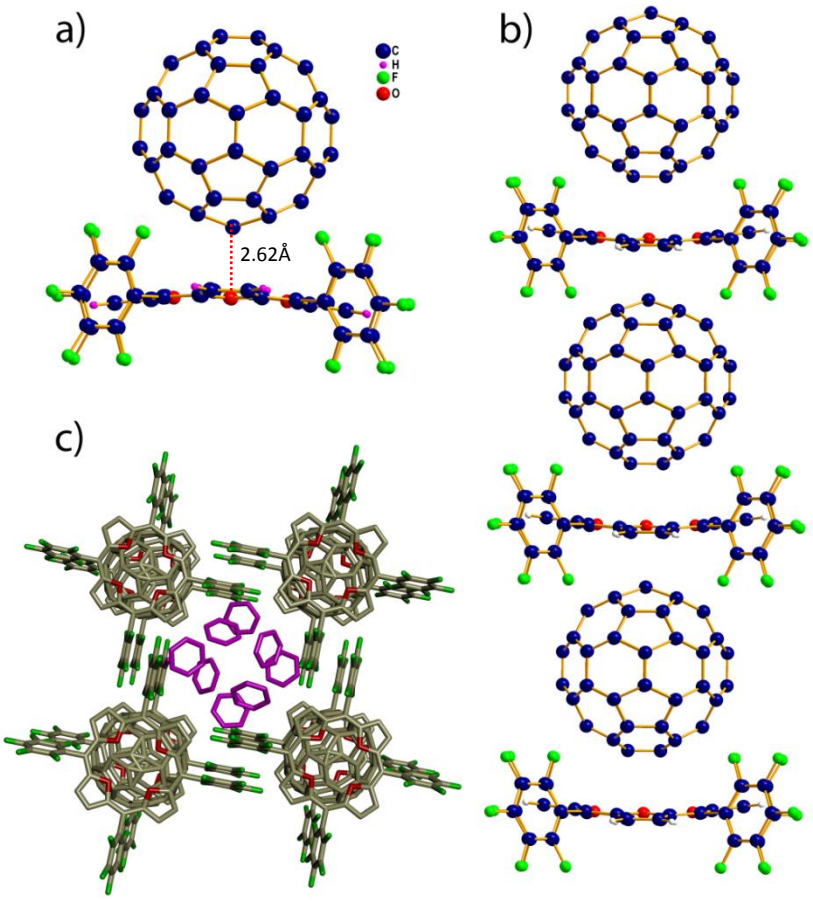

Figure 2.18.(a) Molecular structure of the complex formed by **II.2** and C_{60}; (b) Columnar stacking of alternating isophlorin/C_{60} in **(II.2).C_{60}** complex; (c) The solvent molecules are trapped in the voids.

II.5. Electronic Absorption Studies:

UV-Visible absorption displayed features of isophlorin alone and no salient changes could be observed for all the complexes in solution. This can be attributed to the purely non-covalent interaction, rather than the charge-transfer bands similar to porphyrin-fullerene interaction in solution state.[15] Absence of any charge-transfer bands in the electronic absorption spectra further supported lack of donor-acceptor complexes.

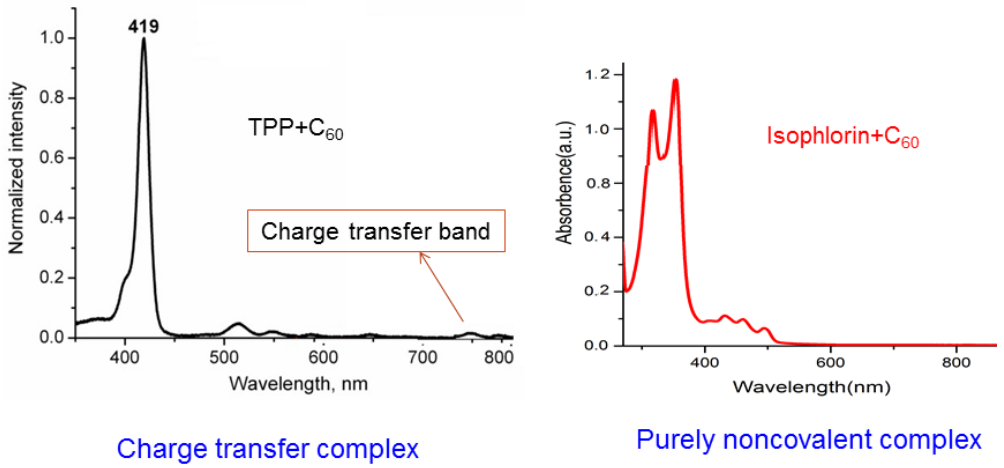

Figure 2.19. Comparison in the electronic spectra of TPP-C_{60} (left)[15] and isophlorin-C_{60} (right) complexes.

II.6. Conclusions

In conclusion, the first molecular complexes of fullerene with anti-aromatic isophlorin were obtained and successfully characterized by single crystal X-ray diffraction studies. The non-covalent interaction between isophlorin and fullerene was confirmed in solution state by ITC and NMR studies. These results strongly favoured the formation of 1:1 complex in solution state and also clearly support the non-covalent interaction between the 20π anti-aromatic tetraoxaisophlorin surface and the curved π surface of C_{60}. These values are much shorter than C_{60} and porphyrin assembly. The close contacts between fullerenes and isophlorin arise from a favorable van der Waals attraction of the curved π surface of a fullerene to the anti-aromatic π surface of isophlorin. These studies suggest that, anti-aromatic characteristics of a π surface can be as good as aromatic surfaces for binding fullerenes. The estimated binding constants also confirmed interaction between the isophlorins and C_{60} in the solution state.

II.7. Experimental Section

Synthetic procedure for 4

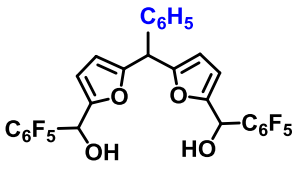

To the stirred solution of 5,5'-Methylenedifuran-2-carbaldehyde,[9b] (6.12 mmol, 1.715gm in 30 ml dry THF) under argon atmosphere at 0 °C, freshly prepared Grignard Reagent (C_6F_5MgBr, 15.3 mmol) was added. Stirring was allowed 2hrs to attain room temperature and the reaction mixture was quenched with saturated NH4Cl solution. The organic layer was extracted with ethylacetate and combined organic layer was washed with water and brine solution. After drying over Na_2SO_4, the solvent was removed under vacuum and purified through silica gel(100-200 mesh) column chromatography to yield the pure compound, **4**, as brown color semi solid.(2 g., Yield: 53%.)

^{1}H NMR (400 MHz, $CDCl_3$): δ 7.28 -7.18 (5H, m), 6.18 (1H, d, *J*=3.6 Hz), 6.06 (1H, s), 5.96 (1H, d, *J*=3.6 Hz), 5.35 (1H, s); **HRMS:** *m/z*: Calcd. for $C_{29}H_{14}F_{10}O_4\ Na^+$: 639.0629; observed: 639.0628 (100.0%, M^+).

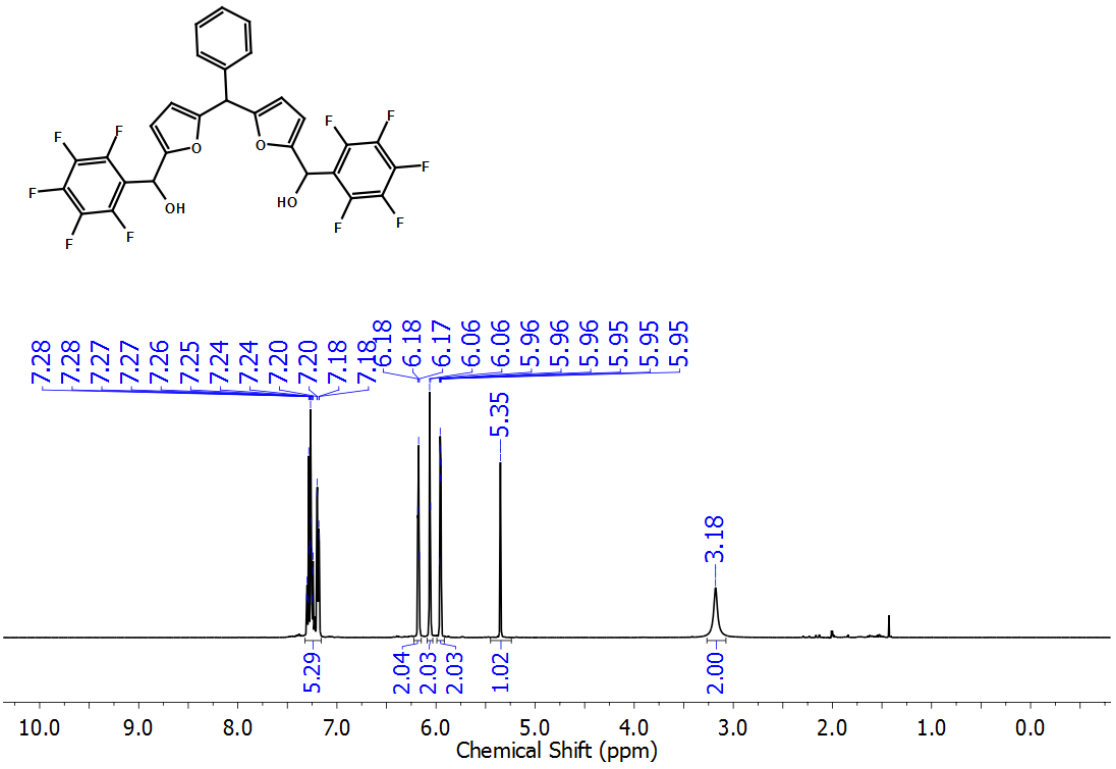

Figure 2.20. ^{1}H NMR of **4** in Chloroform-*d* at 298*K*.

Synthetic procedure for II.1 and II.3

A mixture of *meso*-phenyl difuromethane, **5**, (224 mg, 1 mmol) and the difuro methanedicarbinol, **4**, (616 mg, 1 mmol) were stirred in 100 ml dry dichloromethane. The solution was bubbled with argon for 10 min. $BF_3.OEt_2$ (0.12 ml, 1 mmol) was added under dark, and the resulting solution was stirred for 2h. After adding five

equivalents of $FeCl_3$, solution was opened to air and stirred for additional two hours. The reaction mixture was passed through a short basic alumina column. This mixture was separated by repeated silica gel column chromatography by using CH_2Cl_2/*n*-hexane as eluent. A yellowish green color band obtained was identified as **II.1** in 2.5% yield and also we obtained its higher analog with pink color band identified as **II.3** in 5% yield.

II.1: ^{1}**H NMR:** (400 MHz, Toluene-d_8) δ 6.67 – 6.53 (m, 6H), 6.09 – 5.96 (m, 4H), 2.53 (d, *J* = 4.8 Hz, 4H), 2.17 (d, *J* = 4.8 Hz, 4H); **UV-Vis** (CH_2Cl_2): λ_{max}(ε) L mol^{-1} cm^{-1}: 368 nm (102300), 328 nm (83900); **HRMS:** *m/z*: calcd. For $C_{44}H_{18}F_{10}O_4$: 800.1035; Observed: 800.1045(100.0% M^+); **Crystal data** $C_{44}H_{18}F_{10}O_4$, 2($CHCl_3$) (Mr = 1039.32), monoclinic, space group $P2_1/c$ (no. 14) , a = 10.3234(9), b = 15.5838(14), c = 13.5017(12)Å, α = 90.00° β = 102.531(2)° γ = 90.00°, V = 2120.4(3)Å^3, Z = 2, T = 100(2) K , D_{calcd} = 1.628Mg/m^3, R_1 = 0.0408 (I>2s(I)), R_w (all data) = 0.0475, GOF = 1.268.

II.3: ^{1}**H NMR**: (400 MHz, $CDCl_3$, 298 K): δ 8.28 (d, *J* =4.5Hz, 1H), 8.10 (d, *J* = 7.9Hz, 2H), 7.90 (d, *J* = 4.5Hz, 1H), 7.69-7.58 (m, Phenyl 3H), 2.21 (d, *J* = 4.5 Hz, 1H), 2.32 (d, *J* = 4.5Hz, 1H); ^{19}**F NMR:** (376 MHz, $CDCl_3$, 298 K): δ 137.02 (d, *J* = 18.5 Hz), -154.24 (t, *J* = 20.4 Hz), -162.17 (t, *J* = 18.7 Hz); **UV-Vis** (CH_2Cl_2): λ_{max}(ε) L mol^{-1} cm^{-1}: 566 nm (75049). **HRMS** *m/z*: calcd. For $C_{66}H_{27}F_{15}O_6$: 1200.1568; Observed: 1200.1555 (100.0% M+); **Crystal data**: 2($C_{66}H_{27}F_{15}O_6$).$CHCl_3$ (Mr = 2521.12), Monoclinic, space group P_2/c, (no. 13), a = 27.431(3), b = 12.1634(12), c = 34.398(4) Å, α = 90.00° β = 105.057(2)° γ = 90.00°, V = 11083.2(19) Å^3, Z = 4, T = 100(2) K , D_{calcd} = 1.511 g cm−3, R1 = 0.1073 (I>2s(I)), Rw (all data) = 0.1599, GOF = 2.019.

Table 2.1. Crystallographic data for II.1, $(II.1)_3.C_{60}$, $II.1.(C_{60})_2$, $(II.2)C_{60}$, II.3.

Compound	**II.1**	**$(II.1)_3.C_{60}$**	**$II.1.(C_{60})_2$**	**$(II.2).C_{60}$**	**II.3**
Solvent	Chloroform/ Hexane	Toluene/Acetone	Toluene	Benzene	Chloroform/Methanol
Formula	$C_{44}H_{18}F_{10}O_4$	C_{192} H_{54} F_{30} O_{12}	C_{164} H_{18} F_{10} O_4	C_{104} H_8 F_{20} O_4	$C_{66}H_{27}F_{15}O_6$
Temperature(K)	100(2)	100(2)	100(2)	100(2)	296(2)
Crystal System	Monoclinic	Triclinic	Monoclinic	Tetragonal	Monoclinic
Space group	P2(1)/c	P-1	C2/c	I41/a	P2/c
Volume	2120.4(3) $Å^3$	5218.1(12) $Å^3$	8756(3) $Å^3$	10053.1(13) $Å^3$	11083.2(19) $Å^3$
a	10.3234(9)	15.928(2) Å	26.962(7) Å	28.7283(16) Å	27.431(3)Å
b	15.5838(14)	19.014(2) Å	13.616(3) Å	28.7283(16) Å	12.1634(12) Å
c	13.5017(12)	20.624(3) Å	24.071(5) Å	12.1809(9) Å	34.398(4) Å
α	90°	101.456(7)°	90°	90°	90°
β	102.531(2)°	110.099(7)°	97.746(8)°	90°	105.057(2)°
γ	90°	108.543(7)°	90°	90°	90°
Z	2	4	8	8	4
D_{calc}	1.628 g/cm^{-3}	1.566 g/cm^{-3}	1.701 g/cm^{-3}	1.537 g/cm^{-3}	1.511 g/cm^{-3}
R1	0.0408	0.0992	0.061	0.0648	0.1073
$R2_W$	0.146	0.3163	0.1514	0.1841	0.1599
GOF	1.268	1.197	1.022	1.234	2.019

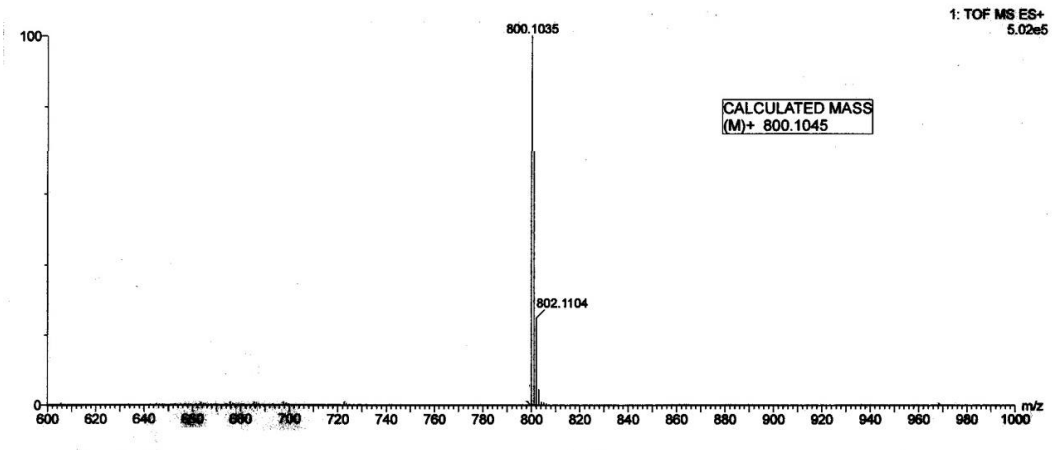

Figure 2.21.HR-ESI-TOF mass spectrum of **II.1**

II.8. References

[1] a) J. L. Atwood, G. A. Koutsantonis, C. L. Raston, *Nature* **1994**, *368*, 229-231; b) T. Suzuki, K. Nakashima, S. Shinkai, *Chemistry Letters* **1994**, 699-702.

[2] Y. Sun, T. Drovetskaya, R. D. Bolskar, R. Bau, P. D. W. Boyd, C. A. Reed, *J Org Chem* **1997**, *62*, 3642-3649.

[3] a) P. D. W. Boyd, M. C. Hodgson, C. E. F. Rickard, A. G. Oliver, L. Chaker, P. J. Brothers, R. D. Bolskar, F. S. Tham, C. A. Reed, *Journal of the American Chemical Society* **1999**, *121*, 10487-10495; b) P. D. Boyd, C. A. Reed, *Acc Chem Res* **2005**, *38*, 235-242; c) A. Hosseini, M. C. Hodgson, F. S. Tham, C. A. Reed, P. D. W. Boyd, *Crystal Growth & Design* **2006**, *6*, 397-403; d) Z. Wang, F. Dotz, V. Enkelmann, K. Mullen, *Angew Chem Int Ed* **2005**, *44*, 1247-1250; e) J. Song, N. Aratani, H. Shinokubo, A. Osuka, *J. Am. Chem. Soc.* **2010**, *132*, 16356-16357.

[4] a) A. Ikeda, M. Yoshimura, H. Udzu, C. Fukuhara, S. Shinkai, *J. Am. Chem. Soc.* **1999**, *121*, 4296-4297; b) N. Kishi, M. Akita, M. Kamiya, S. Hayashi, H. F. Hsu, M. Yoshizawa, *J Am Chem Soc* **2013**, *135*, 12976-12979; c) O. D. Fox, M. G. Drew, P. D. Beer, *Angew Chem Int Ed Engl* **2000**, *39*, 135-140; d) O. D. Fox, E. J. S. Wilkinson, P. D. Beer, M. G. B. Drew, *Chemical Communications* **2000**, 391-392; e) O. D. Fox, J. Cookson, E. J. S. Wilkinson, M. G. B. Drew, E. J. MacLean, S. J. Teat, P. D. Beer, *J. Am. Chem. Soc.* **2006**, *128*, 6990-7002; f) K. Suzuki, K. Takao, S. Sato, M. Fujita, *J. Am. Chem. Soc.* **2010**, *132*, 2544-2545; g) W. Meng, B. Breiner, K. Rissanen, J. D. Thoburn, J. K. Clegg, J. R. Nitschke, *Angew. Chem., Int. Ed.* **2011**, *50*, 3479-3483; h) N. Martìn, J.-F. Nierengarten, *Supramolecular Chemistry of Fullerenes and Carbon Nanotubes; , Germany, 2012.*

[5] a) Z. Chen, J. I. Wu, C. Corminboeuf, J. Bohmann, X. Lu, A. Hirsch, P. Schleyer, *Physical chemistry chemical physics : PCCP* **2012**, *14*, 14886-14891; b) M. M. Olmstead, D. J. Nurco, *Crystal Growth & Design* **2006**, *6*, 109-113.

[6] J. Zhang, J. Tan, Z. Ma, W. Xu, G. Zhao, H. Geng, C. a. Di, W. Hu, Z. Shuai, K. Singh, D. Zhu, *Journal of the American Chemical Society* **2013**, *135*, 558-561.

[7] R. B. Woodward, *Angew. Chem.* **1960**, *72*, 651-662.

[8] a) M. Pohl, H. Schmickler, J. Lex, E. Vogel, *Angew. Chem., Int. Ed.* **1991**, *30*, 1693-1697; b) J. S. Reddy, V. G. Anand, *Journal of the American Chemical Society* **2008**, *130*, 3718-3719.

[9] a) P. Rothemund, *Journal of the American Chemical Society* **1935**, *57*, 2010-2011; b) P. Rothemund, *Journal of the American Chemical Society* **1936**, *58*, 625-627.

[10] E. Vogel, *Pure Appl. Chem.* **1993**, *65*, 143.

[11] F. P. Schmidtchen, *Isothermal Titration Calorimetry in Supramolecular Chemistry, ed. C. A. Schalley, Wiley-VCH,* **2006**, 55-78.

[12] H. A. Benesi, J. H. Hildebrand, *Journal of the American Chemical Society* **1949**, *71*, 2703-2707.

[13] D. V. Konarev, I. S. Neretin, Y. L. Slovokhotov, E. I. Yudanova, N. y. V. Drichko, Y. M. Shul'ga, B. P. Tarasov, L. L. Gumanov, A. S. Batsanov, J. A. K. Howard, R. N. Lyubovskaya, *Chem. - Eur. J.* , **2001**, *7*, 2605-2616.

[14] G. R. Desiraju, T. Steiner, *The Weak Hydrogen Bond in Structural Chemistry and Biology; OUP: Oxford, 1999;* Chapter *3*

[15] A. L. Litvinov, D. V. Konarev, A. Y. Kovalevsky, I. S. Neretin, P. Coppens, R. N. Lyubovskaya, *Crystal Growth & Design* **2005**, *5*, 1807..

Chapter 3

Synthesis and Characterization of meso,meso Linked Anti-aromatic Isophlorin

III.1. Introduction

The components of functional π materials are seldom made from anti-aromatic units,[1,2] even though their relatively higher paramagnetic property can be perceived to be an added advantage in organic electronics.[3-5] The exploration of their employability as functional π materials has not evinced keen interest amongst the researchers, mainly due to the lack of established chemistry based on stable 4nπ systems. The prime reasons for the sluggish growth of anti-aromaticity itself can be attributed to the lack of sufficient synthetic strategies for stable anti-aromatic molecules. Aromatic units such as benzene, is well known to undergo oxidative coupling reactions,[6] which is a key synthetic process in the design of novel poly aromatic hydrocarbons. However, even the simplest of anti-aromatic systems such as cyclobutene or cyclooctatetraene are unknown to dimerize under similar reaction conditions. In this scenario, the 4nπ isophlorins[7-9] offers a rare opportunity to explore the properties and chemistry of anti-aromatic macrocycles. The derivatives of 20π isophlorin with thiophene and furan subunits, **1**, represent the simplest of the stable and planar anti-aromatic systems.[7,8] They can be explored further to understand the chemistry of 4nπ systems in general. Except for the structural resemblance, they exhibit electronic and redox properties very different from the aromatic porphyrin, **2**.

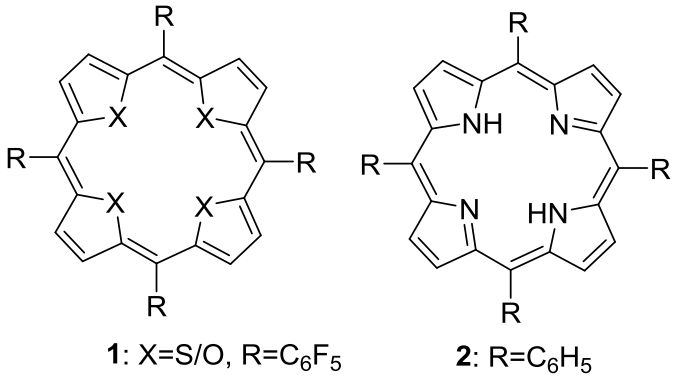

Figure 3.1. 20π isophlorin derivatives of thiophene/furan (**1**); Porphyrin (**2**).

Particularly, the electron density of π-surface in anti-aromatic isophlorin as observed from ^{1}H NMR spectroscopy is found to be the opposite of the aromatic 18π porphyrin. This can be a crucial factor for the electronic effects of the macrocycle in

non-covalent interactions. Yet, isophlorin can bind C_{60}-fullerene through conventional π-π contacts, highlighting the utility of isophlorin as a synthon for supramolecular chemistry.[10]

III.2. Synthesis

The previous chapter illustrated the binding of C_{60} fullerene to the isophlorin surface. Particularly, for porphyrins, the *meso* substituents are known to exert considerable influence in host-guest chemistry through non-covalent interactions. Based on this idea, it was an obvious choice to estimate the strength of such interactions for isophlorins in the absence of *meso* substituents. This led to the synthesis of mono- and di- *meso* free isophlorins by employing MacDonald type condensation of appropriate precursors. Pentafluorobenzaldehyde was reacted with difuromethane[11] **3**, under acidic conditions followed by oxidation to obtain the desired *meso* free isophlorin (Scheme-3.1).

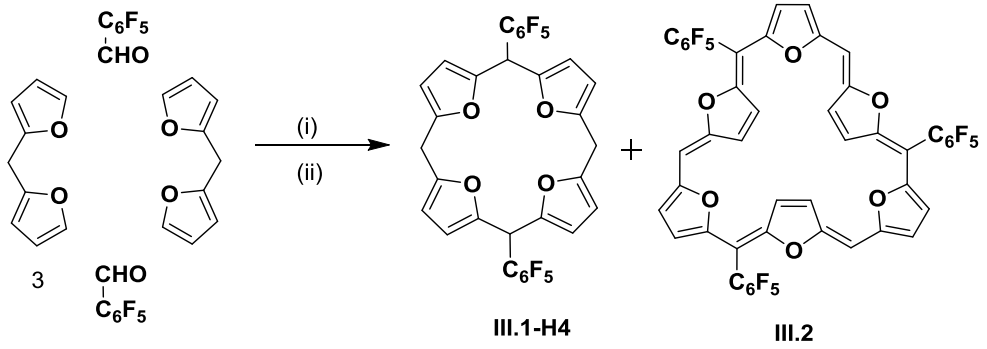

Scheme 3.1. synthesis of **III.1-H4**

Reaction conditions: (i) $BF_3.OEt_2$ (1 eq.), dry DCM (100 ml), rt, N_2, 2h; (ii) $FeCl_3$ (5 eq.), N_2, 2h.

However, the MALDI-TOF-TOF mass spectrum of the reaction mixture revealed the formation of an unconjugated macrocycle, **III.1-H4** (unoxidized form) and another large conjugated macrocycle, **III.2** (oxidized form).The isolated unconjugated macrocycle, **III.1-H4** was subjected to further oxidation with DDQ (Scheme 3.2) to obtain the desired tetraoxaisophlorin.

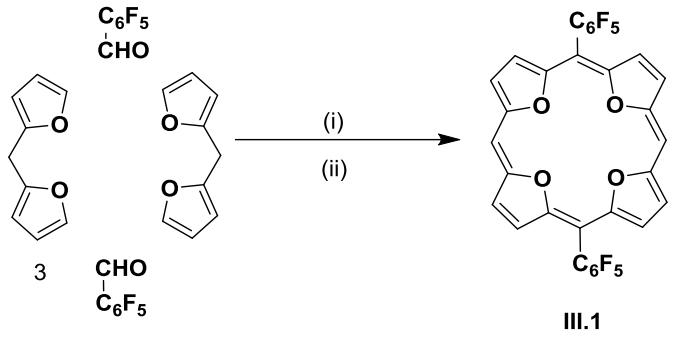

Scheme 3.2. synthesis of **III.1.**
Reaction conditions: (i) $BF_3.OEt_2$ (1 eq.), dry DCM (100 ml), rt, N_2, 2h; (ii) DDQ (5 eq.), N_2, 2h.

The MALDI-TOF-TOF mass spectrum analysis of this DDQ oxidation revealed the formation of three different products, which could be perceived as the over oxidized products (mono keto, diketo and the radical species, see Figure 3.2). This possibility can be envisaged through the reaction of molecular oxygen with the reduced form of DDQ.

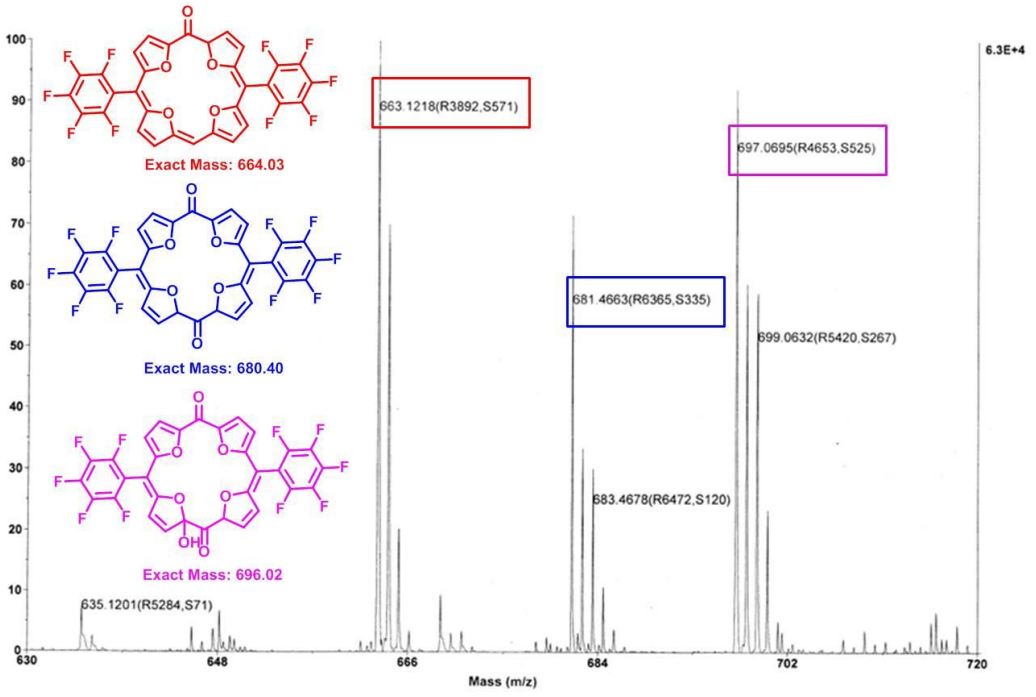

Figure 3.2. MALDI-TOF-TOF mass spectrum of reaction mixture from scheme 3.2.

To overcome this over oxidation, the reaction was performed in a two step process, where in the unconjugated product **III.1-H4** was isolated before oxidation in the one-

pot synthesis. At first it was oxidized with DDQ and later reacted with hydrazine to reduce the unwanted oxygenation of the macrocycle (Scheme 3.3).

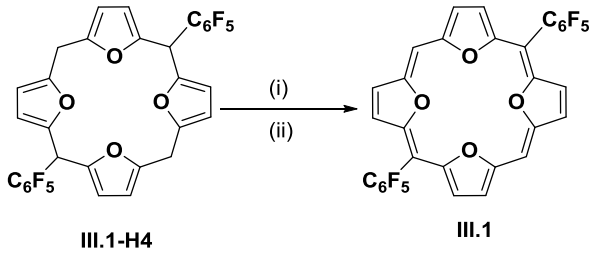

Scheme 3.3. Acid catalysed synthesis of 20π tetraoxaisophlorin **III.1**.
Reaction conditions: (i) DDQ (5 eq.); DCM (100ml); (ii) $N_2H_4.H_2O$, reflux.[11]

The reaction mixture was passed through a short basic alumina column. This mixture was concentrated and further purified by recrystallization in *n*-hexane/ dichloromethane combination, to obtain the desired product as green colored solid, **III.1** (20 mg) in 20% yields.

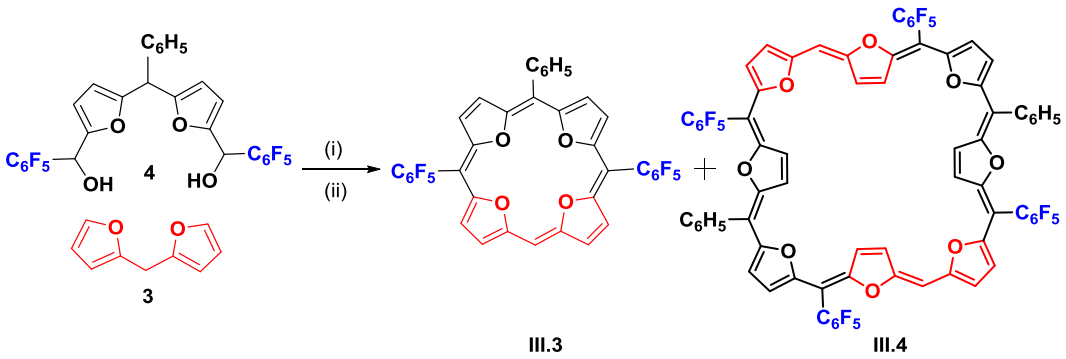

Scheme 3.4. Acid catalysed synthesis of 20π tetraoxaisophlorins **III.3** and **III.4**.
Reaction conditions: (i) $BF_3.OEt_2$ (1 eq.), dry DCM (100 ml), rt, N_2, 2h; (ii) DDQ/$FeCl_3$ (5 eq.), N_2, 2h.

The mono *meso* free tetraoxa isophlorin, **III.3**, was synthesized by a typical Mac Donald type condensation between *bis*(furan)methane **3**, and its corresponding difuromethane dicarbinol **4**, under acidic conditions (Scheme 3.4). In this reaction the 40π octafuran macrocycle **III.4** was also identified from the MALDI-TOF-TOF Mass Spectrum analysis. The reaction mixture was passed through a short basic alumina column and further purified by repeated size exclusion column chromatography with toluene as eluent. A brown color band that eluted in the column was identified as **III.3** while a pink color band was identified as **III.4.** The evaporation of the solvent gave

III.3 as a violet solid in 8% yields, while **III.4** was obtained as green colored solid in 10% yields.

III.3. Spectral Characterization

Isophlorins (**III.1, III.1-H4, III.2, III.3** and **III.4)** were analyzed through high resolution mass spectrometry, UV-Vis, NMR spectroscopy and Single crystal X-ray diffraction analysis.

III.3.1. Electronic Absorption Studies

The synthesized **III.1** and **III.3** isophlorins form green colored solutions when dissolved in common organic solvents. The color of the solution can be attributed to the extensive conjugated network of the macrocycle. They absorb radiation in far UV range from 300-350 nm (Figure 3.3). **III.1** displayed high energy absorptions at 318 nm (ε =97900) and 348 nm (ε=112200) followed by low energy absorptions in the region 400-500 nm. The higher analog **III.2** absorbed at 511 nm (ε = 120800). Compound **III.3** was found to absorb at 322 nm (ε =79800) and 357 nm (ε =91400) followed by low energy absorptions in the region 400-500 nm.

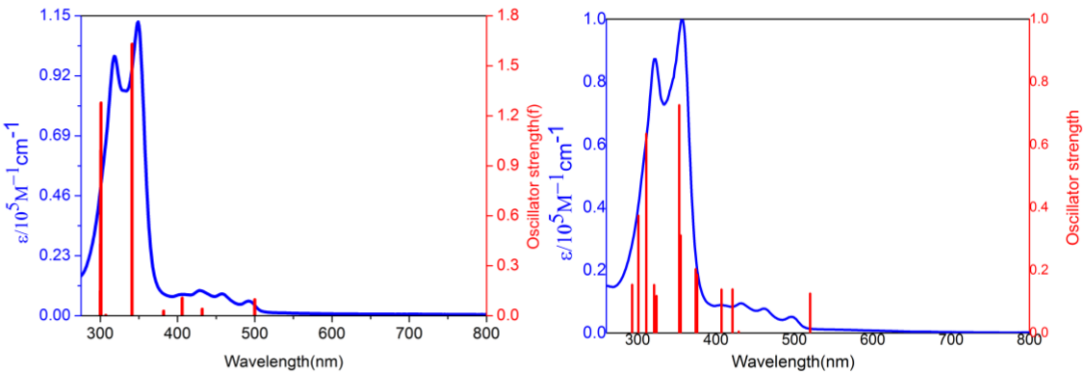

Figure 3.3. The steady state absorption spectra (blue line-experimental) of **III.1** (left) and **III.3** (right) recorded in CH_2Cl_2 along with the theoretical vertical excitation energies (red bar-theoretical) obtained from TD-DFT calculations carried out at the B3LYP/6-31G(d,p) level.

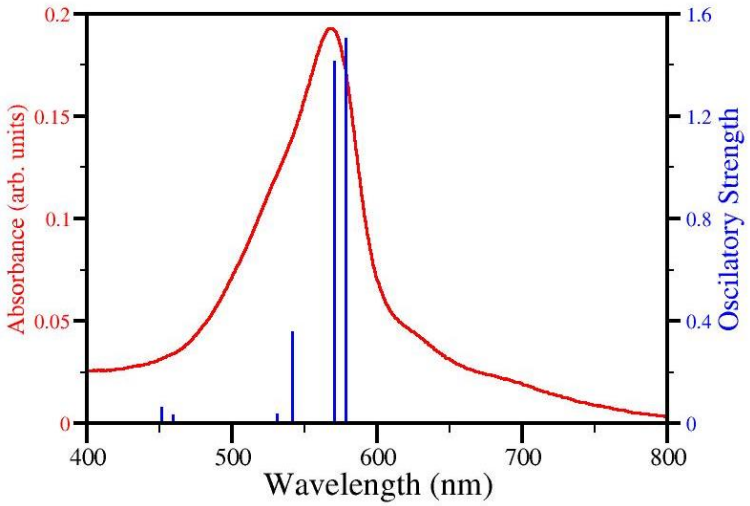

Figure 3.4. The steady state absorption spectra (red line- experimental) of **III.2** recorded in CH_2Cl_2 at 10^{-7}M along with the theoretical vertical excitation energies (blue bar-theoretical) obtained from TD-DFT calculations carried out at the B3LYP/6-31G(d,p) level.

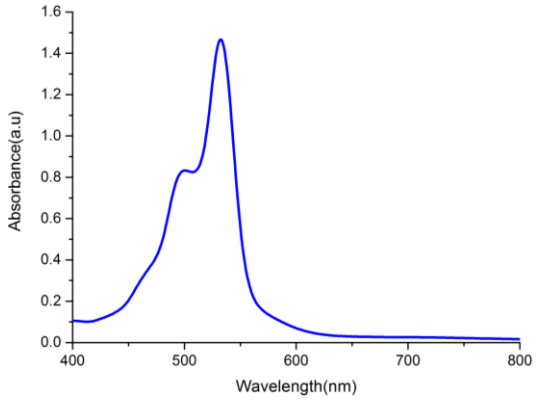

Figure 3.5. The absorption spectra of **III.4** recorded in CH_2Cl_2 at 10^{-5} M.

III.3.2. NMR Characterization

The ^{1}H NMR spectra of the macrocycles, **III.1** and **III.3** confirmed the paratropic ring current effects expected of 4nπ anti-aromatic system because of 20π electrons along the conjugated pathway. The macrocycle **III.1** exhibited very high upfield shifts for both the *meso*-protons and the β-hydrogens of the heterocyclic subunits. The protons of its furan rings resonated as two doublets at δ 2.16 and 1.82 ppm, while a singlet was observed for the *meso*-proton at δ -0.38 ppm (Figure 3.6).

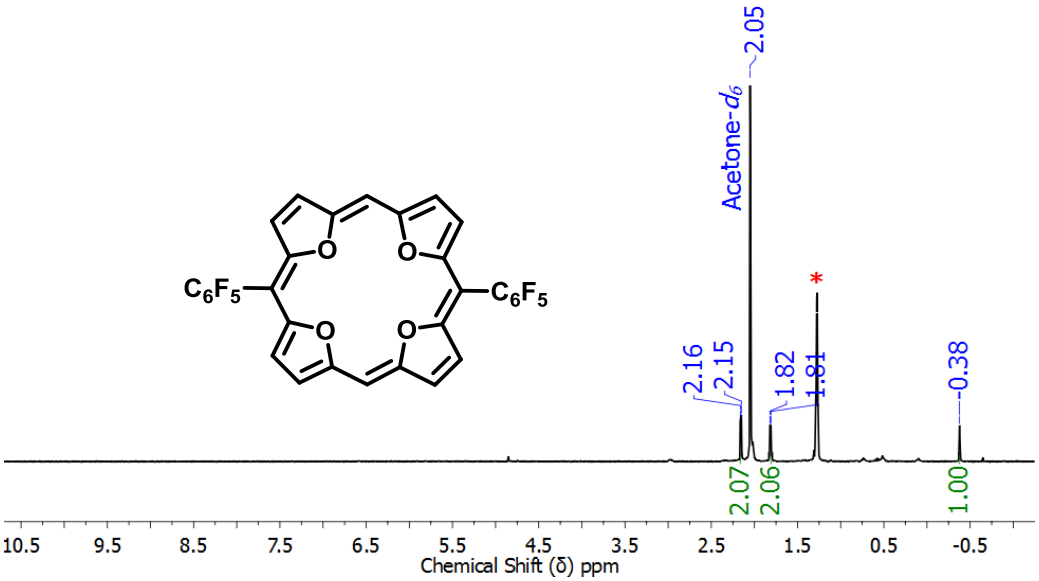

Figure 3.6. ^{1}H NMR of **III.1** in Acetone-d_6 at 298K (* solvent residual peak).

Similarly, compound **III.3** displayed five different signals for the protons: a singlet for the *meso*-proton resonated at δ -0.36 ppm, four doublets for β-protons of the furan were found to resonate in the upfield region between δ 1.82 - 2.24 ppm. The *meso*-phenyl protons were observed in the downfield region as a multiplet and doublet between δ = 5.93 - 6.57 ppm indicating no influence of the strong paratropic ring current effects on the *meso*-phenyl protons (Figure 3.7).

Compound **III.2** displayed four doublets and three singlets in its room temperature ^{1}H NMR spectrum. Of these, four doublets were observed in the down-field region at δ 8.89–8.23 ppm and two singlets for protons on *meso*-carbon atoms could be identified at 9.28 and 9.01. The remaining lone singlet resonated upfield at δ -0.86 ppm (Figure 3.8). This spectrum was suggestive of a C_{2v} symmetry in solution state with diatropic ring current effects and a near planar conformation for the macrocycle. Ideally two doublets are expected for ring inverted β-hydrogens, but both the protons were found to resonate as a singlet even at low temperature, suggestive of fluxional behaviour of macrocycle. The suspected fluxionality of these protons was found to be quite faster than NMR time scale.

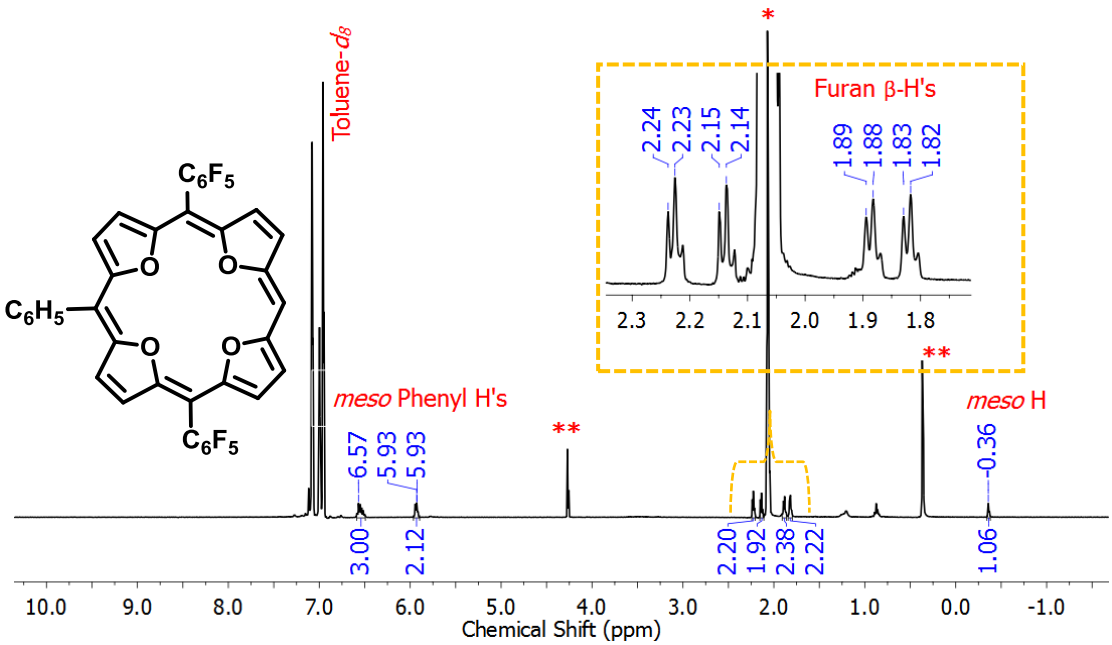

Figure 3.7. ^{1}H NMR spectrum of **III.3** in Toluene-d_8 at 298*K*, (*Toluene-d_8, **H_2O and CH_2Cl_2).

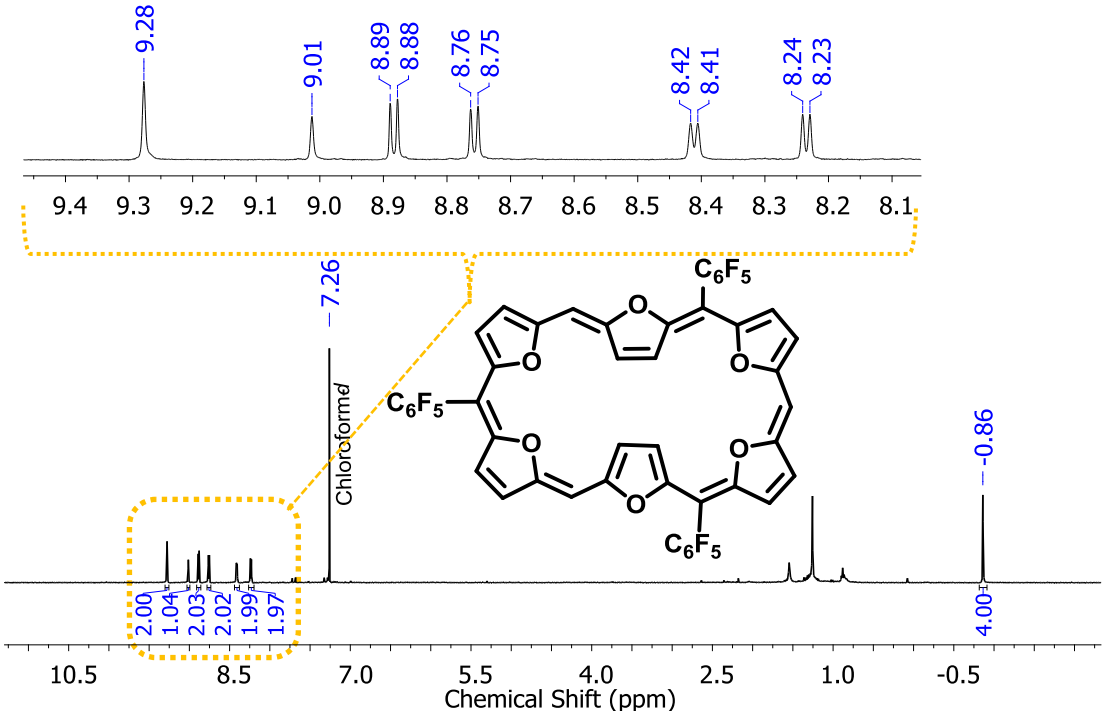

Figure 3.8. ^{1}H NMR of **III.2** in Chloroform-*d* at 298*K*.

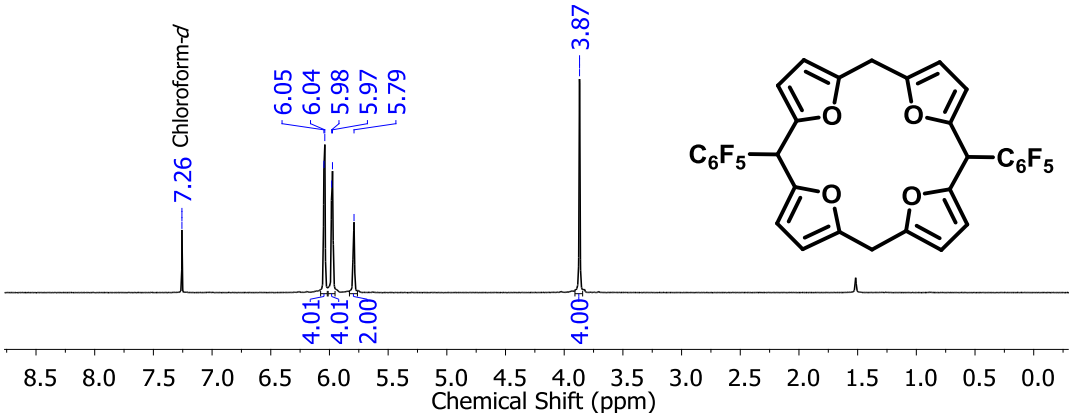

Figure 3.9. ^{1}H NMR of **III.1-H4** in Chloroform-*d* at 298*K*.

The ^{19}F NMR spectra of **III.1, III.1-H4** and **III.3** displayed three different signals each, indicating three sets of fluorines (*ortho*, *meta* and *para* for perfluorophenyl rings).

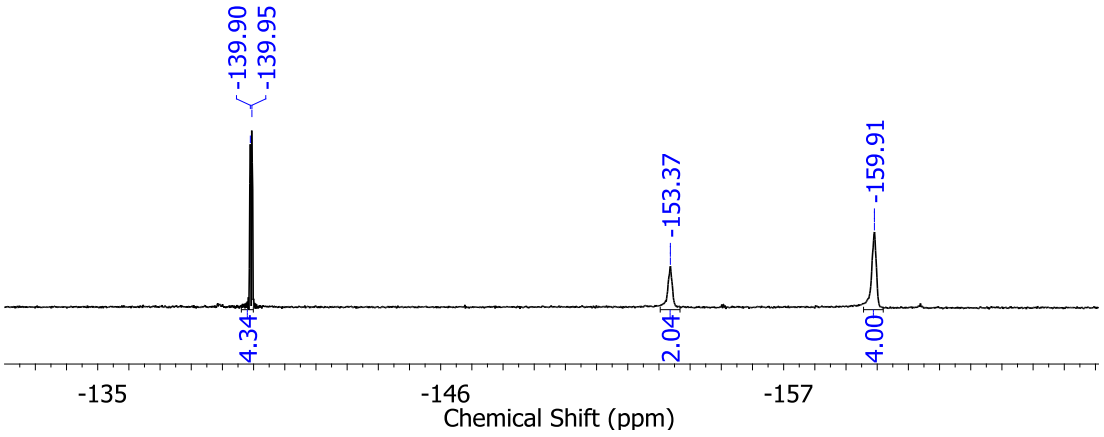

Figure 3.10. ^{19}F NMR spectrum of **III.1** in Acetone-$d_6$at 298*K*

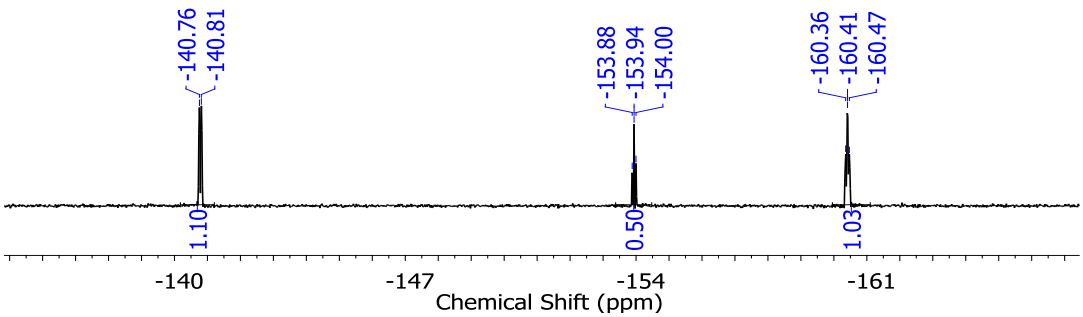

Figure 3.11. ^{19}F NMR spectrum of **III.3** in Toluene-d_8 at 298*K*

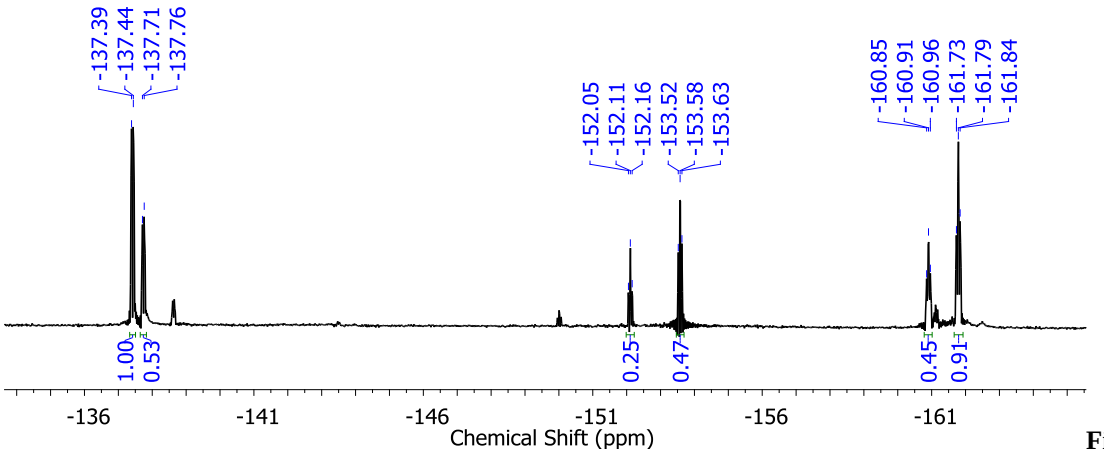

Fi

gure 3.12. ^{19}F NMR spectrum of **III.2** in Chloroform-*d* at 298*K*

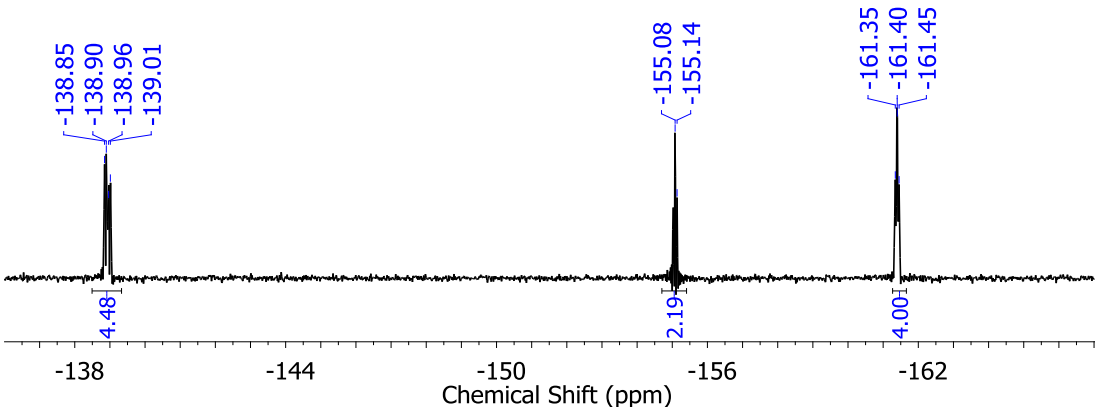

Figure 3.13. ^{19}F NMR of **III.1-H4** in Chloroform-*d* at 298*K*.

Surprisingly, compound **III.4** was found to be NMR silent and EPR active suggestive of its paramagnetic behavior. Such an observation is very rare for neutral and expanded porphyrins. However, it is suspected to have a low energy barrier between its singlet and triplet state due to its D_{2h} symmetry, leading to the formation of paramagnetic species.[12]

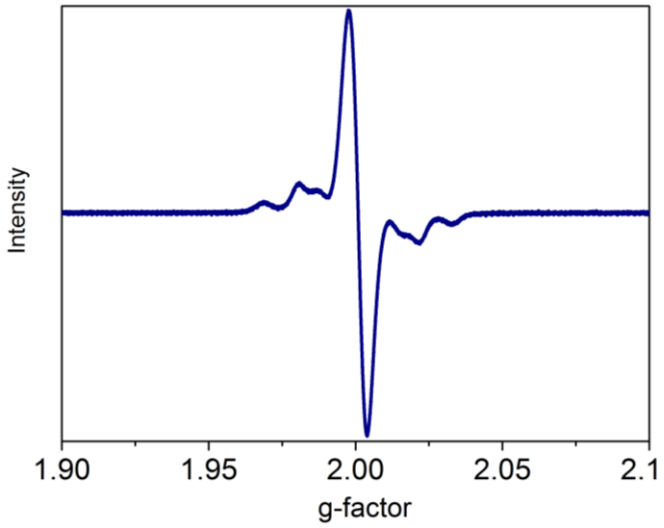

Figure 3.14. EPR spectrum of **III.4** recorded in chloroform at room temperature.

III.3.3. Single Crystal X-ray Diffraction Studies

The structures of the macrocycles were confirmed from single crystal X-ray diffraction analysis. Suitable single crystals were grown in appropriate solvent systems. To confirm the molecular structures of **III.1**, **III.2**, **III.3** and **III.4**, good quality single crystals were grown in chloroform/*n*-hexane by vapor diffusion method. All the macrocycles were crystallized in monoclinic system with $P2_1/c$ space group except **III.4** and exhibited a near planar conformation. The *meso*-phenyl rings were invariably found to adopt an orthogonal orientation with respect to the mean plane of the macrocycle.

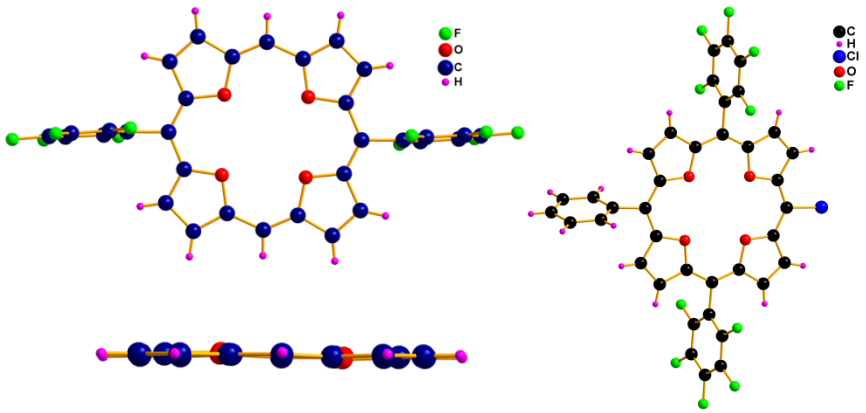

Figure 3.15. Molecular structures of **III.1** (left) and **III.3-Cl**(left). Solvent molecules were omitted for clarity. Phenyl groups are omitted in the side view.

When isophlorin **III.3** was crystallized from chloroform and *n*-hexane, an unexpected chlorination on the *meso*-carbon atom was indentified through X-ray crystallography to obtain **III.3-Cl**. This observation hinted the possibility of a radical mechanism in presence of halogenated solvents.

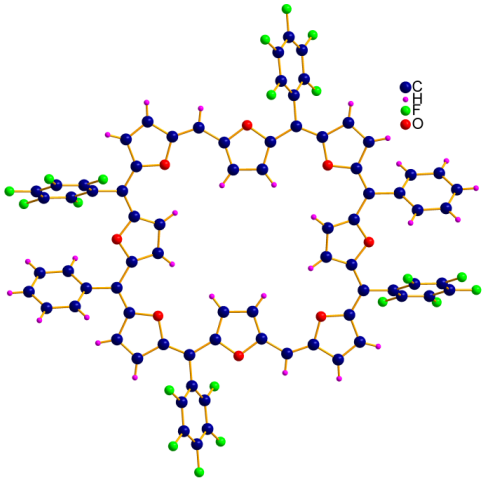

Figure 3.16. Molecular structure of **III.4**.

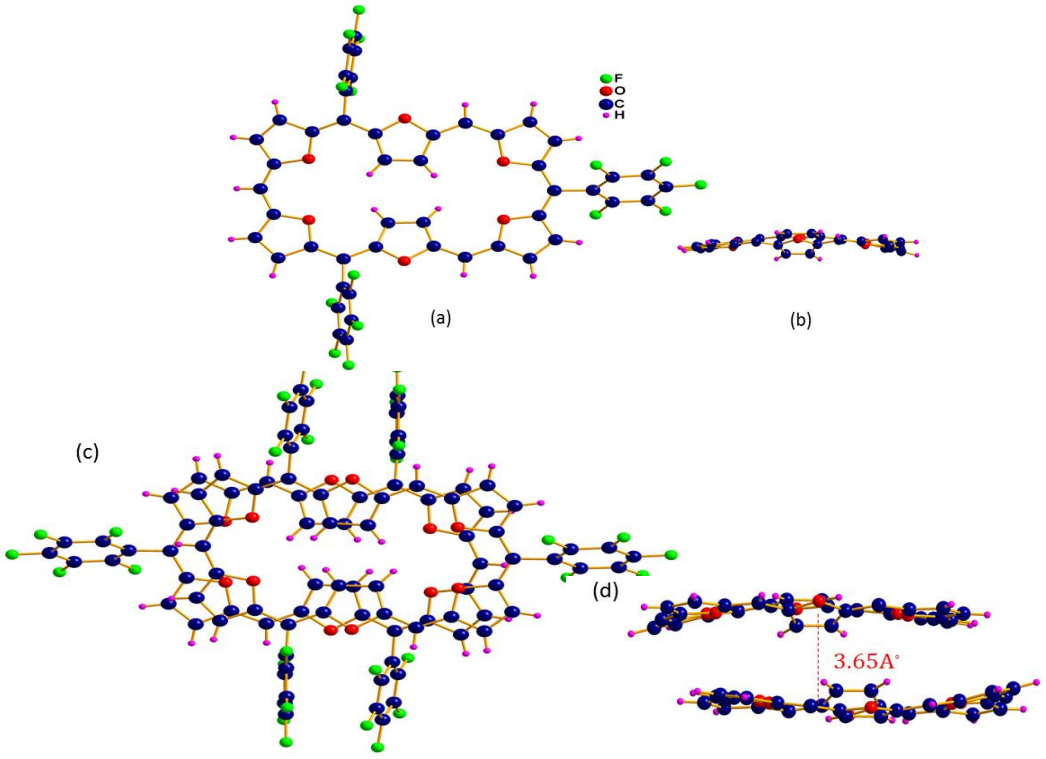

Figure 3.17. Molecular structure of (a) Top view of **III.2** (b) Side view of **III.2,** (c) Top view of intermolecular face to face head to tail π-π stacking interaction in **III.2,** (d) Side view (Pentafluorophenyl rings are omitted for clarity) of intermolecular π-π stacking interaction in **III.2.**

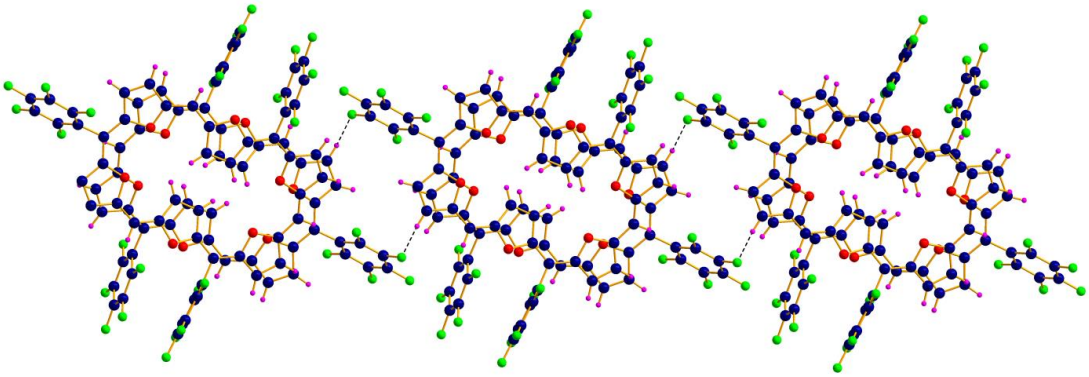

Figure 3.18. Intermolecular C-H…F weak hydrogen bonding interaction between stacked dimers in **III.2**.

Compound **III.4** was crystallized in tetrahydrofuran and its molecular structure displayed the expected D_{2h} symmetry with alternative furan ring inversion, similar to the earlier report on the 40π octafuran macrocycle (Figure 3.16).

The molecular structure of unconjugated macrocycle **III.1-H4** was also confirmed by single crystal X-ray analysis. The orientation of the furan rings did not allow the macrocycle to adopt a planar structure. This is attributed to the sp^3 carbon bridges which do not favour the flat geometry and hence the furan rings are forced to orient the oxygen atoms above and below the mean macrocyclic plane.

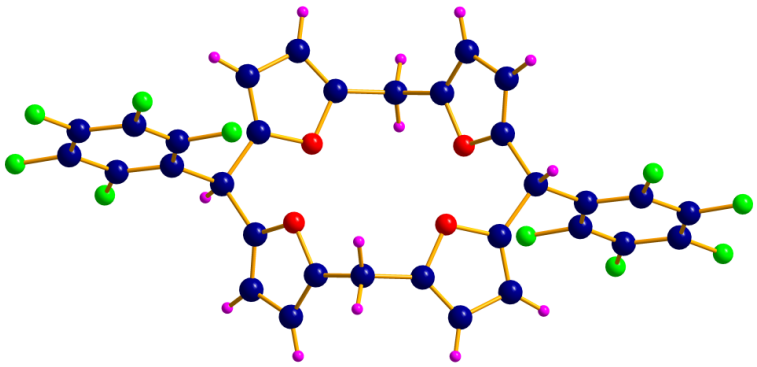

Figure 3.19. Molecular structure of **III.1-H4**.

III.5. Isophlorin-C_{60} interaction

The following experimental techniques were employed to study the nature of interaction between anti-aromatic isophlorins (**III.1** and **III.3**) and C_{60}.

a) MALDI-TOF-TOF Mass Spectrometry
b) Isothermal Titration Calorimetry
c) Fluorescence Spectroscopic Titrations
d) Single Crystal X-ray analysis

III.4. Cocrystallization of Isophlorin (III.1 or III.3) with C_{60}

The solutions of these two anti-aromatic macrocycles were individually treated with a toluene solution of C_{60}. The color of the solution displayed a distinct change from green to brown upon the addition of fullerene, suggesting the formation of the π complex. Cocrystals of isophlorins (**III.1** and **III.3**) and fullerene were grown from a combination of toluene-acetone solvents by slow evaporation method at room temperature, to yield black colored crystals.

III.4.1.a. MALDI-TOF Mass Spectrometry

As mass spectrometry is an excellent tool to observe the composition of non-covalent complexes, the cocrystals of **III.1(C_{60})** were dissolved in toluene and subjected to MALDI-TOF-TOF analysis. In its mass spectrum an *m/z* value corresponding to 1:1 ratio of **III.1(C_{60})** complex was observed at 1366.96, (Figure 3.20). This suggested C_{60} could form a fairly strong non-covalent complex with **III.1** even in gaseous state and represents the first such interaction between anti-aromatic isophlorin-C_{60} in gaseous state till date.

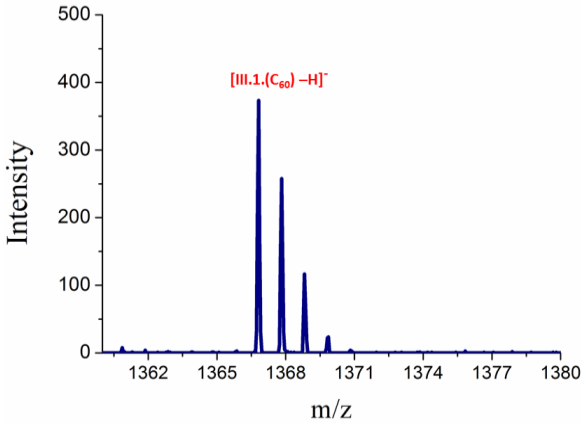

Figure 3.20. MALDI-TOF-TOF mass spectrum of molecular complex **III.1.(C_{60}).**

III.4.1.b. Isothermal Titration Calorimetry

Expecting a strong interaction between the two molecules, the binding constant between isophlorin **III.1** and **C_{60}** was estimated using isothermal titration calorimetry (ITC) and fluorescence spectroscopic titrations.

Isothermal titration calorimetry (ITC) was employed to quantify the complexations of the host (Isophlorin **III.1**) and guest (C_{60}) molecules in solution. The titration was carried out in toluene at 25°C using an isothermal titration calorimeter (Microcal iTC-200) with stirring at 1000 rpm. About 200 µl of host (**III.1**) solution was titrated with the guest (C_{60}) solution. A typical titration experiment consisted of 20 consecutive injections of 2 µl volume and 9s duration each, with a 90s interval between injections. Heat of dilution of the guest (C_{60}) were determined by injecting the guest solution into the solvent alone and the total observed heats of binding were corrected for the heat of dilution. A single set binding model fitted the binding isotherm, from where binding constant (K), binding stoichiometry (N), change of enthalpy (ΔH) and the change of entropy for the binding (ΔS) were obtained. The estimated association constant (K_a) was found to be 7.16 X 10^3 M^{-1} for **(III.1).C_{60}**.

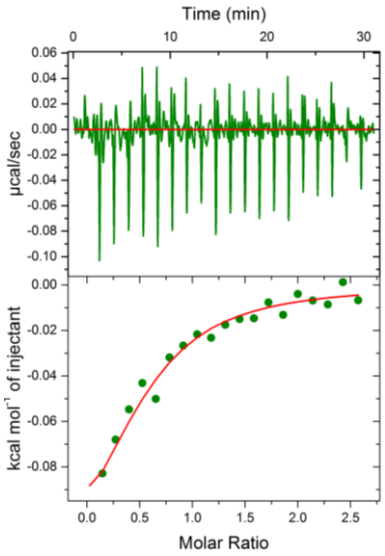

Figure 3.21. ITC profiles for the binding of guest (C_{60}) to host **III.1** at 25 °C in chloroform :toluene (1 : 1 v/v). Top: raw data for the sequential 2 µl injection of C_{60} (0.4 mM) into **III.1** (5 mM). Bottom: plot of the heat evolved (kcal) per mole of C_{60} added, corrected for the heat of C_{60} dilution, against the molar ratio of C_{60} to **III.1**. The data (filled squares) were fitted to a single set binding model and the solid line represents the best fit.

The estimated thermodynamic parameters, ΔG (-4.09 k.cal.mol^{-1}), ΔH (-0.434 k.cal.mol^{-1}), and TΔS (-3.66 k.cal.mol^{-1}), for **(III.1).C_{60}** further confirmed a strong binding between isophlorin and C_{60}.

III.4.1.c. Fluorescence Spectroscopic Titrations

The isophlorins are poor emitters compared to porphyrin. However, it was observed that even the negligible fluorescence intensity reduced upon the addition of fullerene, which can be attributed to complex formation between the two π conjugated molecules (Figure 3.22).

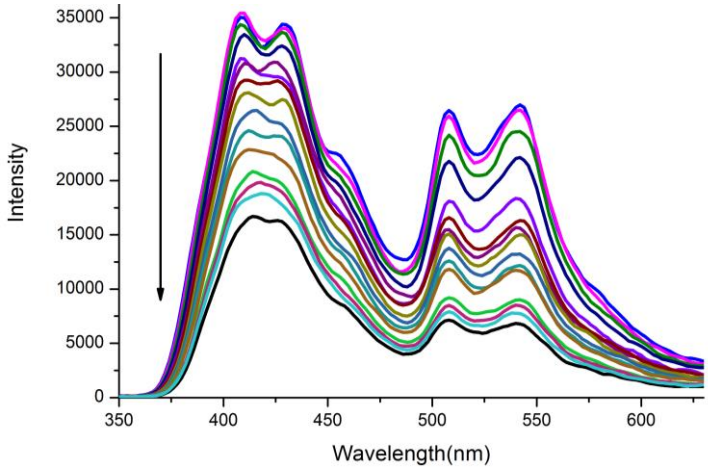

Figure 3.22. Fluorescence spectroscopic titration of Isophlorin **III.1** (1 μM, excited at 326 nm; slit = 2/3 nm) with 0−30 μM of **C_{60}**.

Benesi-Hildebrand plot for binding studies of [C_{60}] towards Isophlorin (III.1).

In order to determine the stoichiometry as well as binding constants of the non-covalent complexes, the fluorescence intensity was analyzed using Benesi-Hildebrand (BH) plot using the following equation (1).

$$\frac{1}{F\text{-}F_0} = \frac{1}{K(F_1\text{-}F_0)[host]} + \frac{1}{F_1\text{-}F_0} \qquad (1)$$

where F_0, F and F_1 are the fluorescence intensities of Isophlorin in absence, presence of host, and in the inclusion complex, respectively.

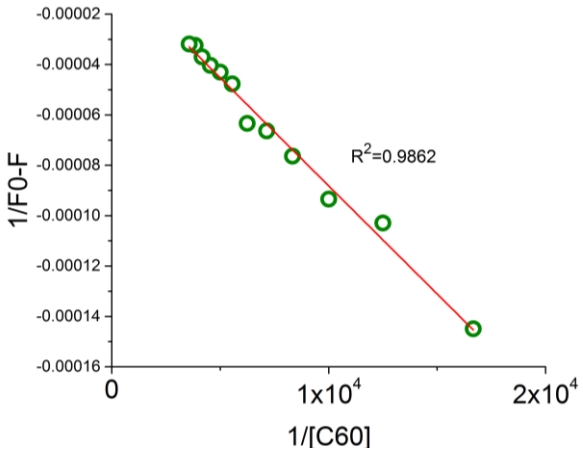

Figure 3.23. Benesi-Hildebrand plot of **III.1** (1 μM) for varying [C_{60}] (0 to 30 μM).

The fluorescence titration was conducted with λ_{Ext} = 326. A good linear fit confirmed the 1: 1 binding stoichiometry in solution and the association constant (K_a) was estimated to be 1.328 x 10^3 M^{-1}. This value further supported the results obtained from ITC measurements.

III.4.1.d. Single Crystal X-ray Diffraction analysis

Fullerene-Isophlorin Binding in Solid State

The attempts at cocrystallization with different composition of C_{60}/isophlorin in various solvents selectively yielded 1:1 ratio of isophlorin **III.1**.

Molecular complex of (III.1).C_{60}

The molecular complex of **(III.1).C_{60}** revealed a zig-zag assembly of alternating isophlorin/C_{60} interactions. The C_{60} is centred over the isophlorin **III.1** with the 5:6 ring junction carbon atoms lying over the centre of the isophlorin ring at distances of 2.64 and 2.66 Å from the 24 atoms mean macrocyclic plane of the isophlorin (Figure 3.24). The isophlorin surface was found to be extremely close to the π-surface of the fullerene, compared to standard values for π-π interactions.[13] These values are comparable to that observed between C_{60} and a free base porphyrin. The closest atom to atom contacts are from the two 5:6 fullerene carbon atoms to the isophlorin oxygen atoms, in the range between 2.96 to 4.31 Å. The *ortho*-F atoms from the *meso*-pentafluorophenyl ring were found to be at a distance of 2.98, 3.12 and 3.13 Å to the

nearest carbon atom of fullerene suggesting their significant contribution in the complexation. The angle between the isophlorin planes was found to be 32.7°. The closest carbon-to-carbon atom distance between fullerenes in adjacent chains was found to be 3.16-3.26 Å.

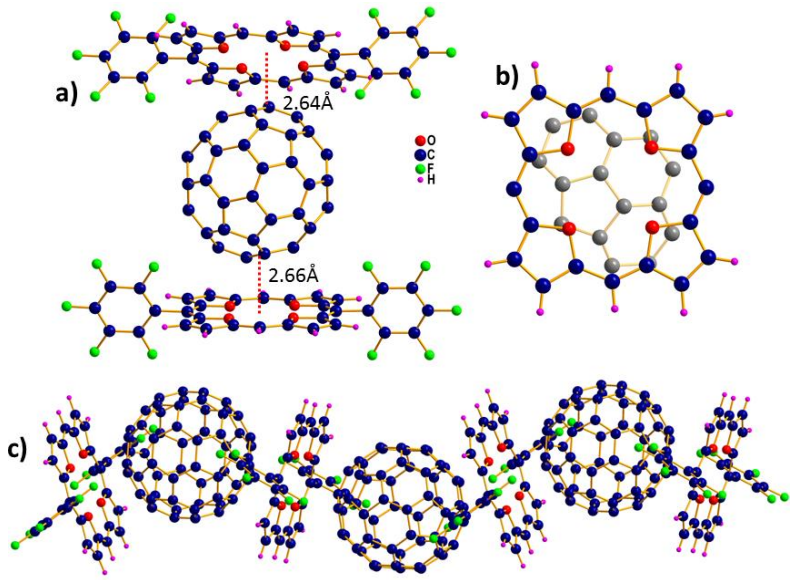

Figure 3.24. (a) Molecular structure of the **(III.1).C_{60}** complex. (b) The 5:6 ring junction carbon atoms of C_{60} lying over the centre of the isophlorin ring (c) Packing diagram in the crystal lattice of **(III.1).C_{60}** reveals a zigzag chain of alternating isophlorin and C_{60}.

In addition to close fullerene-isophlorin π-π interactions, weak C-F…H-C bonds were also observed between the C_6F_5 groups and the furan β-hydrogens of neighbouring macrocycles. No close fullerene/fullerene contacts were observed in the packing diagram for this crystal because the fullerene units were separated by toluene molecules through π stacks in a head-to-tail fashion (Figure 3.25).

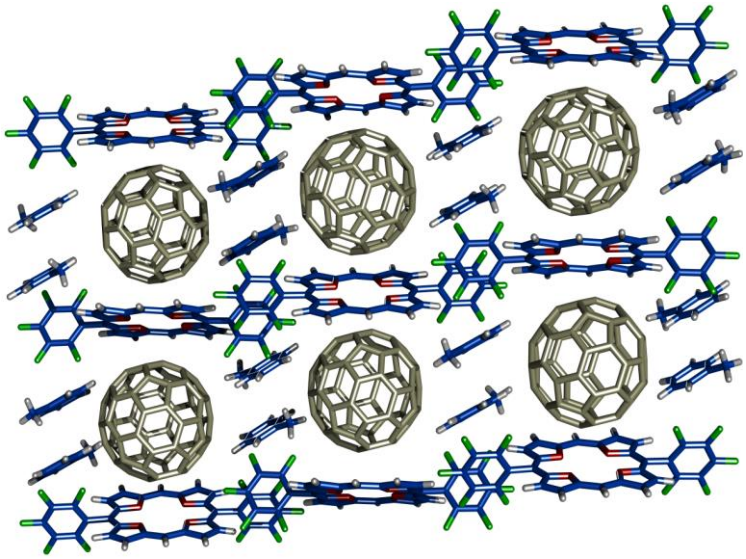

Figure 3.25. Alternate layer of isophlorin sheets (stick model) separated by C_{60} molecules (gray color) in **(III.1).C_{60}** complex. Channels between columns occupied by solvent (Toluene) molecules.

In the process of studying these interactions, serendipitous dimerization of a *meso*-unsubstituted isophlorin, **III.3**, into a *meso*,*meso*-linked isophlorin dimer, **III.5**, in the presence of C_{60}-fullerene (Scheme-3.5) was observed.

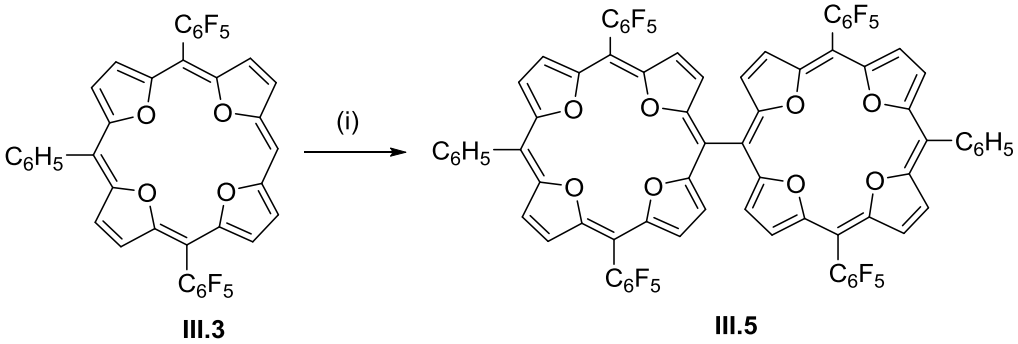

Scheme 3.5. Synthesis of 20π tetraoxa isophlorin dimer **III.5**.
Reaction conditions: (i) Cocrystallization of **III.3** with C_{60} in toluene-acetone.

III.3 forms good quality single crystals over long periods of time (more than 30 days) when cocrystallized with C_{60}-fullerene in toluene-acetone combination. The obtained crystals of **III.3.(C_{60})** were dissolved in dichloromethane and subjected to MALDI-TOF-TOF analysis. Ideally one should expect the monomeric complex in mass spectrum with two different *m*/*z* values corresponding to monomer **III.3** and the C_{60}-fullerene. But the observed unexpected mass 1446.178 was exactly double the

mass of **III.3** along with *m*/*z* values of C_{60}-fullerene, which confirmed the formation of dimeric complex **III.5.(C_{60}).** (Figure 3.26).

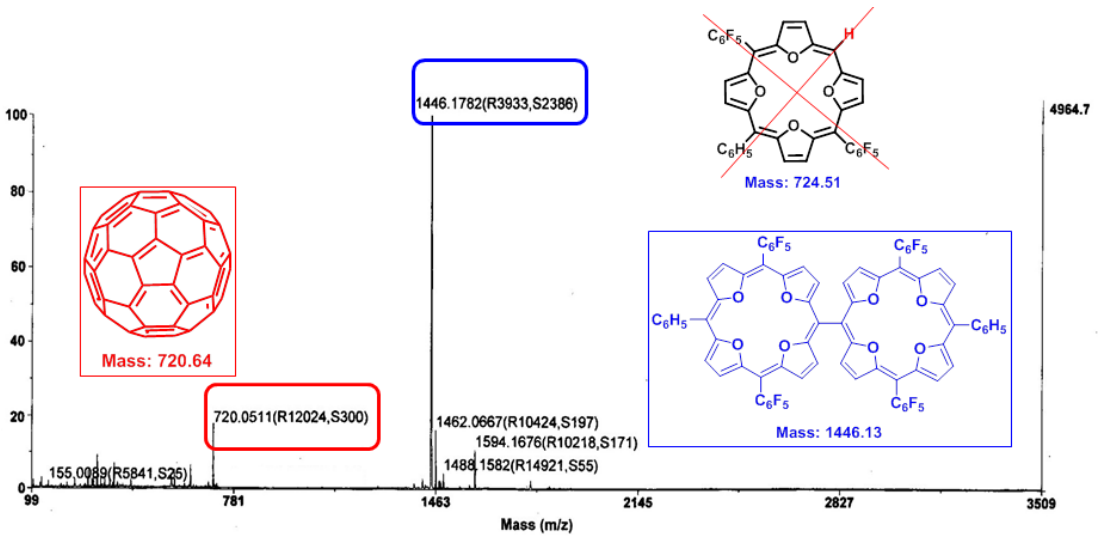

Figure 3.26. MALDI-TOF-TOF mass spectrum of **(III.3).C_{60}** cocrystals revealed two different m/z values corresponding to the dimer **III.5** and the **C_{60}**-fullerene.

X-ray diffraction analysis of these single crystals further support the formation of unexpected *meso,meso* covalent linked dimer, **III.5**, non-covalently bound to C_{60}-fullerene.

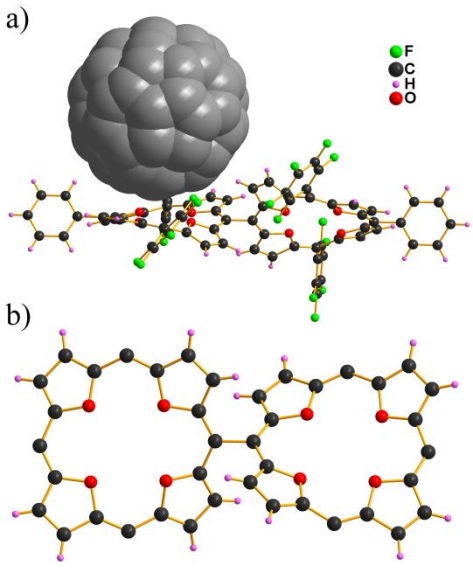

Figure 3.27. (a) Molecular structure of isophlorin dimer **III.5** with C_{60}; (b) Isophlorin dimer **III.5** (top view C_{60} and *meso* substituents omitted for clarity).

The repetition of this cocrystallization method under same conditions, instead of forming dimeric complex **III.5.(C_{60}),** lead to the formation of a monomeric complex **III.3.(C_{60}).**

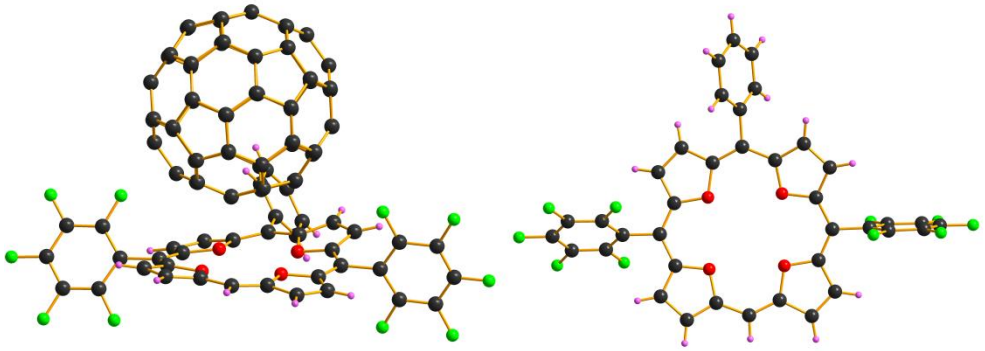

Figure 3.28. Molecular structure of isophlorin **III.3** along with C_{60} side view (left) and isophlorin **III.3** without C_{60} top view (right).

Alternatively, to enhance the rate of this slow reaction, oxidative coupling of *meso* free isophlorin **III.3** was employed in a process similar to that of *meso* free porphyrin. In this process, **III.3** was reacted with a variety of silver salts such as $AgPF_6$, $AgBF_4$ and $AgClO_4$. Surprisingly, none of these reagents could dimerize **III.3** to **III.5**. The reaction monitored through MALDI-TOF-TOF mass spectrometry revealed a minute formation of the dimer **III.5** during the initial few minutes of the reaction and no further increase in its concentration was observed over a period of 1h to 48h in toluene (Figure 3.29).

Reaction with other oxidative coupling reagents such as $FeCl_3$ or $Sc(OTf)_3$/DDQ also did not yield the desired dimer. Unfortunately, this turned out to be an inconsistent reaction with respect to its repeatability and also extremely slow to yield the desired product, **III.2**. The interest in **III.2** was chiefly to explore its electronic and redox properties as the first example of covalently coupled anti-aromatic units. Similar dimers and one-dimensional array from aromatic macrocycles such as porphyrin[14-17] and corrole[18-22] have been explored very routinely. A common observation in the synthesis of all these systems reveal oxidative coupling of aromatic macrocycle, a process comparable to the Scholl reaction.[23] The apparent success of oxidative coupling of arenes can be attributed to electron rich aromatic units as part of

the chromophoric systems. This observation encouraged to design a rational synthesis of covalently linked anti-aromatic isophlorins.

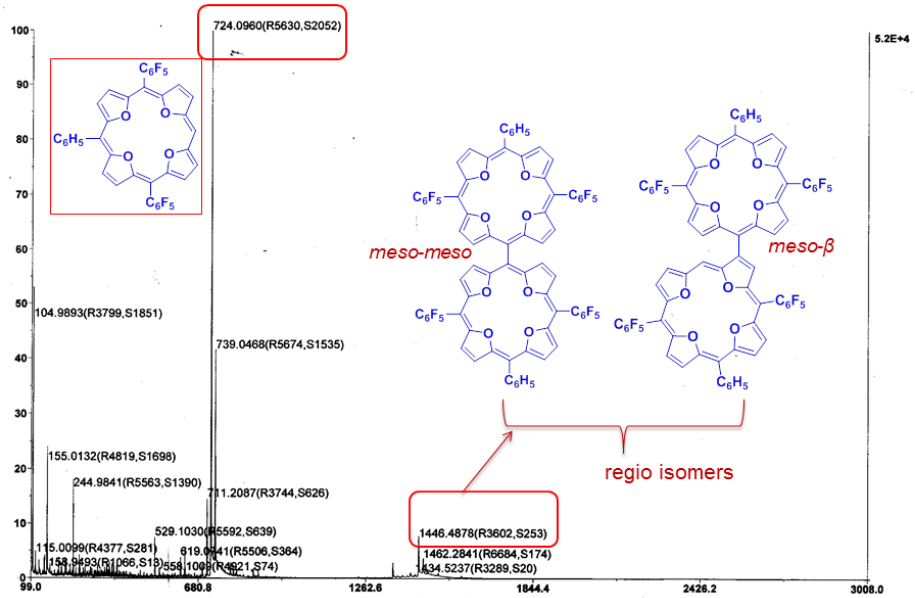

Figure 3.29. MALDI-TOF-TOF mass spectrum revealed a minute formation of the dimer **III.5**.

The effort towards the synthesis of the isophlorin dimer, **III.5,** led to a modified synthetic strategy in which tetrafuroethane[24] **5**, was reacted with two equivalents of difuromethane dicarbinol **4**, under typical MacDonald type reaction conditions (Scheme 3.6.). The reaction mixture was subjected to MALDI-TOF-TOF mass analysis. In its mass spectrum only the *m*/*z* value of 870.051 corresponding to monocyclized mass was identified instead of the expected dicyclization **III.5**. (Figure 3.30)

The failure to obtain the expected dimer could be possibly due to the non-coplanar nature of the difuran units in tetrafuroethane **5,** which probably suppressed the formation of dimer **III.5**. To ensure the possibility of dimerization, a similar reaction was attempted with tetrafuroethene **6,** instead of tetrafuroethane **5** (Scheme 3.7).

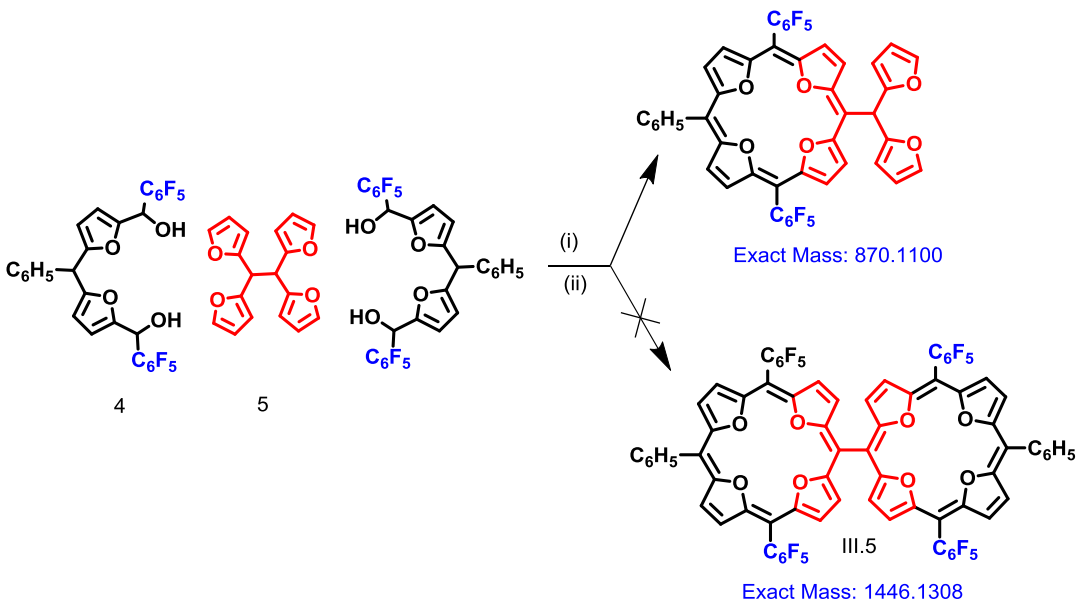

Scheme 3.6. Attempt to synthesis 20π tetraoxaisophlorin dimer **III.5**.
Reaction conditions: (i) $BF_3.OEt_2$ (1 eq.), dry DCM (100 ml), rt, N_2, 2h (ii) $FeCl_3$ (10 eq.), 1h.

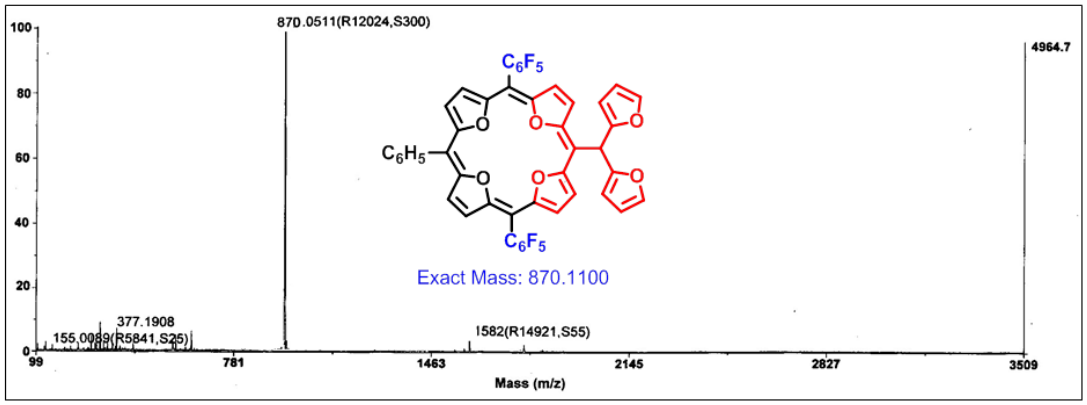

Figure 3.30. MALDI-TOF-TOF mass spectrum confirmed the formation of the monocyclized product.

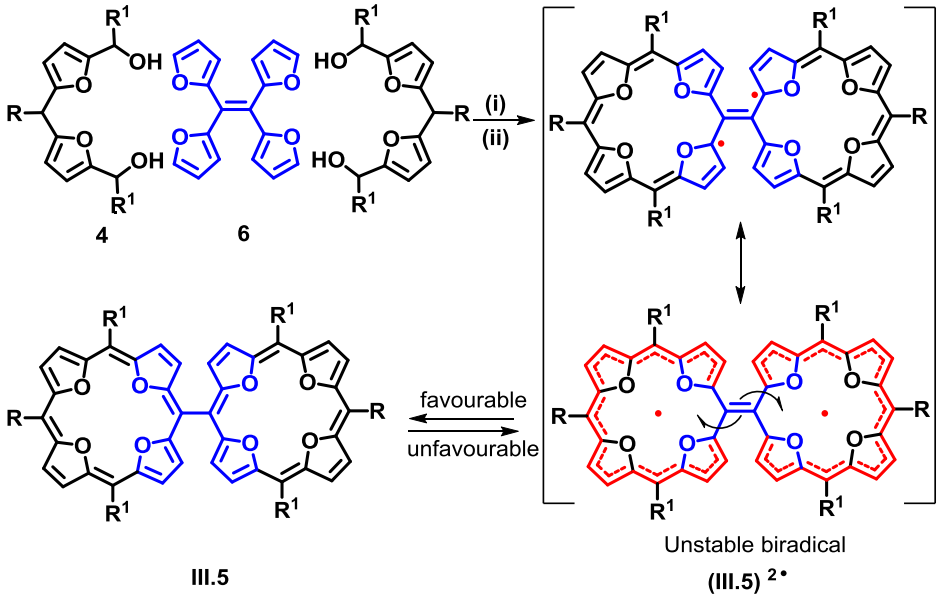

Scheme 3.7. Synthesis of *meso-meso* linked tetraoxa isophlorin dimer **III.5** through biradical intermediate $(\mathbf{III.5})^{2\bullet}$.
Reaction conditions: (i) $BF_3.OEt_2$ (1 eq.), dry DCM (100 ml), rt, N_2, 2h; (ii) $FeCl_3$ (10 eq.), N_2, 1h.

In this reaction, an *m*/*z* value 1446 corresponding to dimer **III.5** was identified in the MALDI-TOF-TOF mass spectrum supporting the cause of planar orientation of furan rings in tetrafuroethene for the facile formation of product. It was observed that **III.5** was sensitive to silica gel and deteriorates through the course of chromatographic separation. However, it could be purified in 4% yields through size exclusion chromatography. The recent reports on 19π[25] and 25π[26] neutral radicals suggested the possibility of a biradical $\mathbf{(III.5)^{2\bullet}}$ of the tetraoxa isophlorin with a rigid exocyclic double bond bridge between the *meso* positions of two individual isophlorins **III.5**. The observed high-resolution mass spectrum of **III.5** exhibited an *m*/*z* value of 1447.1387, corresponding to the calculated mass of $C_{76}H_{26}F_{20}O_8$ (*m*/*z*: 1447.1332). However, the possibility of a biradical was ruled out by its non-paramagnetic behaviour, which was supported by the absence of signal in its ESR (Electron Spin Resonance) spectrum.

The ^{1}H NMR spectrum of **III.5** displayed four doublets between δ = 1.94 - 4.28 ppm for the β-protons of the furan, while the phenyl protons resonated as a multiplet and doublet between δ = 5.80 - 6.51 ppm at room temperature in toluene-d_8. The ^{1}H-^{1}H COSY spectrum displayed two strong correlations between the signals at δ 2.26

and 1.94 ppm, and for signals at δ = 4.28 and 2.47 ppm. These coupling confirmed that four doublets in the upfield region belong to β-protons of the furan. The formation of the covalent *meso-meso* dimer **III.5** suggests the stability of anti-aromatic dimer over the biradical, $(\mathbf{III.5})^{2\bullet}$. This can be envisaged by the homolytic fission of the exocyclic double bond leading to the complete conjugation required for 20π isophlorin.

The anti-aromatic character confirmed by the upfield chemical shift values in the ^{1}H NMR spectrum was further supported by NICS calculations. The estimated NICS(0)[27] values of +30.38 ppm and +12.90 ppm for **III.3** and **III.5** respectively lends further support to paratropic ring current effects expected of 4nπ systems. The reduced anti-aromatic behavior may be attributed to the loss of planar structure upon binding the fullerene C_{60} at the centre of the macrocycle as observed earlier. Ideally **III.5** can be oxidized to a tetracation as observed in case of few tetraoxa dications.[28] Rather it exhibited a strong resistivity towards oxidation as observed for tetraoxa isophlorins.[8] Moreover, **III.5** also resisted the formation of β-β links either with $FeCl_3$ or DDQ in presence of $Sc(OTf)_3$ to yield the completely fused macrocyclic dimer.

III.5. Spectral Characterization of Anti-aromatic dimer

The dimer **III.5** was analyzed through high resolution mass spectrometry, UV-Vis, NMR spectroscopy, X-ray crystallography and cyclic voltammetric studies.

III.5.1. Electronic Absorption Studies

The isophlorins **III.3** and **III.5** displayed green colored solutions when dissolved in common organic solvents, while they were found to be dark green in solid state. The color of the solution is attributed to the extensive conjugation. The electronic absorption spectrum of **III.3** recorded in dichloromethane displayed high energy absorption at 322 nm (ε = 79800) and 357 nm (ε = 91400) followed by low energy absorptions in the region 400-500 nm. The electronic absorption spectrum of dimer **III.5** displayed a red shift with respect to the monomer **III.3**. An intense absorption similar to Soret-like band at 372 nm (ε = 103800), and Q-like bands at 436, 466 and

503nm (Figure 3.31) suggested electronic coupling between the macrocyclic units in spite of the non-coplanar orientation of the both the macrocycles.[13]

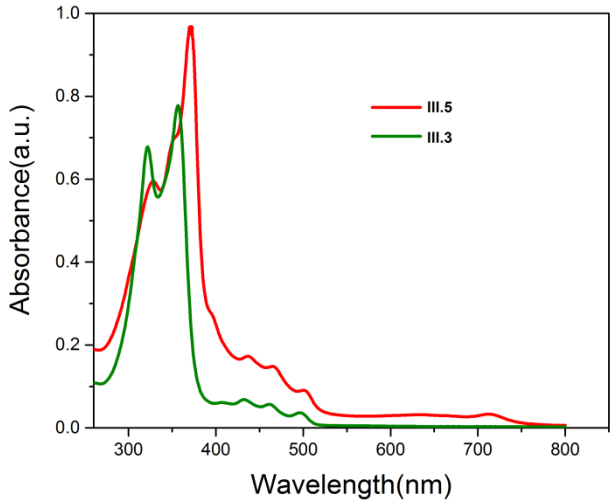

Figure 3.31. The UV-Visible absorption spectrum of **III.3** (~ 10^{-6} M) and **III.5** (~ 10^{-5} M) recorded in methylene dichloride at room temperature.

III.5.2. NMR Characterization

The ^{1}H NMR spectrum of isophlorin dimer **III.5** confirmed the paratropic ring current effects for a 4nπ anti-aromatic system because of 20π electrons along the conjugated pathway in orthogonal rings. Compound **III.5** displayed four doublets between δ = 1.94 - 4.28 ppm for the β-protons of the furan, while the phenyl protons resonated as a multiplet and doublet between δ = 5.80 - 6.51 ppm.

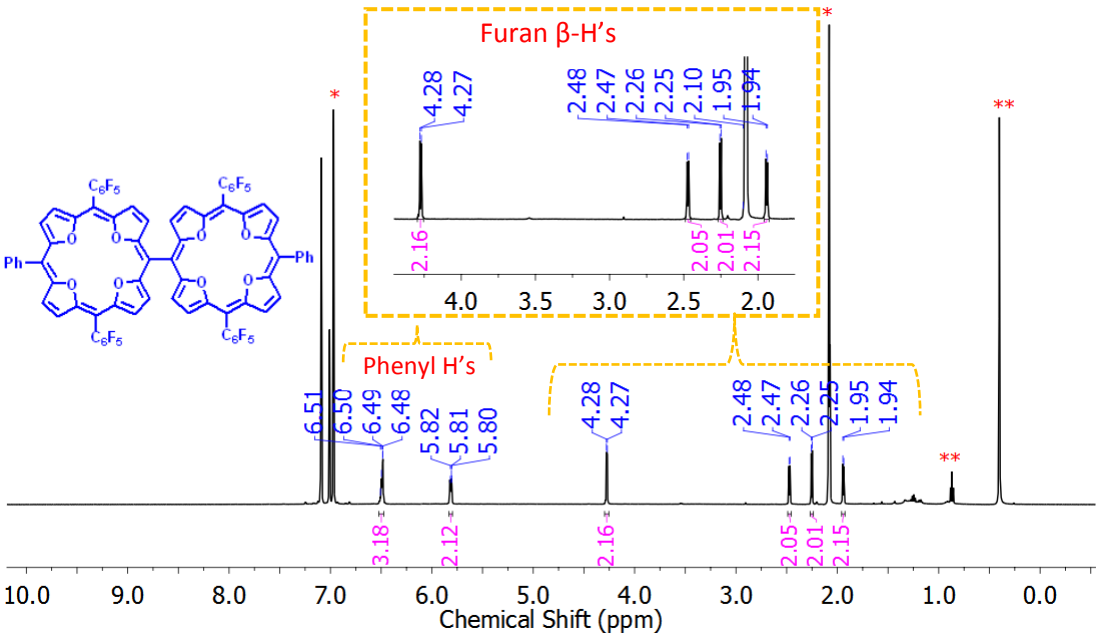

Figure 3.32. ^{1}H NMR spectrum of **III.5** in Toluene-d_8 at 298*K*, (*Toluene-d_8, **H_2O, and *n*-hexane).

The ^{19}F NMR spectrum of dimer **III.5** displayed three different signals each, indicating that three sets of fluorines (*ortho*, *meta* and *para* for perfluorophenyl rings).

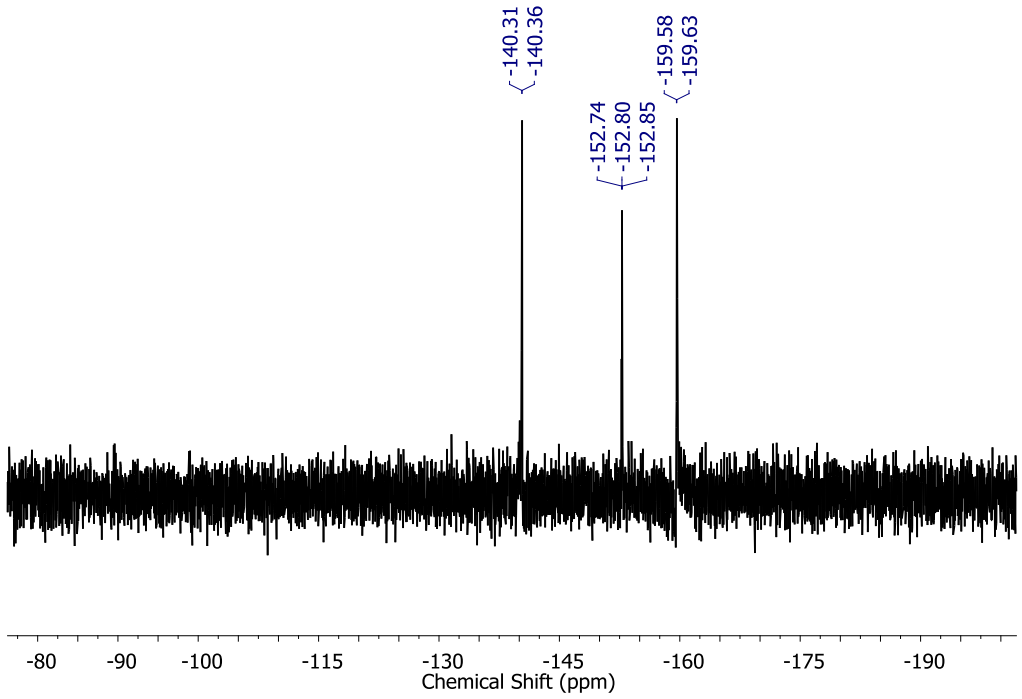

Figure 3.33. ^{19}F NMR spectrum of **III.5** in Chloroform-*d* at 298*K*

The ^{1}H-^{1}H COSY spectrum displayed two strong correlations between the signals at δ 2.26 and 1.94 ppm, and for signals at δ = 4.28 and 2.47 ppm. These coupling confirmed that four doublets in the upfield region correspond to β-protons of the furan. The NOE experiment for **III.5** displayed spatial interaction between *ortho*-protons of *meso*-phenyl groups and the adjacent β-hydrogens of the furan ring.

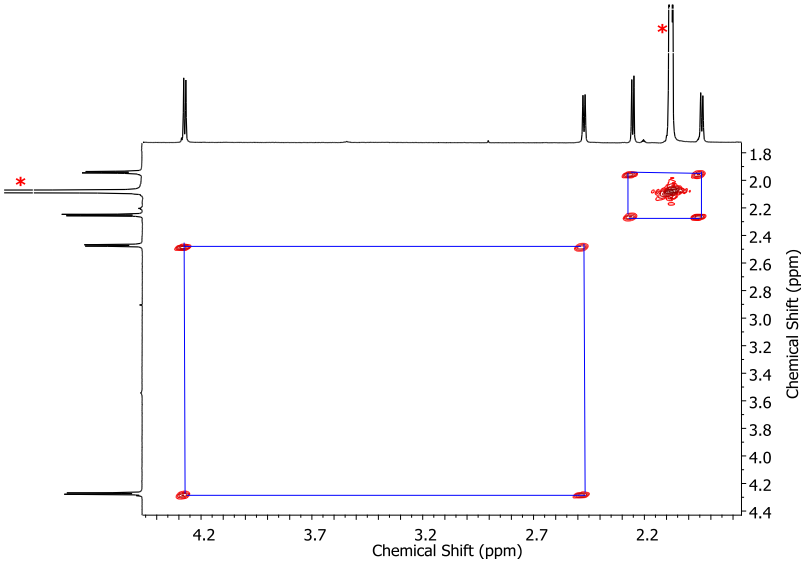

Figure 3.34. ^{1}H-^{1}H COSY spectrum of **III.5** in Toluene-d_8(*) at 298K

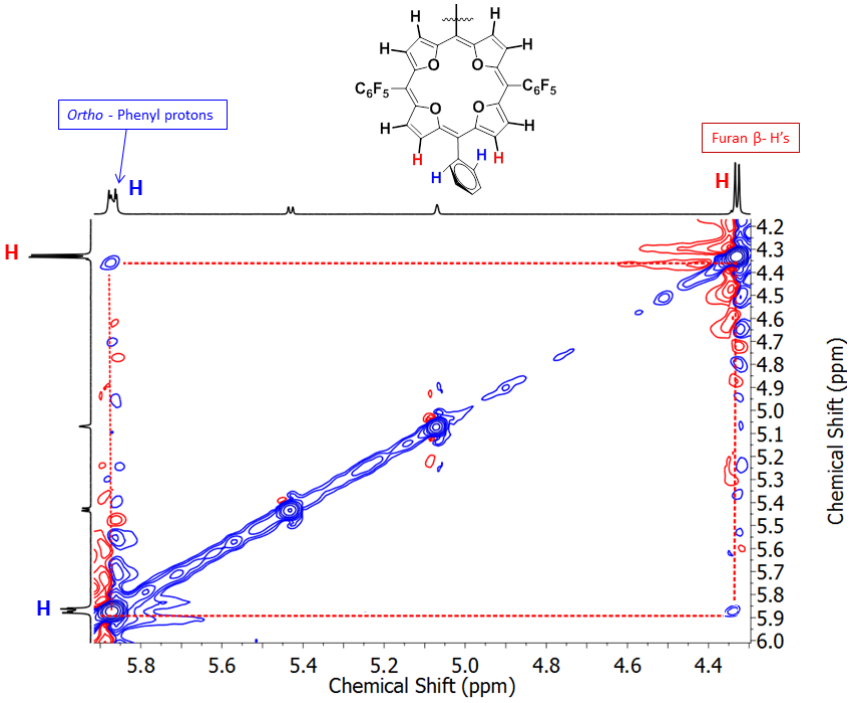

Figure 3.35. NOESY spectrum of **III.5** in Toluene-d_8 at 298K

III.5.3. Single Crystal X-ray Diffraction Studies

The structure of **III.5** was confirmed by single crystal X-ray analysis (Figure 3.35). Attempts to crystallize dimer **III.5** with various organic solvents did not yield good quality single crystals. Finally, C_{60} was utilized as a cocrystallizing agent. The solution of dimer **III.5** was individually treated with a toluene solution of C_{60}-fullerene and allowed to crystallize by slow evaporation method at room temperature to yield black colored crystals. As observed for other tetraoxa isophlorins, dimer **III.5** also exhibited a flat geometry with very close contacts (2.58 and 2.61 Å) between its π-surface and curved surface of C_{60}.

Figure 3.36 displays the solid-state structure of compound **III.5** to confirm the *meso-meso* link expected in the dimer. The near co-planar structure of the bis-furan units that was sustained in the precursor, **6**, was disrupted upon the formation of the dimer. It was much evident from the change in the bond distance from 1.376 Å in **6** to 1.487 Å in **III.5**. Further, the macrocycles were found to make an angle of 35.57˚ in support of the single bond nature of the *meso-meso* link between the two macrocycles. The macrocycles were found to bind fullerene through uncommon short π-π interactions (2.70, 2.78, and 2.93 Å) between its surface and the curved surface of the spheroid.

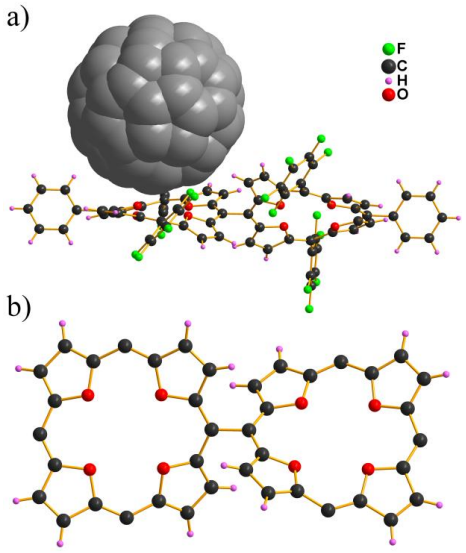

Figure 3.36. (a) Molecular structure of isophlorin dimer **III.5** with C_{60}; b) Isophlorin dimer **III.5** (top view C_{60} and *meso* substituents omitted for clarity).

III.5.4. Cyclic Voltammetric Studies

Cyclic voltammetric studies of **III.3** and **III.5** exhibited reversible redox nature. Compound **III.3** exhibited three reduction waves at -1.55 V, -1.26 V, -1.75 V and two oxidation waves in the region between at +0.22 V to +0.65 V (Figure 3.38). Similarly, compound **III.5** exhibited multiple reduction waves in the region between -1.80 to -1.04 V and three oxidation waves at +0.27 V, +0.36, +0.62 V (Figure 3.37) .

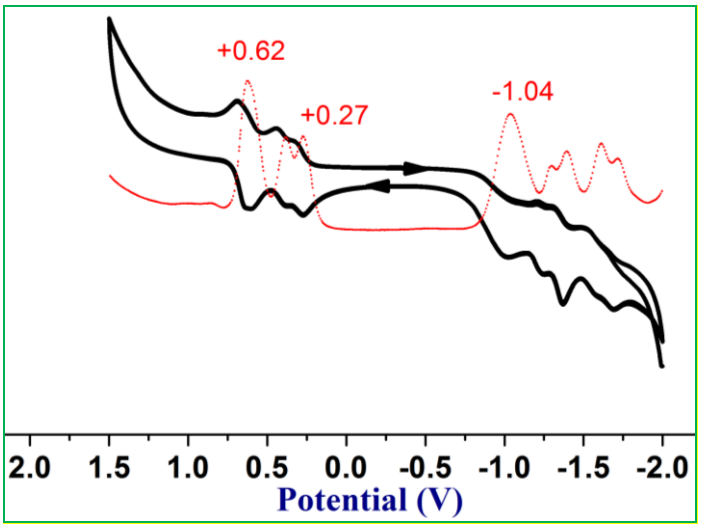

Figure 3.37. Cyclic (black) and Differential Pulse (red) voltammograms of **III.5** in dichloromethane containing 0.1 M tetrabutylammonium perchlorate as the supporting electrolyte recorded at a 50 mV s^{-1} scan rate. Reference electrode: Ag/Ag+; Working electrode: Glassy carbon; Counter electrode: Pt.

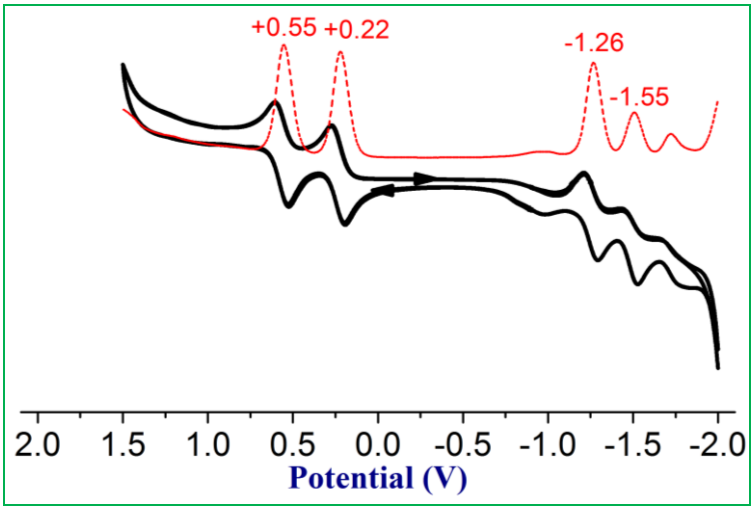

Figure 3.38. Cyclic (black) and Differential Pulse (red) voltammograms of **III.3** in dichloromethane containing 0.1 M tetrabutylammonium perchlorate as the supporting electrolyte recorded at a 50 mV s^{-1} scan rate. Reference electrode: Ag/Ag+; Working electrode: Glassy carbon; Counter electrode: Pt.

III.6. Quantum Mechanical Calculations

Quantum mechanical calculations were performed with the Gaussian09[29] program. All calculations were carried out by Density functional theory (DFT) with Becke's three-parameter hybrid exchange functional and the Lee-Yang-Parr correlation functional (B3LYP) and 6-31G(d,p) basis set for all the atoms were employed in the calculations. The molecular structures obtained from single crystal analysis were used for geometry optimization. To verify the optimized structures, frequency calculations were performed where no imaginary frequency was found. To simulate the steady-state absorption spectra, the time-dependent TD-DFT calculations were employed on the optimized structures. Molecular orbital contributions were determined using GaussSum 2.2 program package. The global ring centres for the NICS (0) values were designated at the non-weighted mean centres of the macrocycles. The NICS (0) value was obtained with gauge independent atomic orbital (GIAO) method based on the optimized geometries.

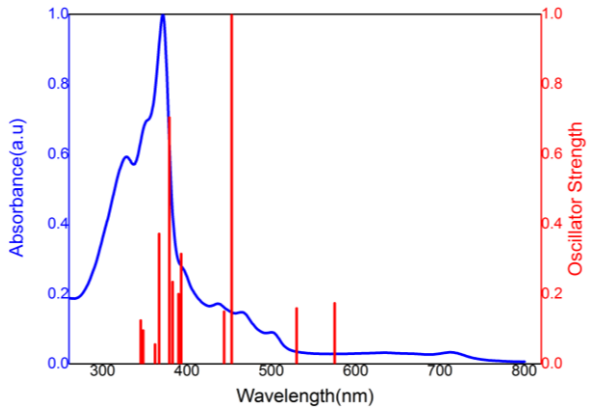

Energy (cm-1)	Wavelength (nm)	Osc. Strength(f)	Major contribtions
12402.47312	806.2908021	0.2584	H-1->L+1 (80%), HOMO->LUMO (19%)
17362.01056	575.97016	0.1731	HOMO->L+2 (89%)
18840.43504	530.7733064	0.1584	H-2->L+1 (15%), H-1->L+2 (32%), HOMO->L+3 (45%)
22038.44544	453.752513	1.0239	H-2->LUMO (65%), H-1->L+3 (15%)
22501.41088	444.416577	0.1489	H-4->LUMO (14%), H-3->LUMO (47%), H-2->L+1 (32%)
25431.64336	393.2109246	0.3142	H-5->L+1 (11%), H-4->LUMO (17%), H-1->L+6 (11%), HOMO->L+7 (33%)
25592.95536	390.7325223	0.1997	H-4->L+1 (41%), H-1->L+7 (12%), HOMO->L+6 (37%)
26062.37328	383.6949111	0.2338	H-5->L+1 (69%), HOMO->L+7 (14%)
26374.512	379.1539347	0.7043	H-4->L+1 (36%), HOMO->L+6 (31%)
27189.94416	367.7830282	0.3715	H-4->LUMO (19%), H-2->L+1 (10%), HOMO->L+7 (39%)
28984.54016	345.0115111	0.1238	H-1->L+11 (17%), HOMO->L+12 (49%)

Figure 3.39. Selected TD-DFT (B3LYP/6-31G(d,p)) calculated energies, oscillator strengths and compositions of the major electronic transitions of **III.5** in DCM at 10^{-5}M.

The estimated NICS (0) value of +39.38 ppm for isophlorin **III.1** is amongst the highest reported positive value for any anti-aromatic macrocycle.

Macrocycle	NICS(0) ppm	Huckel 4nπ rule
III.1	+39.38	Antiaromatic
III.3	+30.38	Antiaromatic
III.5	+12.90	Antiaromatic

Table 1. Computational parameters to classify ring current effects in 20π monomer **III.3** and dimer **III.5** determined from NICS calculations.

III.7. Conclusion

In conclusion, this chapter describes the crucial role of *meso* substituents in isophlorins in binding the C_{6o} fullerene. Less number of substituents enhanced the binding strength as observed from mass spectrometry and ITC titrations. At the same time, the reactivity of *meso* free isophlorins has also been explored for the first time. It appears that *meso* unsubstituted isophlorins are very reactive and perhaps leads to reactive radical species. In this process, the first synthesis of a covalent dimer of an anti-aromatic molecule was discovered. It is apparent that conventional oxidative coupling reactions may not be successful with 4nπ systems and novel methodologies need to be explored for their functionalization. The anti-aromatic property of these molecules remains the same as that of the monomer as the dimer **III.5** resisted chemical oxidation to the expected tetracations with routine oxidizing agents.

III.8. Experimental Section

Synthetic procedure for III.1

To a solution of **III.1-H4** (100 mg, 1.39 mmol) in 20 ml of dichloromethane was added a solution of DDQ (136 mg, 5.7 mmol) in 50 ml of dichloromethane. Upon mixing the two solutions, a black precipitate formed immediately. To this 10 ml of hydrazine (95%) was added. After boiling for 10 min, the reaction mixture was passed through a short basic alumina column and further purified by recrystallization in *n*-hexane-dichloromethane combination. A green color solid was identified as **III.1** (20mg) in 20% yield.

^{1}H NMR (400 MHz, (Acetone-d_6): δ 2.16 (d, *J* = 4.8 Hz, 4H), 1.81 (d, *J* = 4.6 Hz, 4H), -0.38 (s, 2H); **UV-vis** (CH_2Cl_2): $\lambda_{max}(\varepsilon)$ L mol^{-1} cm^{-1}: 348 nm (112200), 318 nm (97900); **HR-MS** (ESI-TOF): *m/z*: Calcd. for $C_{32}H_{10}F_{10}O_4$: 648.0419; observed: 648.0419 (100.0%, M+); **Crystal data:** $C_{32}H_{10}F_{10}O_4$ (Mr = 648.40), monoclinic, space group $P2_1/c$, a = 14.649(4), b = 10.269(3), c = 8.425(2) Å, α = 90.00° β = 99.013(6)° γ = 90.00°, V = 1251.7(6)Å^3, Z = 2, T = 100(2) K , D_{calcd} = 1.720 Mg/m^3, R_1 = 0.0497 (I>2s(I)), R_w (all data) = 0.0380, GOF = 1.035.

Synthetic procedure for III.1-H4.

A mixture of *meso* free difuromethane **3**, (400 mg, 2.7 mmol) and the pentafluoro benzaldehyde, (0.32 ml, 2.7 mmol) were stirred in 500 ml dry dichloromethane. The solution was bubbled with argon for 10 min. $BF_3.OEt_2$ (0.33 ml, 2.7 mmol) was added under dark, and the resulting solution was stirred for 3h. A few drops of triethylamine were then added and the reaction mixture passed through a short basic alumina column. This mixture was further separated by silica gel column chromatography by using 1% ethylacetate / *n*-hexane as eluent. A white color solid obtained as **III.1-H4** (160mg) in 2% yield.

^{1}H NMR (400 MHz, $CDCl_3$): δ 6.04 (d, *J* = 3.0 Hz, 4H), 5.98 (d, *J* = 2.8 Hz, 4H), 5.79 (s, 2H), 3.87 (s, 4H); **HRMS** *m/z*: calcd. For $C_{32}H_{14}F_{10}O_4Na^+$: 675.0625; Observed: 675.0625 (100.0% $(M+Na)^+$); **Crystal data** $C_{33}H_{14}F_{10}O_4$, (Mr = 652.43), monoclinic, space group $P2_1/c$ (no. 14) , a = 13.963(15) Å, b = 6.282(7) Å, c = 15.787(17) Å, α = 90.00° β = 106.758(18)°. γ = 90.00°, V = 1326(3) Å^3, Z = 2, T = 296(2) K ,D_{calcd} = 1.634 Mg/m^3, R_1 = 0.1021 (I>2s(I)), R_w (all data) = 0.3161, GOF = 1.795.

Synthetic procedure for III.5

A mixture of tetrafuroethene **6**, (146 mg, 0.5 mmol) and the difuromethanediol **4**, (616 mg, 1 mmol) were stirred in 100 ml dry dichloromethane. The solution was bubbled with argon for 10 min. $BF_3.OEt_2$ (60µl, 0.5 mmol) was added under dark, and the resulting solution was stirred for 2h. After adding ten equivalents of $FeCl_3$ under inert atmosphere, solution was stirred for additional one hour. The reaction mixture was passed through a short basic alumina column. This mixture was separated by repeated size exclusion column chromatography by using toluene as eluent. A brown color band obtained was identified as **III.5** in 30mg, 4.1% yield.

^{1}H NMR (500 MHz, Toluene-d_8): δ 6.49(dd, *J* = 9.0, 3.2Hz, 3H), 5.81 (dd, *J* = 7.5, 2.3 Hz, 2H), 4.27 (d, *J* = 4.8 Hz, 2H), 2.47 (d, *J* = 4.8 Hz, 2H), 2.25 (d, *J* = 4.8 Hz, 2H), 1.94 (d, *J* = 4.8 HZ, 2H); **^{19}F NMR** (376 MHz, Chloroform-*d*): δ -140.31 (d), -152.82 (t), -159.61 (d); **UV-Vis** (CH_2Cl_2): $\lambda_{max}(\varepsilon)$ L mol^{-1} cm^{-1}: 371 nm (103822); **HRMS:** *m/z*: Calcd. for $C_{38}H_{14}F_{10}O_4$: 1447.1386; observed: 1447.1332 (100.0%, M+H). **Crystal data:** $C_{76}H_{26}F_{20}O_8$, 2(C_{61}) (Mr = 2912.19), cubic, space group F d -3 (no. 203) , a = 57.756(6) Å, b = 57.756(6) Å, c = 57.756(6) Å, α = 90.00° β = 90.00° γ = 90.00°, V = 192656(58) Å^3, Z = 112, T = 100(2) K , D_{calcd} = 1.205g cm^{-3}, R_1 = 0.1296 (I>2s(I)), R_w (all data) = 0.1940, GOF = 1.557.

Synthetic procedure for III.3

A mixture of *meso* free difuromethane **3**, (148 mg, 1 mmol) and the difuromethane dicarbinol **4**, (616 mg, 1 mmol) were stirred in 100 ml dry dichloromethane. The solution was bubbled with argon for 10 min. $BF_3.OEt_2$ (0.12 ml, 1 mmol) was added under dark, and the resulting solution was stirred for 2h. After adding five equivalents of DDQ under inert atmosphere, solution was stirred for additional one hour. The reaction mixture was passed through a short basic alumina column. This mixture was separated by repeated size exclusion column chromatography by using toluene as eluent. A brown color band obtained was identified as **III.3** in 60 mg 8% yield.

^{1}H NMR (400 MHz, Toluene-d_8): δ 6.57 (s, 3H), 5.93 (d, *J* = 1.3 Hz, 2H), 2.23 (t, *J* = 5.1 Hz, 2H), 2.13 (dd, *J* = 10.2, 4.5 Hz, 2H), 1.91 – 1.86 (m, 2H), 1.82 (t, *J* = 5.1 Hz, 2H), -0.36 (s, 1H): **^{19}F NMR** (376 MHz, Chloroform-*d*): δ -140.79 (d, J = 21.6 Hz), -153.94 (t, *J* = 21.7 Hz), -160.41 (t, *J* = 21.1 Hz); **UV-Vis** (CH_2Cl_2): $\lambda_{max}(\varepsilon)$ L mol^{-1} cm^{-1}: 357 nm (91411), 322 nm (79800); **HRMS:** *m/z*: Calcd. for $C_{38}H_{14}F_{10}O_4$: 724.0732; observed: 724.0725 (100.0%, M^+); **Crystal data** $C_{38}H_{14}F_{10}O_4$, (C_{60}) (Mr = 1445.09), orthorhombic, space group F d d 2 (no. 43) , a = 35.203(6), b = 55.389(9), c = 12.2274(19)Å, α = 90.00° β = 90.00° γ = 90.00°, V = 23842(7)Å^3, Z = 16, T = 100(2) K , D_{calcd} = 1.610 Mg/m^3, R_1 = 0.0678 0.0408 (I>2s(I)), R_w (all data) = 0.1225, GOF = 0.971.

Synthetic procedure for 6.

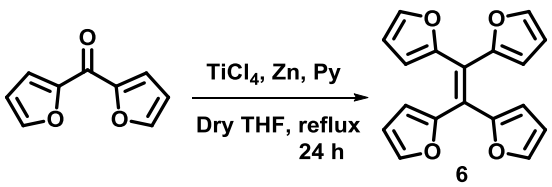

6

To a mixture of Zn dust (19.26g) in dry THF (200 ml) $TiCl_4$ (16.4 ml, 150 mmol) was carefully added and argon was bubbled through it. The resulting black slurry was refluxed for 2 hrs, then add pyridine 11.78ml at room temperature and again reflux 1h. A solution of difuryl ketone[30] (2 g, 12 mmol) in THF (100 ml) was added drop wise to the black slurry and the resulting mixture was refluxed for 12 h. The reaction mixture was cooled to 0 °C and quenched by the addition of distilled water (200 ml). The organic phase was extracted in $CHCl_3$, washed with water and concentrated under reduced pressure. The compound **6** was purified by column chromatography on silica gel (100-200 Mesh) eluted with *n*-hexane yielded in 20%.

^{1}H NMR (400 MHz, $CDCl_3$): δ 7.33 (d, *J* = 2.0 Hz, 4H), 6.42 (d, *J* = 2.0 Hz, 4H), 6.28 (m, 4H); **HRMS** *m/z*: Calcd. for $C_{18}H_{12}O_4$: 293.0814; observed: 293.0811 (100.0%, M+); **Crystal data** $C_{18}H_{12}O_4$, (Mr = 292.28), monoclinic, space group C2/c (no. 15) , a = 21.876(3) Å, b = 22.174(3) Å, c = 15.3753(18) Å, α = 90.00° β = 130.230(4)°. γ = 90.00°, V = 5694.2(12) Å^3, Z = 16, T = 100(2) K, D_{calcd} = 1.364 Mg/m^3, R_1 = 0.0532 (I>2s(I)), R_w (all data) = 0.0791, GOF = 1.222.

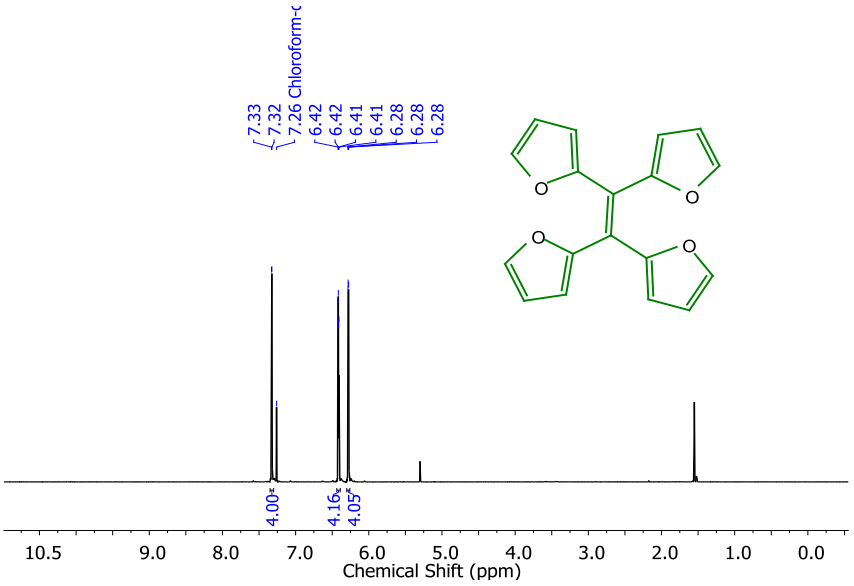

Figure 3.40. ^{1}H NMR spectrum of **6** in Chloroform-*d*at 298*K*.

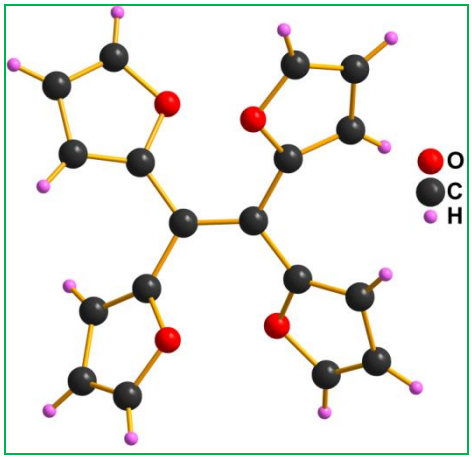

Figure 3.41. Molecular structure of **6.**

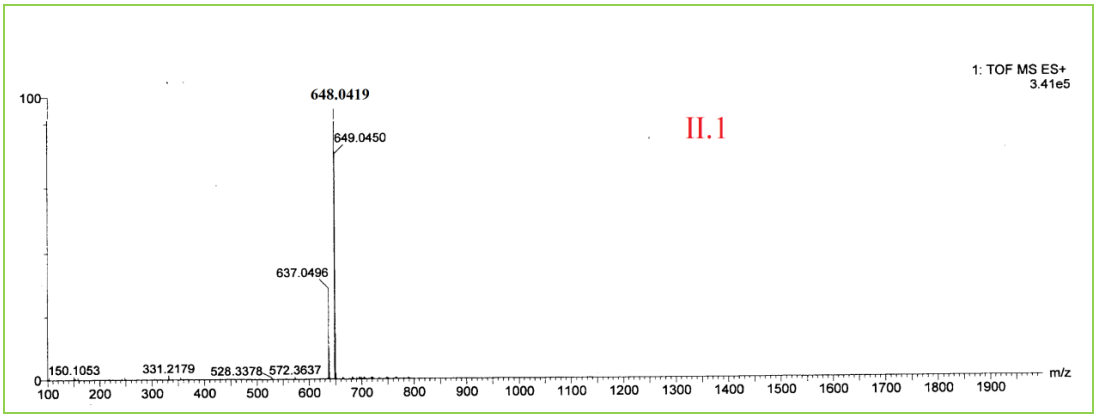

Figure 3.42. HR-ESI-TOF mass spectrum of **III.1.**

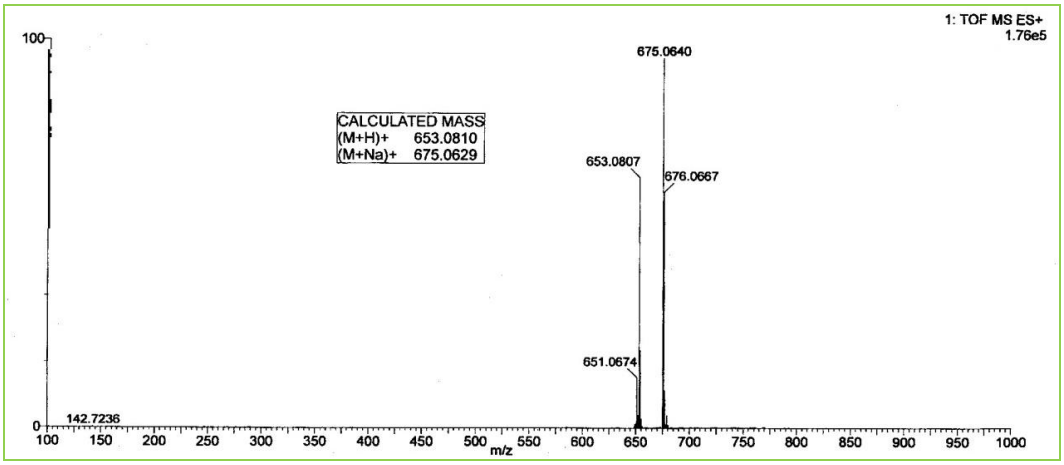

Figure 3.42. HR-ESI-TOF mass spectrum of **III.1-H4.**

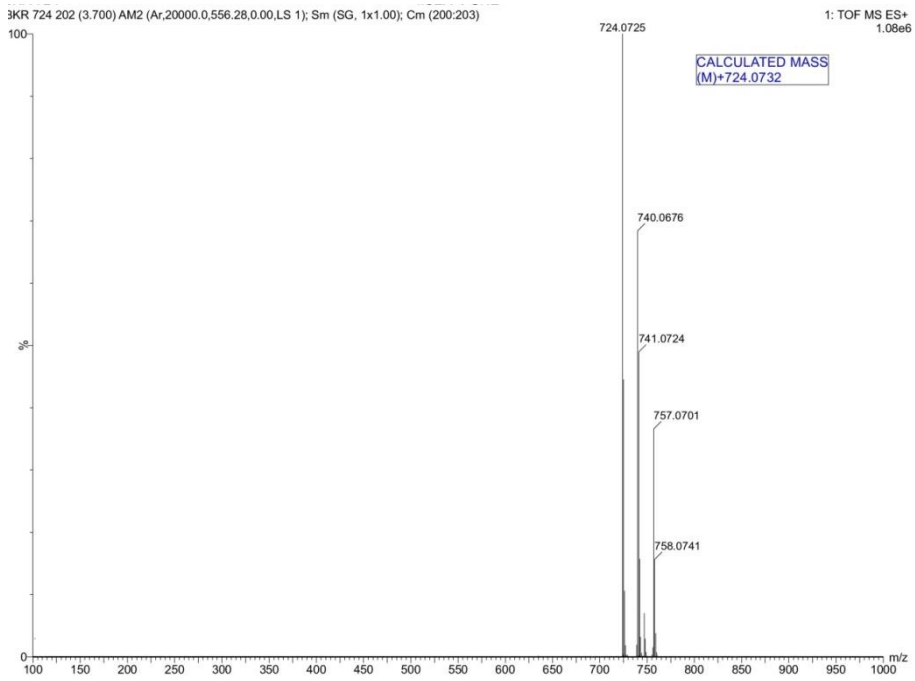

Figure 3.43. HR-ESI-TOF mass spectrum of III.3

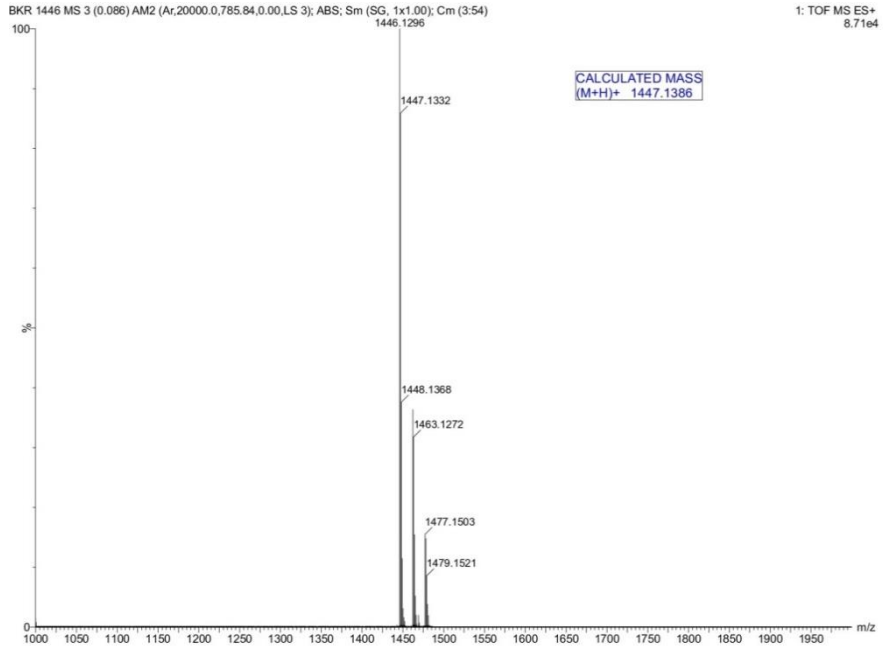

Figure 3.44..HR-ESI-TOF mass spectrum of III.5.

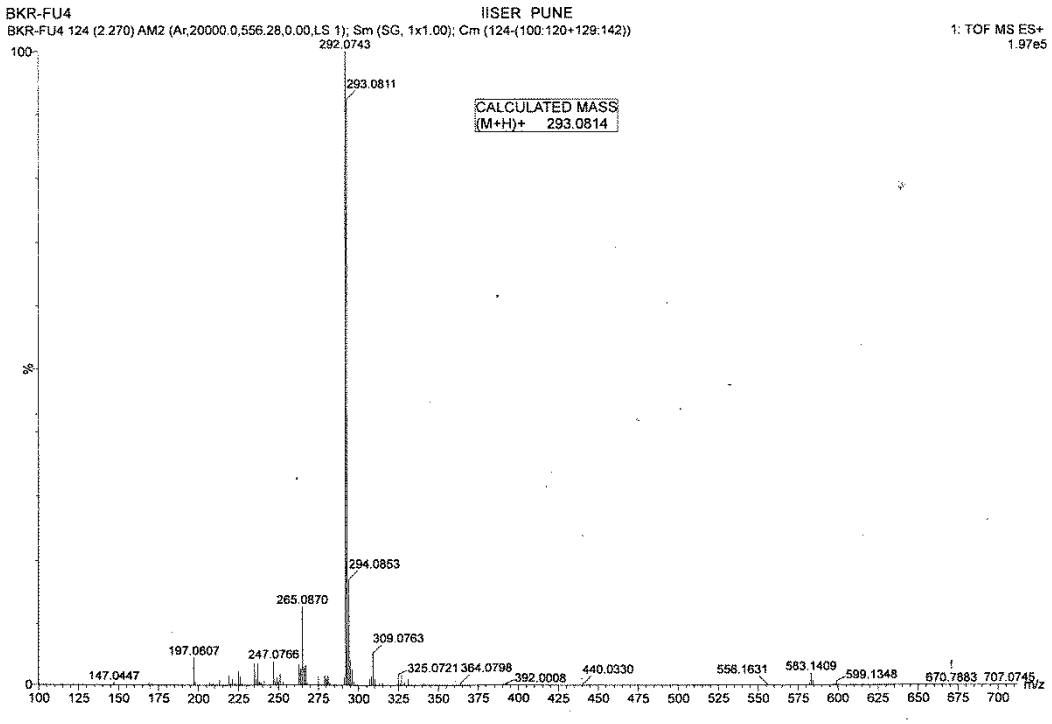

Figure 3.45. HR-ESI-TOF mass spectrum of 6.

III.9. References

[1]. T. J. J. Müller and U. H. Bunz, in *Functional Organic Materials: syntheses, strategies and applications;*, Wiley-VCH **2007**.

[2]. P. M. Beaujuge and J. M. J. Fréchet, *J. Am. Chem. Soc.*, **2011**, *133*, 20009-20029.

[3]. R. Breslow, *Acc. Chem. Res.*, **1973,** *6*, 393-398.

[4]. R. Breslow, B. Jaun, R. Q. Kluttz and C.-z. Xia, *Tetrahedron*, **1982**, *38*, 863-867.

[5]. P. J. Garratt, *Aromaticity*, Wiley:, New York, 1986.

[6]. E. Clar, C. T. Ironside and M. Zander, *J. Chem. Soc.*, **1959**, 142-147.

[7]. R. Bachmann, F. Gerson, G. Gescheidt and E. Vogel, *J. Am. Chem. Soc.*, **1992**, *114*, 10855-10860.

[8]. J. S. Reddy and V. G. Anand, *J. Am. Chem. Soc.*, **2008**, *130*, 3718-3719.

[9]. M. Kon-no, J. Mack, N. Kobayashi, M. Suenaga, K. Yoza and T. Shinmyozu, *Chem. Eur. J.*, **2012**, *18*, 13361-13371.

[10]. B. K. Reddy, S. C. Gadekar and V. G. Anand, *Chem. Commun.*, **2015**, *51*, 8276-8279.

[11]. Z. Hu, J. L. Atwood and M. P. Cava, *J. Org. Chem.*, **1994**, *59*, 8071-8075; b) M. E. Schwenter, P. Vogel, *Chemistry – A European Journal* **2000**, *6*, 4091.

[12]. R. Breslow, B. Jaun, R. Q. Kluttz, C.-z. Xia, *Tetrahedron* **1982**, *38*, 863.

[13]. a) P. D. W. Boyd, M. C. Hodgson, C. E. F. Rickard, A. G. Oliver, L. Chaker, P. J. Brothers, R. D. Bolskar, F. S. Tham, C. A. Reed, *Journal of the American Chemical Society* **1999**, *121*, 10487-10495; b) P. D. Boyd, C. A. Reed, *Acc Chem Res* **2005**, *38*, 235-242; c) A. Hosseini, M. C. Hodgson, F. S. Tham, C. A. Reed, P. D. W. Boyd, *Crystal Growth & Design* **2006**, *6*, 397-403.

[14]. A. Osuka and H. Shimidzu, *Angew. Chem., Int. Ed.*, **1997,** *36*, 135-137.

[15]. A. Tsuda and A. Osuka, *Science*, **2001**, *293*, 79-82.

[16]. H. Mori, T. Tanaka, S. Lee, J. M. Lim, D. Kim and A. Osuka, *J. Am. Chem. Soc.*, **2015,** *137*, 2097-2106.

[17]. N. Fukui, H. Yorimitsu, J. M. Lim, D. Kim and A. Osuka, *Angew. Chem., Int. Ed.*, **2014**, *53*, 4395-4398.

[18]. B. Koszarna and D. T. Gryko, *Chem. Commun.,* **2007**, 2994-2996.

[19]. S. Ooi, T. Tanaka, K. H. Park, S. Lee, D. Kim and A. Osuka, *Angew. Chem., Int. Ed.,* **2015**, *54*, 3107-3111.

[20]. S. Ooi, T. Yoneda, T. Tanaka and A. Osuka, *Chem. Eur. J.,* **2015**, *21*, 7772-7779.

[21]. M. Murugavel, R. V. R. Reddy and J. Sankar, *Rsc Advances*, **2014**, *4*, 13669-13672.

[22]. J. Sankar, H. Rath, V. Prabhuraja, S. Gokulnath, T. K. Chandrashekar, C. S. Purohit and S. Verma, *Chem. Eur. J.*, **2007**, *13*, 105-114.

[23]. M. Grzybowski, K. Skonieczny, H. Butenschön and D. T. Gryko, *Angew. Chem., Int. Ed.*, **2013**, *52*, 9900-9930.

[24]. M. E. Schwenter, K. Schenk, R. Scopelliti, P. Vogel, *Heterocycles* **2002**, *57*, 1513.

[25]. T. Yoshida, W. Zhou, T. Furuyama, D. B. Leznoff and N. Kobayashi, *J. Am. Chem. Soc.*, **2015**, *137*, 9258-9261.

[26]. T. Y. Gopalakrishna, J. S. Reddy and V. G. Anand, *Angew. Chem., Int. Ed.*, **2014**, *53*, 10984-10987.

[27]. P. V. Schleyer, C. Maerker, A. Dransfeld, H. J. Jiao and N. J. R. V. Hommes, *J. Am. Chem. Soc.*, **1996**, *118*, 6317-6318.

[28]. E. Vogel, P.Rohrig, M. Sicken, B. Knipp, A.Herrmann, M.Pohl, H. Schmickler, J. Lex, *Angew. Chem.Int. Ed.* **1989**, *28*, 1651-1655.

[29]. Gaussian 09, Revision D.01, M. J. Frisch, G. W. Trucks, H. B. Schlegel, G. E. Scuseria, M. A. Robb, J. R. Cheeseman, G. Scalmani, V. Barone, B. Mennucci, G. A. Petersson, H. Nakatsuji, M. Caricato, X. Li, H. P. Hratchian, A. F. Izmaylov, J. Bloino, G. Zheng, J. L. Sonnenberg, M. Hada, M. Ehara, K. Toyota, R. Fukuda, J. Hasegawa, M. Ishida, T. Nakajima, Y. Honda, O. Kitao, H. Nakai, T. Vreven, J. A. Montgomery, Jr., J. E. Peralta, F. Ogliaro, M. Bearpark, J. J. Heyd, E. Brothers, K. N. Kudin, V. N. Staroverov, R. Kobayashi, J. Normand, K. Raghavachari, A. Rendell, J. C. Burant, S. S. Iyengar, J. Tomasi, M. Cossi, N. Rega, J. M. Millam, M. Klene, J. E. Knox, J. B. Cross, V. Bakken, C. Adamo, J. Jaramillo, R. Gomperts, R. E. Stratmann,

O. Yazyev, A. J. Austin, R. Cammi, C. Pomelli, J. W. Ochterski, R. L. Martin, K. Morokuma, V. G. Zakrzewski, G. A. Voth, P. Salvador, J. J. Dannenberg, S. Dapprich, A. D. Daniels, Ö. Farkas, J. B. Foresman, J. V. Ortiz, J. Cioslowski, and D. J. Fox, Gaussian, Inc., Wallingford CT, 2009.

[30]. K. T. Meilert, M.-E. Schwenter, Y. Shatz, S. R. Dubbaka, P. Vogel, *The Journal of Organic Chemistry* **2003**, *68*, 2964.

Chapter 4

Stable Singlet Diradical Character of Fused Bicyclic Expanded Isophlorin

IV.1. Introduction

The synthesis of a covalently linked isophlorin dimer described in the previous chapter opens a new pathway to explore the chemistry of inter-linked anti-aromatic molecules. Such dimerization of anti-aromatic molecules is very rare, to date. The interest in such connectivity arises from the perceived paramagnetic property of anti-aromatics, which can be better suited for application in molecular wires than the aromatic sub-units. Unfortunately, the dimerization of 4nπ systems appears to be unsuccessful from a monomeric unit. In principle it would be ideal to have organic conductors in the form of a molecular wire with free electrons. In the process of identifying a plausible mechanism (Scheme 4.1) for the synthesis of tetroxaisophlorin dimer, it was envisaged that a neutral biradical could be the most possible intermediate in the formation of the dimer.

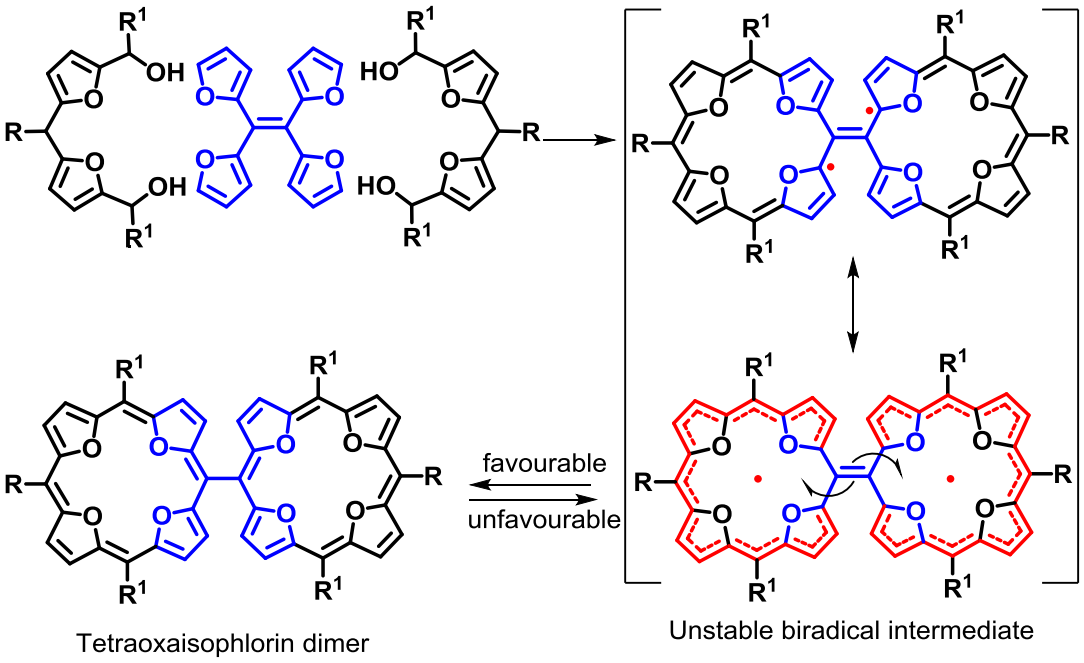

Scheme 4.1. Plausible mechanism for the synthesis of tetroxaisophlorin dimer.

Synthesis of such radicals is a challenge for chemists for two main reasons; a) to control the reactivity of radical species and b) to prevent the dimerization of any two radicals into the formation of a covalent diamagnetic molecule. Both the causes mentioned above are fundamental to the concepts of chemical bonding and structure.

Nevertheless, a rational approach to the synthesis of covalent diamagnetic dimer appears to be feasible with appropriate precursors. More than hundred years ago, Gomberg reported the synthesis and discovery of the first ever organic radical, trimethylenemethane.[1,2] Later reports revealed the discovery of quinodimethane (QM)[3] with a diradical behaviour, which still remains as a key building block in the design of biradicals. These molecules are employed to construct stable diradicals or poly radicals because of their diverse chemical and physical properties.

A process to dimerize a mono radical into biradical, albeit against the fundamental concepts of bonding, seems near impossible. As a prerequisite, it requires a stable free radical to be a successful synthetic strategy. However, organic molecules with a radical behaviour are very reactive. Yet, few π-conjugated molecules tend to offer stability for such radicals which is so far understood based on the Clar's sextet. The phenalenyl mono radical (Scheme 4.2) represents a rare π-conjugated system with a highly spin delocalized molecule.

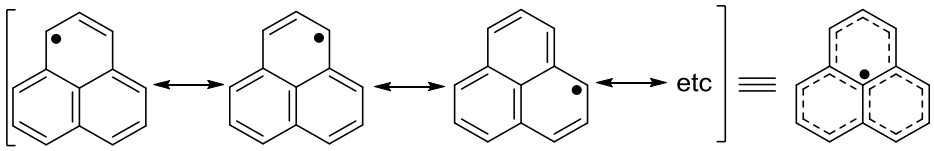

Scheme 4.2. Spin delocalization of phenalenyl radical.

It provides an opportunity to explore the dimerization of stable mono radical species, since it can be chemically oxidized/reduced to a stable cation/anion respectively from the stand alone mono radical. This radical and its derivatives are known to be persistent, and many of them have been successfully isolated.[4-6] In a recent study, it was established that sigma dimerization of the phenalenyl radical leads to a covalent diamagnetic dimer, satisfying the Hund's rule of multiplicity.[7] But, it is observed that the phenalenyl radical can be dimerized into a biradical with a suitable aromatic spacer in-between the two radical species (Scheme-4.3). The hydrocarbon **1** consists of *para*-quinodimethane and two phenalenyl moieties. The quinoid Kekule compound **1** would resonate well with biradical structure **1a**' as a result of gaining the aromatic stabilization energy of the central benzenoid ring (Scheme 4.3). The

unpaired electrons located on the terminal carbon atoms of the *para*-quinodimethane moiety can undergo delocalization on the phenalenyl moieties (**1a**). Out of these resonating structures **1a** would be thermodynamically stabilize the singlet diradical than *para*-quinodimethane **1**.[8]

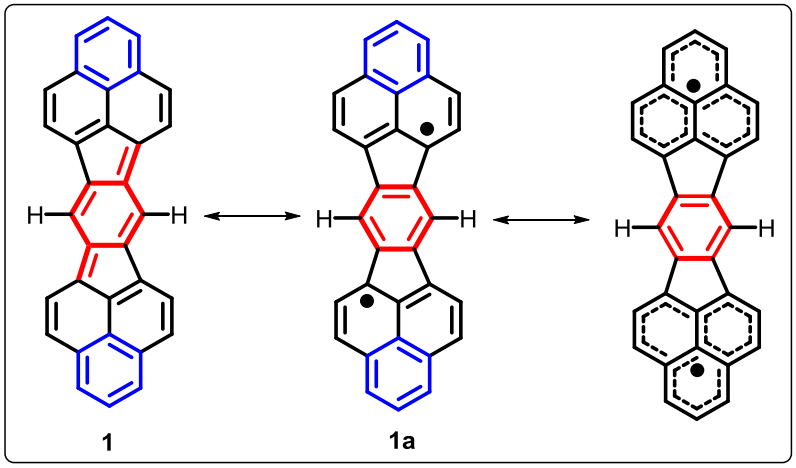

Scheme 4.3. Resonance structures of **1**.

Clar's aromatic sextet rule, which can be applied to estimate the stability and reactivity of PAHs, predicts that the most stable resonance structure will always bear more number of aromatic sextets.[9] According to Clar's sextet rule, structure **1a** is more stable and hence stabilizes the diradical form. This is in stark contrast to the majority of known quinoidal Kekule hydrocarbons that are highly reactive and easily dimerizes or polymerizes at normal temperature.[10]

The π-conjugation in cyclic systems with odd number of atoms leads to incomplete network of π bonds. As a result of this frustration, such cyclic systems can tend to form a radical which can be stabilized by the delocalized π-bonds. Very recently, such a macrocyclic system with five thiophene sub-units was isolated and characterized as an air- and water-stable neutral 25π pentathiophenemono radical **2**.[11] This radical undergoes chemical oxidation or reduction to form the respective 24π cation and 26π anion. Ideally, this macrocycle can also be dimerized through one of its *meso* carbon atoms, very similar to that observed for porphyirns. However, such dimreization can lead to altered properties in structure and bonding to favor a diamagnetic dimer. As described (Scheme 4.4) below, the macrocycle requires an

unsubstituted *meso* carbon, *i.e.* C-H moiety (**3**). It can be subjected to a dehydrogenation reaction leading to the dimer, **4**, through a direct C-C bond between the two macrocycles. In accordance with the principles of the chemical bonding, it can be envisaged that this can lead to the formation of covalent diamagnetic dimer **5** as observed in the case of phenalenyl dimerization. However, the dimerization of **3** generates a double bond link in between the macrocycles in order to be a diamagnetic system **5**. The synthesis of **5** can now be more easily targeted with appropriate precursors from thiophene units.

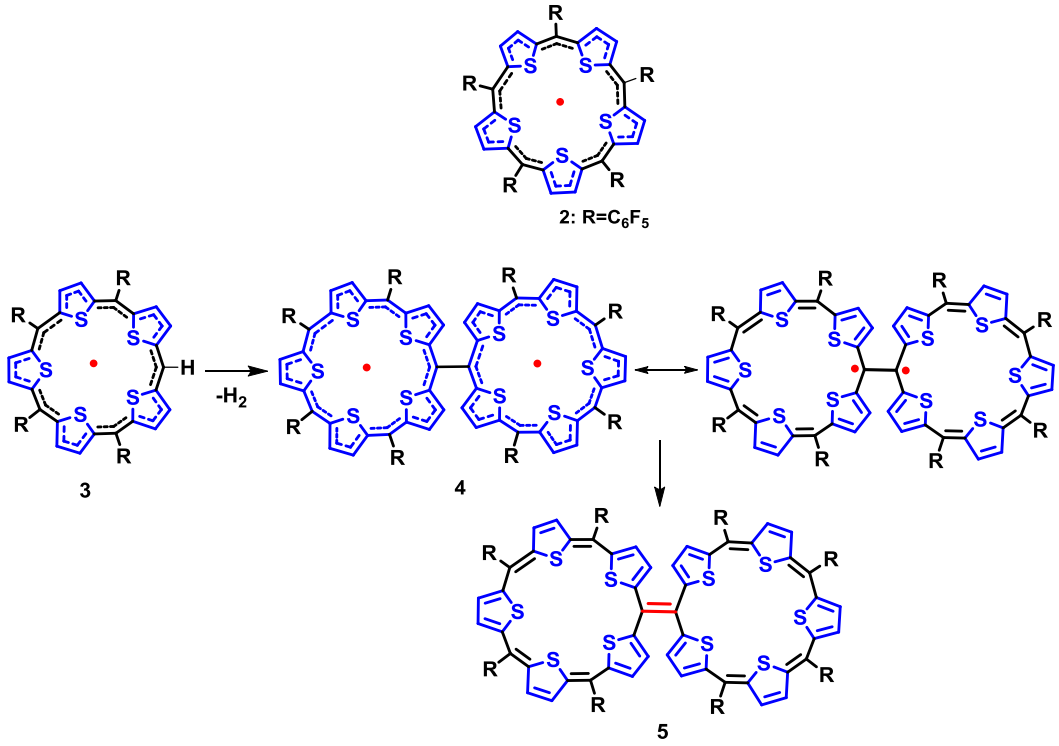

Scheme 4.4. Schematic representation of diradical **4.**

IV.2. Synthesis

The synthesis of pentathiophene expanded isophlorin dimer, **5**, was attempted by employing MacDonald type condensation of appropriate precursors. 5,5'-Methylenetristhiophene-2-carbinol **7**, was reacted with tetrathienylethene **6**, under acidic conditions followed by oxidation to obtain the desired expanded isophlorin (Scheme 4.5). Apart from the expected dimer, this reaction can yield either bicyclic

compound **IV.1** or dimeric compound **IV.2** depending on the orientation of the tetrathienylethane towards 5,5'-Methylenetristhiophene-2-carbinol.

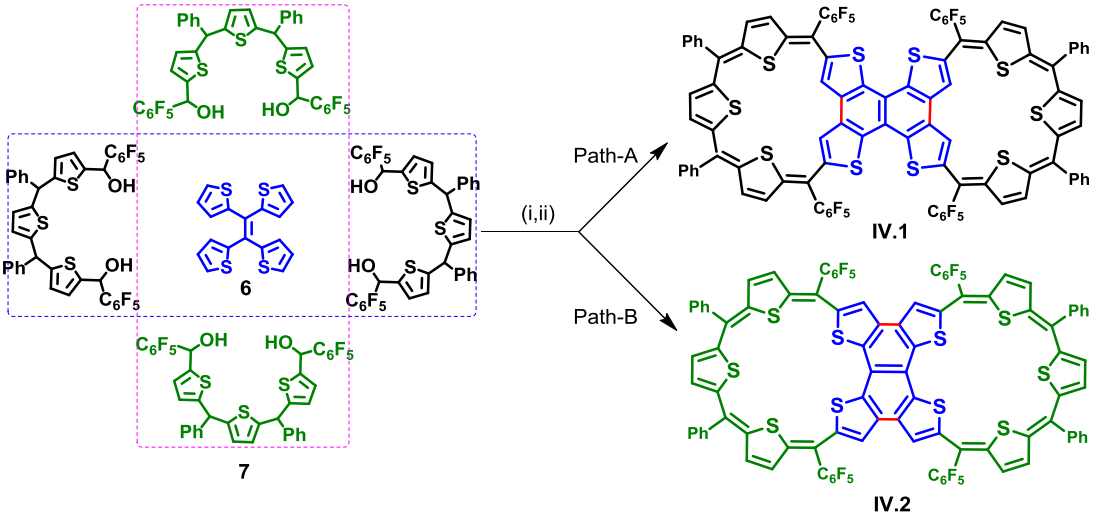

Scheme 4.5. Acid catalysed synthesis of 50π expanded isophlorins **IV.1** or **IV.2.**

Reaction conditions: (i) $BF_3.OEt_2$(1 eq.), dry DCM (100 ml), rt, N_2, 2h (ii) $FeCl_3$(10 eq.), 2h.

The product was purified by silica gel column chromatography and subjected to MALDI-TOF-TOF mass analysis. Its mass spectrum displayed an *m*/*z* value of 1911.720 corresponding to a mass four units less than the excepted 1915.0018. It suggested the formation of the desired product along with a possible oxidative dehydrogenation in the presence of $FeCl_3$. However, the reactivity of the precursors could be suspected for the unexpected mass. It could also be envisaged that depending on the orientation of the central tetrathiophene unit, another macrocyclic product could also be feasible with a similar mass of the expected dimer, **5**. Both the macrocycles have a possibility of oxidative dehydrogenation at β-carbons of the tetrathiophene units.

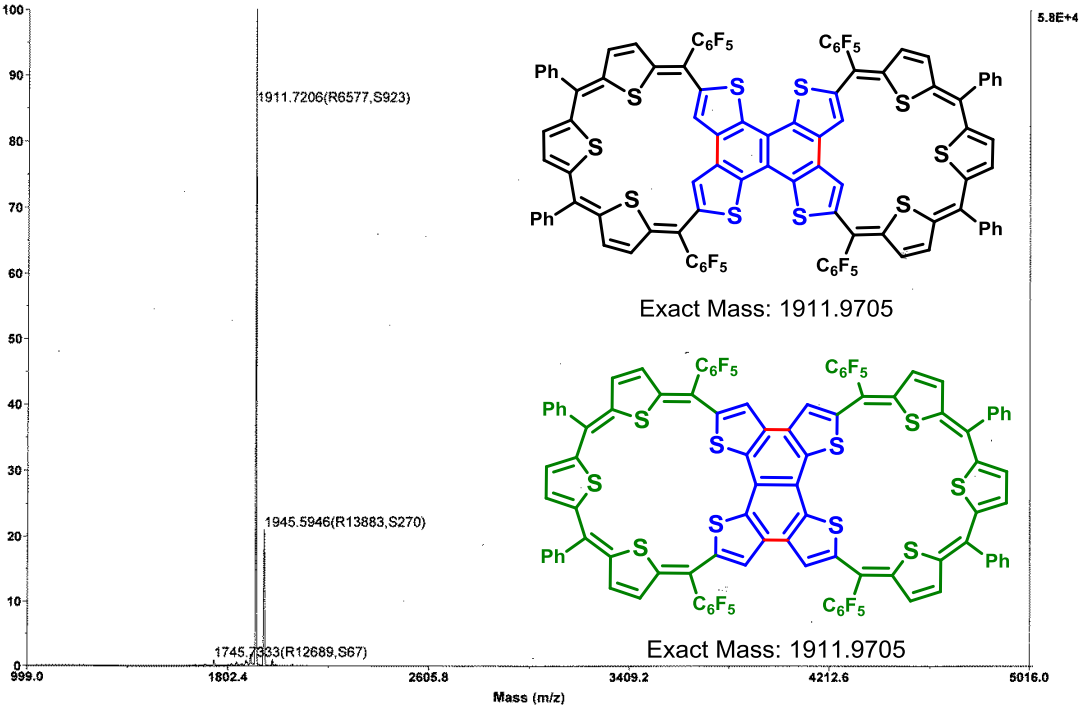

Figure 4.1. MALDI-TOF-TOF mass spectrum of **IV.1** or **IV.2**.

The mass spectrum analysis was ambiguous enough to distinguish either of the bicyclized compounds **IV.1**or **IV.2** formed during the reaction. The suspected purified expanded isophlorin dimer forms pink colored solutions when dissolved in common organic solvents, while it was found to be dark green in solid state. The color of the solution is attributed to the extensive conjugation and was found to absorb in the visible region at 554 nm (ε = 101110) (Figure 4.2).

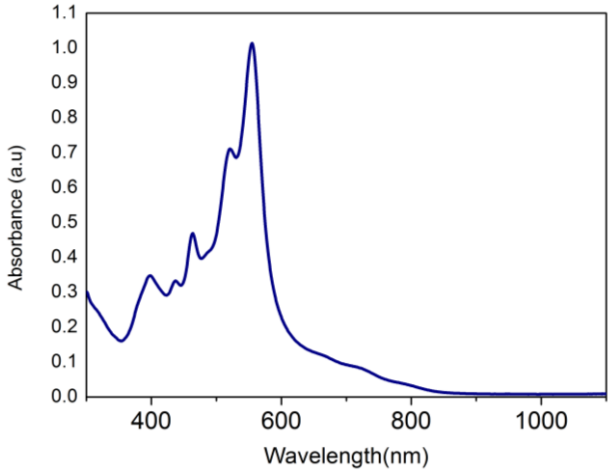

Figure 4.2. UV-Vis absorption spectra of **IV.1**or **IV.2** recorded in THF 10^{-5}M at room temperature.

Electronic absorption spectrum also did not support the formation of one product over another. ^{1}H NMR spectroscopy is an ideal analytical tool to confirm the most probable structural isomer, based on the β-protons resonance of the thiophene in the macrocycle. Due to ring current effects it could be expected that any proton at the centre of the macrocycle would show a significant difference in its resonance signal compared to the peripheral protons. Surprisingly, the molecule was found to be NMR silent even at low temperature (-100 °C in Tetrahydrofuran-d_8) suggesting the possibility of a radical behavior. Interestingly, the molecule was indeed paramagnetic as confirmed from its ESR spectrum recorded at room temperature. Based on this unexpected outcome, the molecule was subjected to paramagnetic studies based on magnetic measurements and ESR spectroscopy. The expected dimer is supposed to be a combination of two 25π systems and hence it should contain 50π electrons. With even number of π electrons, it could be envisaged that homolytic bond fission could have perhaps led to the formation of a biradical. Such instances are rare but possible with a few π-conjugated systems.[8,12]

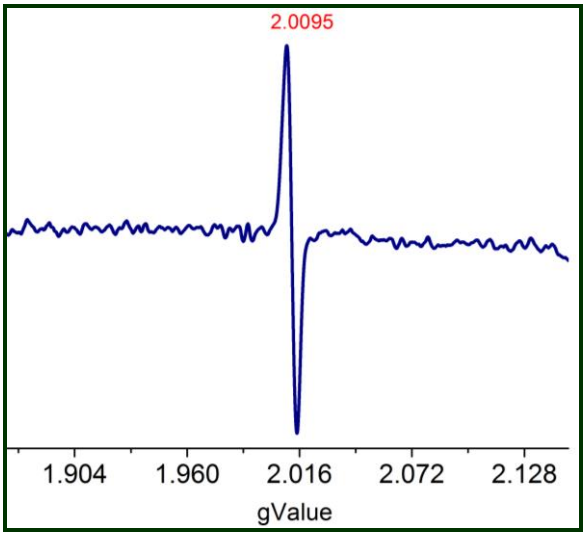

Figure 4.3. EPR spectrum of compound (**IV.1**or **IV.2)** recorded in solid state at room temperature.

The ESR spectrum of **IV.1** or **IV.2** at 298 K in the solid state exhibited a signal at g = 2.009 characteristic of an organic free radical. The VT-ESR measurements for the powder sample of **IV.1** or **IV.2** disclosed the significant temperature dependency of the signal intensities; the intensity decreased with decreasing temperature indicating that

the compound has a singlet diradical ground state, which is in equilibrium with a higher energy triplet diradical state[12] (Figure 4.4).

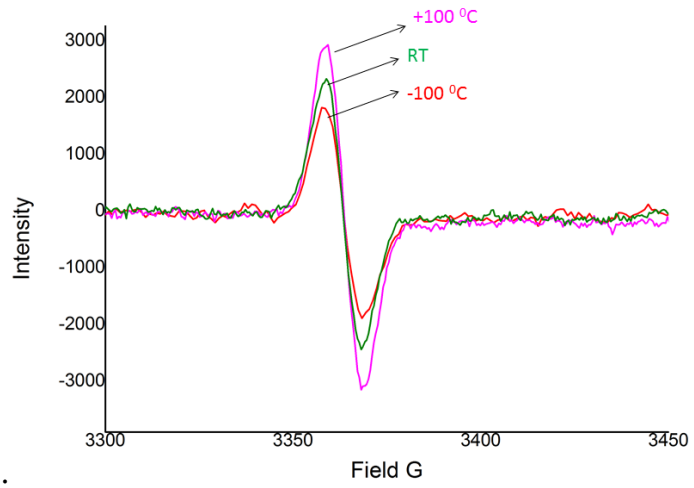

Figure 4.4. VT-EPR spectra of compound (**IV.1** or **IV.2)** recorded in solid state.

The singlet−triplet energy gap ΔE_{S-T} (i.e., −2 J/kB) was estimated by SQUID measurements on the powder form of **IV.1** or **IV.2** at 5−320 K by means of careful fitting of the curves by the Bleaney−Bowers equation[13] (Figure 4.5).

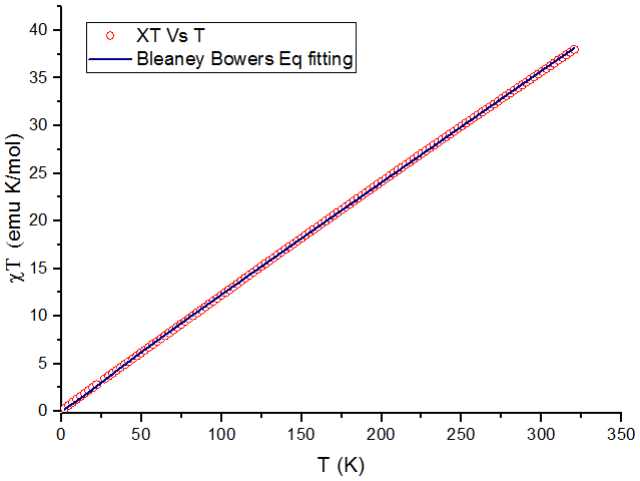

Figure 4.5. χT−T curve in the SQUID measurement for the powder of **IV.1** or **IV.2**. The solid lines are the fitting curves according to Bleaney−Bowers equation; g-factor was taken to be 2.

The energy gap between singlet (S_0) and triplet (T_1) states was determined to be 0.3113 k.cal./mol. Such small ΔE_{S-T} value allows the facile thermal excitation to the higher energy triplet diradical state.[12]

To confirm one structure out of two possible structures (**IV.1** or **IV.2**), crystals were grown in various organic solvents and finally the compound crystallized in Chloroform/TFA combination. From single crystal X-ray diffraction analysis it was confirmed to have ring inverted molecular structure as **IV.1.**

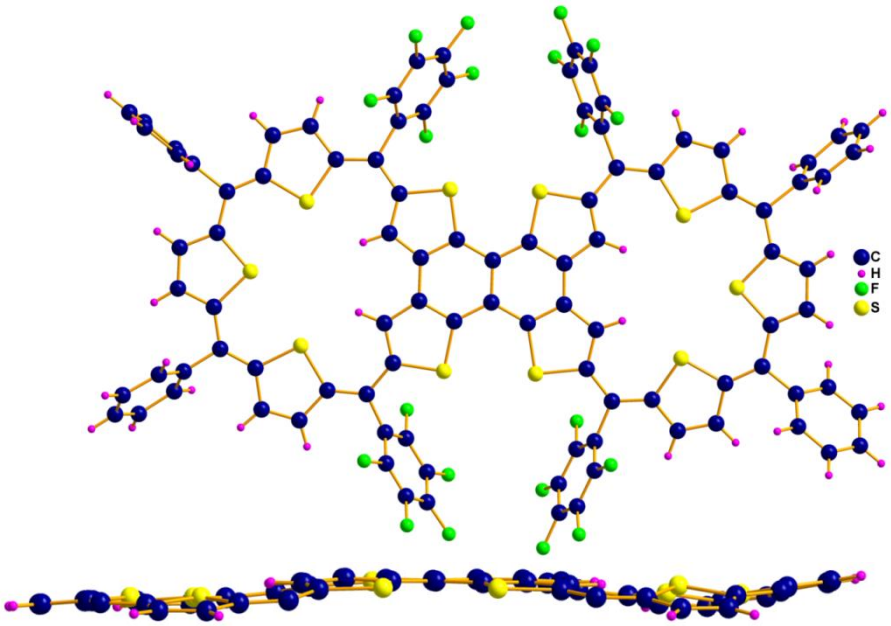

Figure 4.6. Molecular structure of compound **IV.1**.Top view (upper) and side view (below).

Compound **IV.1** displayed a near planar structure and the crystal packing shows slipped sandwich kind of π-π interaction with an interplanar distance of 3.79 Å between adjacent layers.

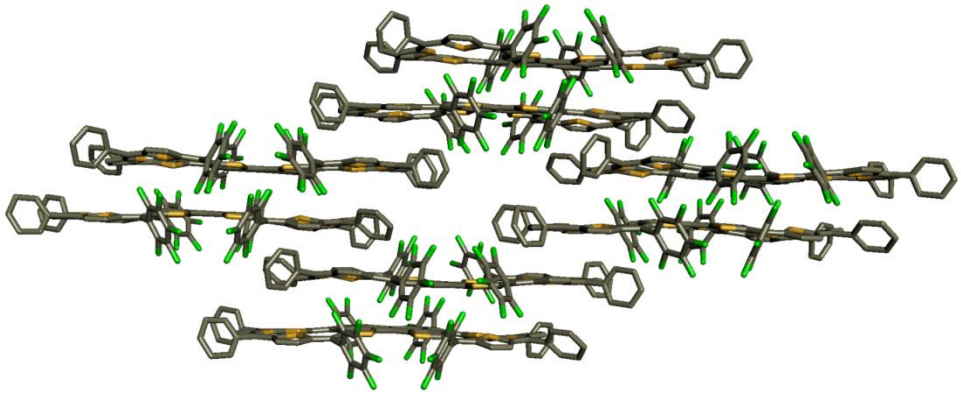

Figure 4.7. π–π stacking in molecular packing of **IV.1**

Based on molecular structure it could be confirmed that the cyclization followed by fusion occurred selectively in path-A instead of path-B (Scheme 4.1).

The above investigations led to the curiosity of chemical redox as observed for the 25π mono radical. The dimer **IV.1** was subjected to chemical oxidation through Meerwien's salt[14] or $[NO]^+[BF_4]^-$. However no significant change in its absorption was observed suggesting stability towards to oxidizing agents. Cyclic voltammetry and differential pulse voltammetry measurements were performed to investigate the electrochemical properties of compound **IV.1**. The compound displayed chemically reversible four reduction potentials in the region between at -0.46 V to -2.15 V (Figure 4.8), while no oxidations could be recorded to support the resistance observed for chemical oxidation.

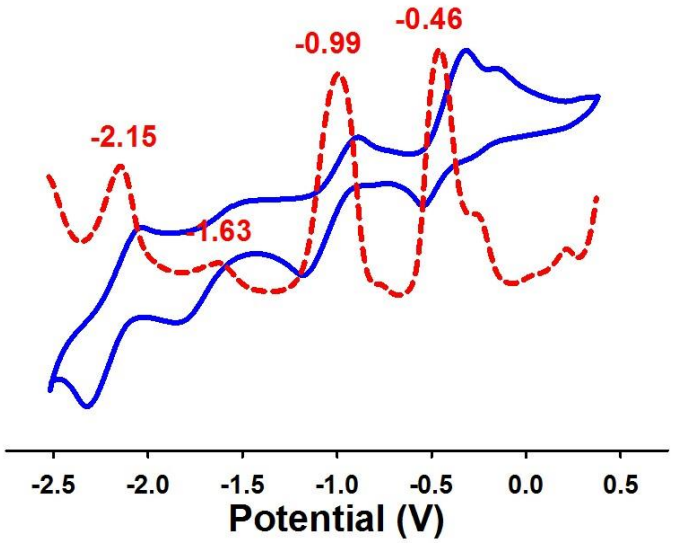

Figure 4.8. Cyclic voltammograms of **IV.1** in dry THF with 0.1 M Bu_4NPF_6 as supporting electrolyte, Ag/AgCl as reference electrode, Glassy carbon as working electrode, Pt wire as counter electrode, and scan rates at 20 mV/s, respectively.

The paramagnetic bicyclic macrocycle **IV.1** can exist either in closed shell **IV.1a** or open shell **IV.1b.** The ESR and SQUID measurements confirmed that macrocycle **IV.1** existed in a diradical form (open shell configuration) instead of closed shell **IV.1a.** Macrocycle **IV.1a** has a combination of aromatic 26π stabilization in one core of the molecule and another core attained anti-aromatic 24π destabilization. The experimental studies revealed that such systems could not be sustained and instead,

lead to splitting of a double bond into two radicals. Envisaging such a scenario, the aromatic character of the dimer was estimated by NICS calculations. The NICS(0) at the centre of the two pentathiophene cores was -4.05 ppm indicating symmetrical ring current effects. The estimated NICS(0) value for the central napthalene core was found to be -18.40 ppm, suggesting a strong aromatic character. However, a symmetrical aromatic strength does not justify the unsymmetrical distribution of 26π and 24π electrons in the two rings. Rather, it does not even support the possibility of 26π and 22π electrons to justify the aromatic character in either of them. It can be only possible when both the macrocycles have same number of π electrons to have equal distribution of electron density over the naphthalene core. Such a possibility exists only if both the macrocycles are stabilized by 22π electrons to make them aromatic in character. This accounts for only 44π electrons of the total 50π electrons. The other six electrons are expected to be equally distributed over the naphthalene unit, to further increase the aromatic behaviour of the fused core. This concept is similar to the Clar's aromatic sextet rule, which proposes that a biradical can be stabilized by a resonance structure that can accommodate maximum number of aromatic units.

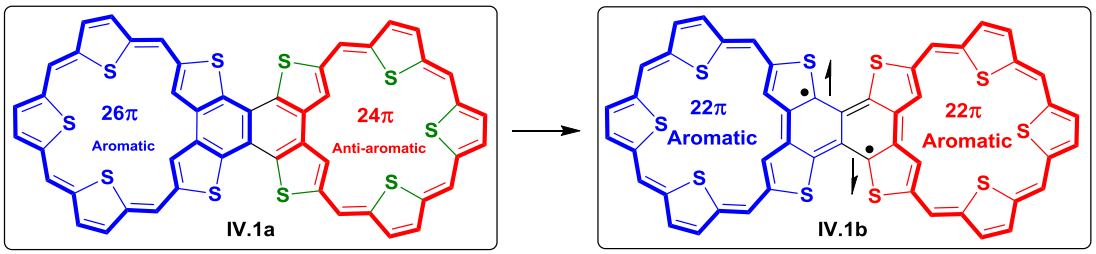

In this context only two symmetrical 22π aromatic cores are only possible when the two diradicals are accommodated in the naphthalene ring. The NICS and AICD calculations also support that **IV.1b** could be the most possible structure.

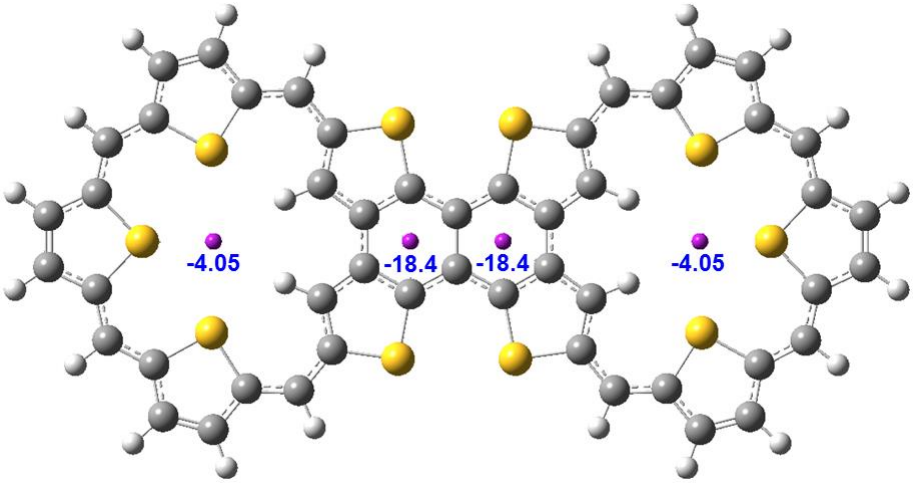

Figure 4.9. Computational parameters to classify ring current effects in **IV.1** determined from NICS calculations.

The symmetrical ring current effects strongly correlated with the proposed structure and also the negative NICS value confirmed that aromatic nature of **IV.1**. The effect of delocalization for **IV.1** was further supported by Anisotropy Induced Current Density (AICD) plots.

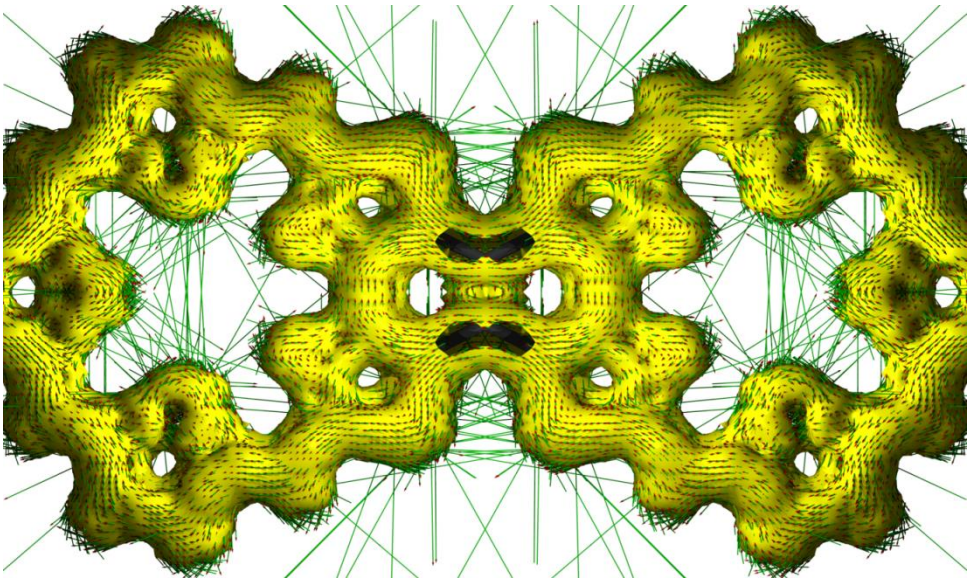

Figure 4.10. AICD plot for macrocycle **IV.1**.

The AICD plot for **IV.1** displayed clockwise ring current favouring aromatic character of the macrocycle (Figure 4.10).

On the basis of calculated NICS(0), both the thiophene macrocycles and the central naphthalene moiety exhibited aromatic character. Hence for the estimation of biradical charecter, the NICS(0) proposed 22π structure was taken as the starting geometry. The optimized closed-shell geometry of the **IV.1b** exhibits C_{2v} symmetry. The open-shell broken-symmetry singlet and closed shell energy difference ΔE_1 was evaluated according to Eqn (1). The negative ΔE_1 indicate that the singlet state of **IV.1b** is best described by the unrestricted symmetry-broken method[16] (Table 4.1).

$$\Delta E_1 = E_{UDFT} - E_{RDFT} \quad (1)$$

Further, to classify a molecule as a diradicaloid, the singlet–triplet energy gap ΔE_2 was calculated using Eqn (2).

$$\Delta E_2 = E_{UDFT\,(triplet)} - E_{RDFT\,(closedshell)} \quad (2)$$

The large deviation in the computed value of ΔE_2 (-36.19 kcal.mol^{-1}) as compared to the experimental value obtained from SQUID measurements, suggesting the challenges to calculate a large open-shell system. [17]

The spatial diradical distribution in the singlet diradical structures was examined by inspecting the HOMOs and LUMOs for α and β spin electrons. Figure 4.11 represents the frontier orbitals for α and β spin electrons of **IV.1b**, calculated using the unrestricted symmetry-broken method. α-HOMO and β-LUMO, as well as β-HOMO and α-LUMO occupy practically the same part of space, thus allowing the π-electrons to delocalize.

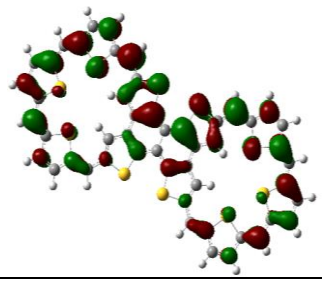	
α-HOMO	β –HOMO

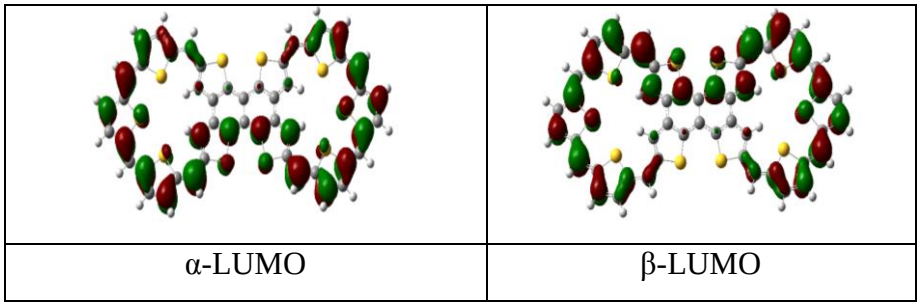

α-LUMO	β-LUMO

Figure 4.11. Calculated frontier molecular orbitals of **IV.1b**

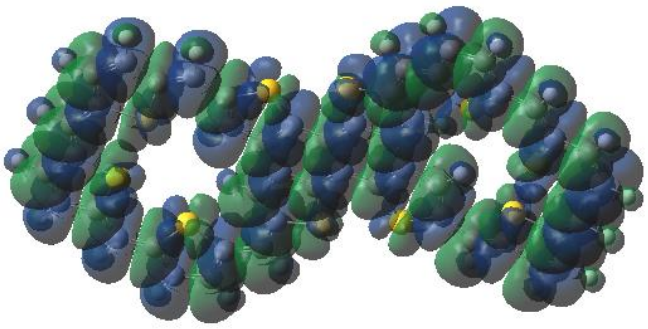

Figure 4.12. Spin density calculated at the UBH and HLYP/6-31G (*d,p*) level for the singlet state **IV.1b**. Green and blue surfaces represent positive and negative spin densities, respectively.

The percent biradical charecter can also be estimated by using the Yamaguchi method. The diradical index y_{PUHF}, related to the HOMO and LUMO for singlet states, is defined by the weight of the doubly-excited configuration in the multi-configurational MC-SCF theory, and is formally expressed in the case of the spin-projected UHF (PUHF) theory (Eqns 3 and 4)

$$Y = 1 - \frac{2T}{1+T^2} \qquad \text{Equation 3}$$

$$T = \frac{\text{HOMO-LUMO}}{2} \qquad \text{Equation 4}$$

Here *T* is the orbital overlap between the corresponding occupied and unoccupied orbital pairs (HOMO and LUMO) and *T* is determined by using the occupation numbers (η) of the unrestricted formalism natural orbitals. The large value

of ΔE_2 is in correlation with the small biradical charecter value 9% for **IV.1b**. The current trend is in agreement with literature values[16,18].

Table IV.1: The Eigen value of the stability matrix, the differences between open-shell broken-symmetry singlet and closed shell solution (ΔE_1)[a], Singlet–triplet gap (kcal/mol),[a] the biradical character (BRC)[a] and the LUMO natural orbital occupation number (y_{NOON})[b]

ΔE_1 **(kcal.mol^{-1})**	-3.531
ΔE_2 **(kcal.mol^{-1})**	-36.19
BRC	9%
y_{NOON}	8.6%

[a]*UBH and HLYP functional,* [b]*Calculated by performing CASSCF(2,2)/6-31G(d) single point calculations at B3LYP optimized geometries*

IV.3. Spectral Characterization

The monomers were analyzed through high resolution mass spectrometry and NMR spectroscopy.

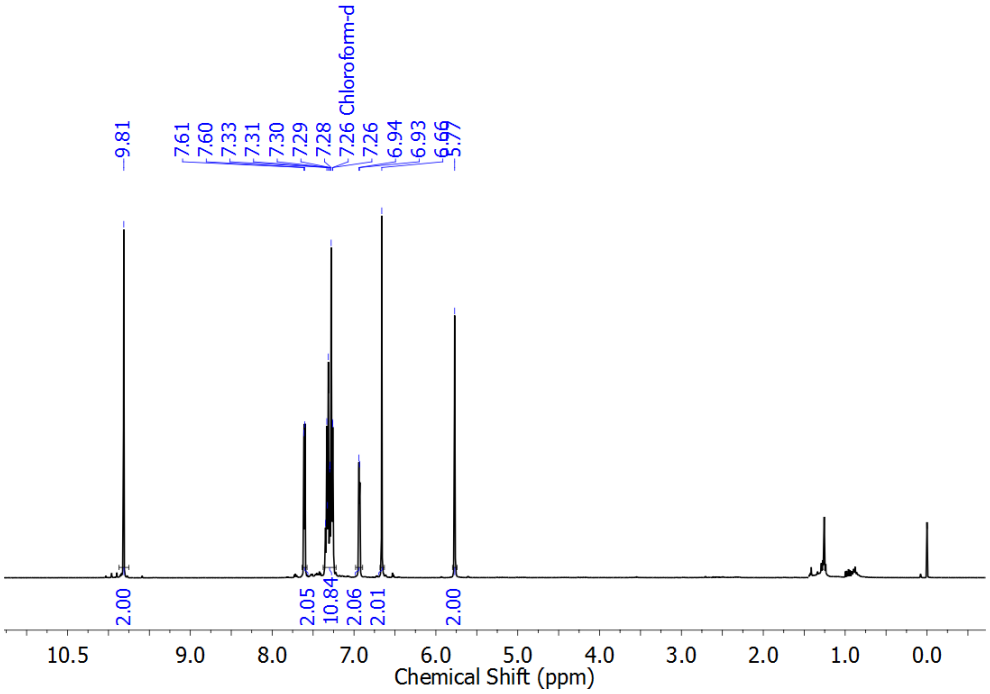

Figure 4.13. ^{1}H NMR spectrum of trithiophene dicarbaldehyde in $CDCl_3$at 298*K*.

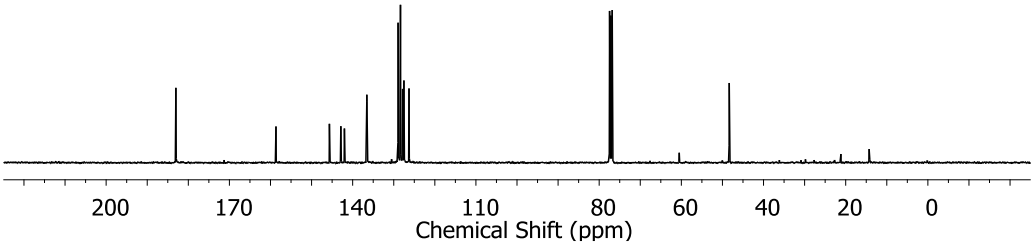

Figure 4.14. ^{13}C NMR spectrum of trithiophene dicarbaldehyde in $CDCl_3$ at 298*K*.

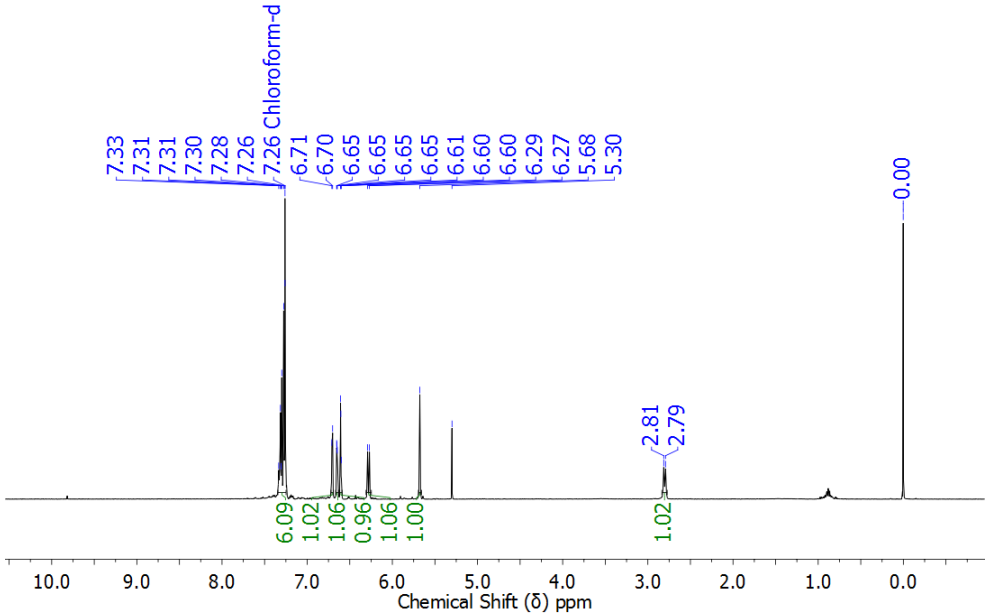

Figure 4.15. ^{1}H NMR spectrum of trithiophene dicarbinol **7** in $CDCl_3$ at 298*K*.

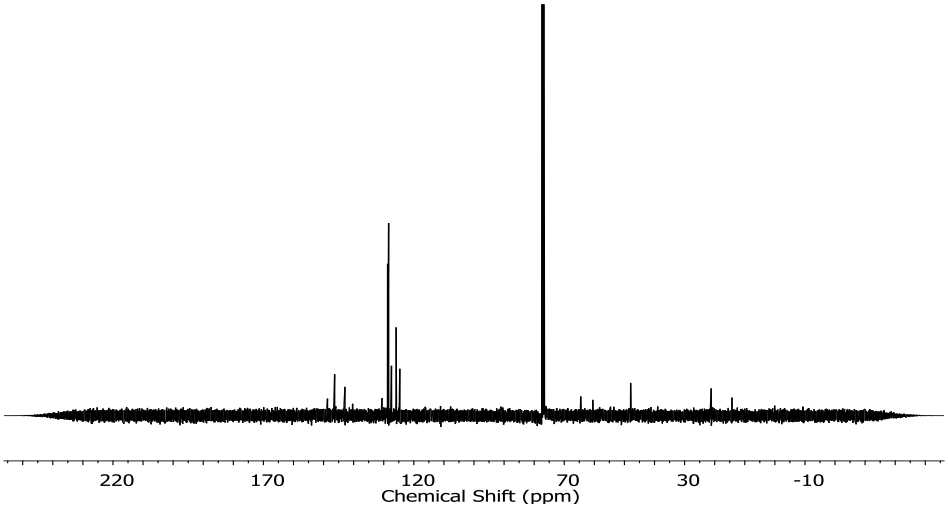

Figure 4.16. ^{13}C NMR spectrum of trithiophenedicarbinol **7** in $CDCl_3$ at 298*K*.

IV.4. Conclusion

The first example of bicyclic expanded isophlorin was obtained from a one-pot synthesis and it has a distinct singlet diradical character. It is believed that, the molecule may not exist with the combination of both aromatic and anti-aromatic closed shell system; instead it could exit in a stable aromatic-aromatic delocalized open shell system. To date, there are no examples of fusion between aromatic and anti-aromatic sub-units. This molecule represents one such unexplored situation that tries to understand the electronics of fusing anti-aromatic behaviour with aromaticity. It can be foreseen that such covalent interactions predominantly support aromatization leading the formation of a biradical. This possibly opens a new pathway to generate novel and stable organic biradicals which can have potential in applications based on organic electronics.

IV.5. Experimental Section

5,5'-Methylenetristhiophen-2-carbaldehyde

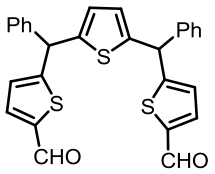

To a mixture of thiophene, 2,5-bis(phenyl-2-thienylmethyl), (0.5 g., 1.1 mmol), dry ether (15ml.), and *n*-butyl lithium 2.5 M in Hexane (1.91ml, 4.8 mmol), prepared as before, dimethylformamide (0.37ml, 4.8 mmol) in 3ml dry ether was added dropwise with stirring at room temperature, and stirring was continued for a further 2h. The mixture was washed successively with water; dilute hydrochloric acid, water, and sodium hydrogen carbonate solution, dried and evaporated. The residue purified by (Silica gel 100-200 mesh) column chromatography gave 5,5'-Methylene tristhiophen-2-carbaldehyde as orange color semisolid (0.34 g., Yield: 61%).

^{1}H NMR (400 MHz, $CDCl_3$): δ 9.81 (2H, s), 7.28-7.33 (10H, m), 7.61 (d, *J* =3.6 Hz, 2H), 6.94 (d, *J* =3.6 Hz, 2H), 6.66 (2H, s), 5.77 (2H, s); **^{13}C NMR** (100 MHz, $CDCl_3$) δ 183.02 (s), 158.66 (s), 145.65 (s), 142.88 (s), 142.01 (s), 136.55 (s); **HRMS:** *m/z*: Calcd. for $C_{28}H_{20}S_3O_2$: 484.0625; observed: 484.0603 (100.0%, M^+).

5,5'-Methylenetristhiophen-2-carbinol (7)

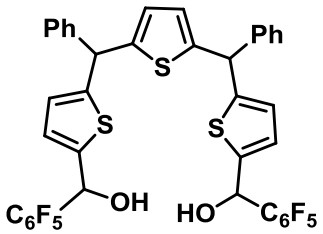

To the stirred solution of 5,5'-Methylenetristhiophen-2-carbaldehyde (1.1 mmol, 0.746g in 15 ml THF) under argon atmosphere at 0 °C, freshly prepared Grignard Reagent (C_6F_5MgBr, 2.7 mmol) was added. Stirring was allowed 2hrs to attain room temperature and the reaction mixture was quenched with saturated NH_4Cl solution. The organic layer was extracted with ether and combined organic layer was washed with water and brine solution. After drying over Na_2SO_4, the solvent was removed under vacuum and purified through silica gel(100-200 mesh) column chromatography to yield the pure compound, **7**, as brown color semi solid.(0.9 g., Yield: 41%.)

^{1}H NMR (400 MHz, $CDCl_3$): δ 7.33 -7.26 (5H, m), 7.71 (1H, d, *J*=3.6 Hz), 6.65 (1H, s), 6.61 (1H, s), 6.29 (1H, d, *J*=3.6 Hz), 5.68 (1H, s) 2.81(1H, d, *J*=3.6 Hz) ; **^{13}C NMR** (101 MHz, $CDCl_3$) δ 148.61 (s), 146.24 (s), 143.10 (s), 142.81 (s), 128.61 (s), 128.29 (s), 127.33 (s), 125.75 (s), 124.55 (s), 77.32 (s), 77.00 (s), 76.68 (s), 64.47 (s), 47.89 (s); **HRMS:** *m/z*: Calcd. for $C_{40}H_{22}F_{10}S_3O_2\,Na^+$: 843.0519; observed: 843.0513 (100.0%, M^+).

Synthetic procedure for IV.1

A mixture of tetrathienylethene[15], **6**, (178 mg, 0.5 mmol) and the trithiophene dicarbinol **7**, (820 mg, 1 mmol) were stirred in 100 ml dry dichloromethane. The solution was bubbled with argon for 10 min. $BF_3.OEt_2$ (60µL, 0.5 mmol) was added under dark, and the resulting solution was stirred for 2h. After adding ten equivalents of $FeCl_3$ under open atmosphere, solution was stirred for additional 2h. The reaction mixture was passed through a short basic alumina column. This mixture was purified on silica gel column followed by recrystallization in dichloromethane at 0 °C. A metallic green color solid obtained was identified as **IV.1** in 100mg, 10.4% yield.

UV-vis (THF): $\lambda_{max}(\varepsilon)$L mol^{-1} cm^{-1}: 554 nm (101176). **MALDI-TOF m/z:** Calcd. for $C_{98}H_{36}F_{20}S_{10}$: 1911.9705; observed: 1911.7206 (100.0%, M^+). **Crystal data:**

$C_{99}H_{37}Cl_3F_{20}S_{10}$ (Mr = 2033.23), Triclinic, space group P-1 (no. 2) , a = 15.552(3) Å, b = 17.106(3) Å, c = 20.345(4) Å, α = 109.332(4)° β = 104.391(4)° γ = 96.259(4)°, V = 4837.3(15) $Å^3$, Z = 2, T = 100(2) K , D_{calcd} = 1.396mg cm^{-3}, R_1 = 0.1198 (I>2s(I)), R_w (all data) = 0.2465, GOF = 1.143.

IV.6. References

1) P. Dowd, *Acc. Chem. Res.***1972**, *5*, 242.

2) S. Yamago, E. Nakamura, *Org. React.***2002**, *61*, 1.

3) M. Szwarc, *Discuss. Faraday Soc.***1947**, *2*, 46.

4) K. Goto, T. Kubo, K. Yamamoto, K. Nakasuji, K. Sato,D. Shiomi, T. Takui, M. Kubota, T. Kobayashi, K. Yakusi, J. Ouyang, *J. Am. Chem. Soc.* **1999**, *121*, 1619 – 1620.

5) Y. Morita, T. Ohba, N. Haneda, S. Maki, J. Kawai, K. Hatanaka, K. Sato, D. Shiomi, T. Takui, K. Nakasuji, *J. Am. Chem. Soc.***2000**, *122*, 4825 – 4826.

6) P. A. Koutentis, Y. Chen, Y. Cao, T. P. Best, M. E. Itkis, L. Beer, R. T. Oakley, A.W. Cordes, C. P. Brock, R. C. Haddon, *J. Am. Chem. Soc*.**2001**, *123*, 3864 – 3871.

7) K. Uchida, S. Ito, M. Nakano, M. Abe, T. Kubo, Journal of the American Chemical Society **2016**, *138*, 2399–2410.

8) T. Kubo, A. Shimizu, M. Sakamoto, M. Uruichi, K. Yakushi, M. Nakano, D. Shiomi, K. Sato, T. Takui, Y. Morita, K. Nakasuji, *Angew. Chem., Int. Ed.,***2005**, *44*, 6564.

9) E. Clar, *The Aromatic Sextet*, *Wiley*, London, **1972**.

10) M. S. Platz in Diradicals (Ed.:W. T. Borden), *Wiley*, New York, **1982**, pp. 195–258.

11) T. Y. Gopalakrishna, J. S. Reddy and V. G. Anand, *Angew. Chem.*, *Int. Ed.*,**2014**, *53*, 10984-10987.

12) Z. Zeng, M. Ishida, J. L. Zafra, X. Zhu, Y. M. Sung, N. Bao, R. D. Webster, B. S. Lee, R.-W. Li, W. Zeng, Y. Li, C. Chi, J. T. L. Navarrete, J. Ding, J. Casado, D. Kim, J. Wu, Journal of the American Chemical Society **2013**, *135*, 6363–6371.

13) B. Bleaney, K. D. Bowers, *Proc. R. Soc.* London, Ser. A **1952**, *214*, 451−465.

14) R. Rathore, A. S. Kumar, S. V. Lindeman, J. K. Kochi, *The Journal of Organic Chemistry* **1998**, *63*, 5847

15) E. Fischer, J. Larsen, J. B. Christensen, M. Fourmigué, H. G. Madsen, N. Harrit, The Journal of Organic Chemistry **1996**, *61*, 6997–7005.

16) A. Thomas, K. Bhanuprakash and K. M. M. K. Prasad, *J. Phys. Org. Chem*., **2011**, *24*, 821–832.

17) Z. Zeng, S. Lee, J. L. Zafra, M. Ishida, N. Bao, R. D. Webster, J. T. Lopez Navarrete, J. Ding, J. Casado, D. Kim, J. Wu, *Chemical Science* **2014**, *5*, 3072.

18) S. Marković, S. Radenković, Z. Marković, I. Gutman, *Russian Journal of Physical Chemistry A* **2011**, *85*, 2368.